The Investigation of Gold Nanoparticles as Radiosensitizers to Treat Prostate Cancer in 3D *In Vitro* models

by

Saduni Udeesha Sumithrarachchige Don

A thesis

presented to the University of Waterloo

in fulfillment of the

thesis requirement for the degree of

Master of Science

in

Pharmacy

Waterloo, Ontario, Canada, 2026

© Saduni Udeesha Sumithrarachchige Don 2026

Author's Declaration

I hereby declare that I am the sole author of this thesis. This is a true copy of the thesis, including any required final revisions, as accepted by my examiners.

I understand that my thesis may be made electronically available to the public.

Abstract

Prostate cancer (PCa) is the most prevalent cancer among Canadian men (1). Despite advancements in PCa treatment, castration resistant PCa (CRPC) and metastatic CRPC (mCRPC) remain difficult to treat with the currently limited treatment options, and radioresistance and recurrence persist (169,170). Radiation therapy and surgery are the primary treatments for localised PCas; however, if the cancer has metastasized, systemic treatments like chemotherapy may be used (26). To address the challenge of radioresistance, we investigated gold nanoparticles (GNPs) that leverage both the photoelectric properties of gold and the anti-cancer effects of phytochemicals, like curcumin (135,158,188). This research focused on synthesizing, characterizing and evaluating curcumin-coated gold nanoparticles (Curc-GNPs) for their efficacy as radiosensitizers for prostate cancer therapy using three-dimensional DU145 prostate cancer spheroids.

In this study, two gold nanoparticle formulations, citrate-coated GNPs (Cit-GNPs) and Curc-GNPs were synthesized and characterized. Curc-GNPs were synthesized using an eco-friendly single-step green synthesis method, where curcumin acted as both a reducing and stabilizing agent (188,202). Cit-GNPs were synthesized using a citrate reduction method, known as the Turkevich method (203-205). Ultraviolet-visible spectroscopy was used to confirm the successful formation of spherical GNPs, where surface plasmon resonance peaks (SPR) were observed in the 520-530 nm range (188,202,204). Dynamic light scattering (DLS) analysis demonstrated that both formulations produced small nanoparticles with hydrodynamic diameters ranging from 18 – 25 nm. The average hydrodynamic diameter of Curc-GNPs and Cit-GNPs were 18.36 ± 0.27 and 22.55 ± 0.18 nm respectively. Both formulations had negative zeta potentials with Curc-GNPs measuring -44.5 ± 1.2 mV and Cit-GNPs measuring -40.0 ± 4.6 mV. Inductively coupled plasma optical emission spectroscopy (ICP-OES) showed that Curc-GNPs had a higher final gold concentration than Cit-GNPs, with measured concentrations of 361 ± 15 μg/mL and 20 ± 4 μg/mL, respectively. Overall, these results confirmed the successful synthesis and characterization of stable Curc-GNPs and Cit-GNPs suitable for downstream biological evaluation.

In vitro studies supported the therapeutic efficacy of Curc-GNPs as radiosensitizers in three-dimensional DU145 prostate cancer spheroids, which better reflect the tumour-like architecture compared to conventional monolayer culture, and the therapeutic resistance seen in CRPC and mCRPC (148,188). Cellular uptake was quantified using ICP-OES after three-dimensional DU145 prostate

cancer spheroids were exposed to different GNP formulations, concentrations and incubation times (148,188,202). The results demonstrated that nanoparticle uptake in spheroids was influenced by GNP coating type, dose, exposure time and the interaction of these variables. Curc-GNP uptake was generally greater than Cit-GNP uptake, with the strongest uptake observed for 100 μg/mL Curc-GNPs at 24 hours. At this concentration and time point Curc-GNP uptake was 4.76-fold higher than Cit-GNP uptake, suggesting that functionalizing curcumin onto GNPs improved nanoparticle internalization in DU145 spheroids (188,202).

Clonogenic assay was used to evaluate the radiosensitizing potential of Curc-GNPs after exposure to clinically relevant 6 MV photon radiation doses of 0, 2, 4, and 6 Gy (33,137,188). Linear-quadratic model fitting demonstrated concentration-dependent radiosensitization, where with increasing Curc-GNP concentration, a progressive downward shift in survival was observed. This was supported by the increased α values, decreased β values, reduced D_{50} values, increased sensitization enhancement ratios, and elevated α/β ratios (206-207). The D_{50} decreased from 2.012 Gy in untreated controls to 1.295 Gy at 200 μg/mL Curc-GNPs, while the sensitization enhancement ratio (SER) increased from 1.000 to 1.554. These results suggest that Curc-GNPs were able to enhance radiation-induced cell killing through single-track DNA damage in DU145 spheroids, where the greatest radiosensitizing effect was seen at the highest concentration investigated 200 μg/mL (137,158,188).

This thesis demonstrates the successful synthesis and characterization of Cit-GNPs and Curc-GNPs and supports the potential of Curc-GNPs as radiosensitizers for prostate cancer therapy. The findings show that curcumin functionalization improved GNP uptake in DU145 spheroids and enhanced radiation-induced cell death with increasing concentration. These results provide an important foundation for the development and optimization of Curc-GNPs as radiosensitizers, where future studies should investigate nanoparticle localization within tumour spheroids, confirm the biological mechanisms of radiosensitization, and optimize Curc-GNP formulations so they have improved uptake, stability, and localization in prostate cancer models (148,158,188). Overall, this work supports the continued development of Curc-GNPs as a promising radiosensitizers in prostate cancer.

Acknowledgements

I sincerely acknowledge the University of Waterloo School of Pharmacy community for supporting me throughout my thesis project. I am fortunate to have been supported by a wide-reaching network of people, without whom this research would not have been possible.

I am immensely grateful to my supervisors, Dr. Ernest Osei and Dr. Shawn Wettig, for their belief and trust in me. Dr. Osei, thank you for taking a chance on me in 2022 as an undergraduate student. I am forever grateful for the opportunities you have entrusted me with, and I have learned so much from you as both a mentor and supervisor. In particular, you taught me that "if at first the idea is not absurd, then there is no hope for it." I am truly grateful for your support throughout this journey. You have shown me that sometimes a leap of faith, combined with hard work, is exactly what is needed to accomplish something meaningful. Dr. Wettig, thank you for your unwavering support and guidance. Without you, this project would not have been possible. You have been an exceptional mentor and supervisor, providing me with an invaluable window into the world of pharmaceutical science. I am incredibly grateful for your thoughtful support, guidance, and mentorship throughout this project, and for your reassurance and trust along the way. I could not have asked for a better team of supervisors.

I am deeply grateful to my MSc committee members, Dr. Tom McFarlane, Dr. Roderick Slavcev, and the late Dr. Kostadinka Bizheva, for their valuable and diverse expertise, thoughtful encouragement, and guidance. Dida, thank you for serving as a member of my thesis committee during the early stages of this work. Your guidance, expertise, encouragement, and feedback helped shape the direction of this thesis and my growth as a researcher. I will remember your support with deep appreciation and gratitude.

Beyond my MSc committee, I was incredibly privileged to be surrounded and supported by highly qualified and kind individuals. Dr. Mohammed Kohandel and his research group, thank you for graciously sharing your laboratory space with me at the start of my research and for giving me a place to grow and store my cells. Ron Snelgrove and the WHRN Cancer Centre staff, thank you for accommodating my work and trusting me with the equipment necessary for my studies. Dr. Faten Salim and the Chemical Engineering Analytical Laboratory, thank you for taking the time to teach me how to use the ICP-OES and for answering my many questions. Dr. Mohamed Aborig, thank you for patiently and graciously teaching me how to synthesize and characterize GNPs, and for your support, guidance, and valuable insight throughout this project.

I am also fortunate to have worked alongside many generous, brilliant, and hardworking people. Steph Swanson, thank you for taking me under your wing and for being an exceptional mentor. I am forever grateful for your patience, guidance, support, and trust. You taught me how to be a researcher, and without you, I would not have developed the healthy dose of skepticism, confidence, and love for spreadsheets that I was missing. You have truly helped me become a better person and researcher. Nicole MacNeil, thank you for welcoming me so warmly into the Wettig research group, for teaching me new skills, holding me accountable and for being an invaluable friend. Mohamed El-Rayani, thank you for being a sounding board for my ideas and a source of emotional support through the trenches of lab work. From working late in the BSC to irradiating cells at WHRN, this research would not have made it out of our office without you. I have also had the pleasure of helping supervise Nikita Ramchandani. Thank you for inspiring me to strive to be a better mentor and person.

Finally, to the people in my personal life who have undoubtedly influenced my professional trajectory. To my friends Jovana Haag, Tina Nguyen, and Olympia To, thank you for being my cheerleaders, for sticking with me despite the distance, and for reminding me what is important in life. Thank you for the laughter and respite. Manrohit Uppal, you have supported me through thick and thin, through every crisis and every moment of doubt. Thank you for pushing me to become a better person and to build a life I never thought was possible. To my family, thank you for your unwavering support, which has carried me through this journey.

Dedication

To my father, Uditha Sumithrarachchige, whose curiosity and dedication to learning inspired me to pursue graduate studies. To my mother, Nayana, whose love and support have carried me through every moment. To my siblings, Hiru and Samadi, thank you for always supporting me and for showing me what balance and hard work look like. This achievement belongs to all of you as much as it does to me, and it truly would not have been possible without you.

To the late Pathaka Jayatilaka Aunty, you are my first role model and mentor, even from a young age you taught me how important hard work, kindness and faith are. Thank you for instilling these qualities in me. I hope to become even half as great a person as you were. This work is for you.

Table of Contents

Author's Declaration ii

Abstract iii

Acknowledgements v

Dedication vii

List of Figures xii

List of Tables xiii

List of Abbreviations xiv

List of Symbols xviii

Chapter 1 : Introduction 1

1.1 The Prostate and Prostate Cancer 1

1.1.1 Diagnosis of Prostate Cancer 1

1.1.2 Types of Prostate Cancer 4

1.1.3 Stages of Prostate Cancer 5

1.2 Current Prostate Cancer Treatment Modalities 7

1.2.1 Radiation Therapy 7

1.2.2 Types of Radiation Therapy 8

1.2.3 Chemotherapy 10

1.2.4 Hormone Therapy 10

1.2.5 Surgery 11

1.3 Cell Culture 12

1.3.1 2D and 3D Cell Culture in prostate cancer research 13

1.4 Prostate Cancer Resistance and Recurrence 14

1.4.1 Radiotherapy Resistance in Castration-Resistant Prostate Cancer 15

1.5 Novel approaches to improve the treatment efficacy of Prostate Cancer 17
1.5.1 Radiosensitizers 17
1.5.2 Drug Repurposing 19
1.6 Novel Therapeutics for Prostate Cancer 22
1.6.1 Nutraceuticals 22
1.6.2 Gold nanoparticles 24
1.6.3 High Atomic Number 25
1.6.4 Ease of Synthesis and Functionalization of GNPs 25
1.6.5 Mechanistic Approach 28
1.6.6 Uptake of GNPs in Cells 29
1.7 GNPs in Radiation Therapy 34
1.7.1 Mechanisms of Radiosensitization 35
1.7.2 Physical Process 35
1.7.3 Chemical Processes 36
1.7.4 Biological Processes 37
1.8 Research Gap and Rational 39
1.9 Aim and Objectives of Research Undertaken 42
1.9.1 Hypothesis: 42
1.9.2 Objective 1.1 (Synthesis & Characterization): 42
1.9.3 Objective 1.2 (Cellular Uptake & Cytotoxicity in 3D Models): 43
1.9.4 Objective 1.3 (Radiosensitization Efficacy in 3D Spheroids): 43
1.9.5 Thesis Structure: 43
Chapter 2 : Synthesis and Characterization of Gold Nanoparticles 44
2.1 Introduction 44

2.2 Materials....46
2.3 Synthesis....47
2.3.1 Citrate-coated Gold Nanoparticles....47
2.3.2 Curcumin-coated Gold Nanoparticles....47
2.4 Characterization....48
2.4.1 UV-Vis Spectroscopy....48
2.4.2 DLS....48
2.4.3 ICP-OES....49
2.5 Results and Discussion....50
2.5.1 UV-Vis Spectroscopy....50
2.5.2 DLS....52
2.5.3 ICP-OES....58
2.6 Conclusion....59
References:....61
Chapter 3 : In Vitro Study of Gold Nanoparticles in Prostate Cancer Spheroids....65
3.1 Introduction....65
3.2 Materials....68
3.3 Methods....69
3.3.1 Spheroid Culture....69
3.3.2 GNP Treatment....70
3.3.3 Radiation Treatment....71
3.3.4 Disaggregating Spheroids....72
3.3.5 Clonogenic Assay....72
3.3.6 ICP-OES Cellular Uptake....77

3.4 Results and Discussion 79
3.4.1 ICP-OES Cellular Uptake 79
3.4.2 Clonogenic Assay 89
3.5 Conclusion: 100
References 101
Chapter 4 : Conclusions and Future Directions 106
4.1 Conclusions 106
4.2 Challenges and Future Directions 107
4.2.1 Improving Nanoparticle Penetration and Uptake in 3D Spheroids 108
4.2.2 Linking GNP Uptake to Radiosensitization 109
4.2.3 Investigating the Mechanisms of Curc-GNP-Mediated Radiosensitization 110
4.2.4 Future In Vitro Evaluation of Curc-GNPs 111
4.2.5 Future In Vivo Evaluation of Curc-GNPs 113
References: 115

List of Figures

Figure 1.1: Schematic illustration of gold nanoparticles synthesis by Turkevich method 26

Figure 1.2: Influence of cell size on cellular uptake of GNPs. 31

Figure 2.1: UV-Vis Spectra of Citrate- and Curcumin- GNPs 52

Figure 2.2: DLS Sizes and Apparent Zeta Potentials of Curc- and Cit-GNPs 54

Figure 3.1: Process of seeding spheroids in gels. 70

Figure 3.2: GNP treatment of spheroids and preparation for radiation. 71

Figure 3.3: Gold nanoparticle uptake in DU145 spheroids following treatment with citrate-coated and curcumin-coated GNPs. 81

Figure 3.4: Survival Curves of DU145 Spheroids exposed to Curc-GNPs and radiation. 91

List of Tables

Table 1.1: Prostate Cancer Tumour Staging 6

Table 2.1: DLS Parameters for GNPs 54

Table 2.2: ICP-OES Parameters for Curc-GNPs 59

Table 2.3:ICP-OES Parameters for Cit-GNPs 59

Table 3.1: Aligned rank transform ANOVA summary for the effects of coating type, dose, and incubation time on gold nanoparticle uptake in DU145 spheroids. 82

Table 3.2: Post hoc comparisons of Curc-GNP and Cit-GNP uptake in DU145 spheroids across dose and incubation time. 82

Table 3.3: Curc-GNP radiosensitization parameters derived from linear-quadratic model fitting. 90

List of Abbreviations

2D — Two-dimensional

3D — Three-dimensional

3DCRT — Three-dimensional conformal radiotherapy

ADT — Androgen deprivation therapy

ANOVA — Analysis of variance

AR — Androgen receptor

ART — Aligned rank transform

ATM — Ataxia telangiectasia mutated

ATR — Ataxia telangiectasia and Rad3-related

Au — Gold

Chk1/2 — Checkpoint kinases 1 and 2

Cit-GNPs — Citrate-coated gold nanoparticles

CRPC — Castration-resistant prostate cancer

CSC — Cancer stem cell

CT — Computed tomography

Curc-GNPs — Curcumin-coated gold nanoparticles

DAC — Ductal adenocarcinoma

DDR — DNA damage repair

DF — Dilution factor

DHT — Dihydrotestosterone

DLS — Dynamic light scattering

DNA — Deoxyribonucleic acid
DNA-PKcs — DNA-dependent protein kinase catalytic subunit

DRE — Digital rectal examination

DSB — Double-strand break

EBRT — External beam radiation therapy

ECM — Extracellular matrix

EGCG — Epigallocatechin gallate

EMT — Epithelial–mesenchymal transition

FBS — Fetal bovine serum

FDA — Food and Drug Administration

FSH — Follicle-stimulating hormone

G_0 — Resting phase of the cell cycle

G_1 — Gap 1 phase of the cell cycle

G_2 — Gap 2 phase of the cell cycle

GNPs — Gold nanoparticles

GnRH — Gonadotropin-releasing hormone

HIF-1α — Hypoxia-inducible factor 1-alpha

HR — Homologous recombination

Hsp90 — Heat shock protein 90

ICP-OES — Inductively coupled plasma optical emission spectroscopy

IGRT — Image-guided radiotherapy

IMRT — Intensity-modulated radiation therapy

LINAC — Linear accelerator

LH — Luteinizing hormone

LOQ — Limit of quantitation

LQ — Linear-quadratic

M — Mitotic phase of the cell cycle

mCRPC — Metastatic castration-resistant prostate cancer

MDL — Method detection limit

mpMRI — Multiparametric magnetic resonance imaging

MRI — Magnetic resonance imaging

NF-κB — Nuclear factor kappa-light-chain-enhancer of activated B cells

NHEJ — Non-homologous end joining

Nrf2 — Nuclear factor erythroid 2-related factor 2

PARP — Poly(ADP-ribose) polymerase

PBS — Phosphate-buffered saline

PCa — Prostate cancer

PCA3 — Prostate cancer antigen 3

PDI — Polydispersity index

PE — Plating efficiency

PEG — Polyethylene glycol

PEG-GNPs — Polyethylene glycol-coated gold nanoparticles

PHI — Prostate Health Index

PI3K — Phosphoinositide 3-kinase

PMMA — Polymethyl methacrylate

PSA — Prostate-specific antigen

PSMA — Prostate-specific membrane antigen

RNA — Ribonucleic Acid

ROS — Reactive oxygen species

RPMI — Roswell Park Memorial Institute medium

S — Synthesis phase of the cell cycle

SBRT — Stereotactic body radiation therapy

SCC — Squamous cell carcinoma

SER — Sensitization enhancement ratio

SF — Surviving fraction

SIRT6 — Sirtuin 6

SPR — Surface plasmon resonance

TCC — Transitional cell carcinoma

TEM — Transmission electron microscopy

TERT — Telomerase reverse transcriptase

TME — Tumour microenvironment

TNM — Tumour, Node, Metastasis

UV-Vis — Ultraviolet-visible spectroscopy

WRHN — Waterloo Regional Health Network

XTT — 2,3-bis-(2-methoxy-4-nitro-5-sulphophenyl)-2H-tetrazolium-5-carboxanilide

List of Symbols

α — Linear component of cell killing in the linear-quadratic model

β — Quadratic component of cell killing in the linear-quadratic model

α/β — Ratio describing the relative contribution of linear and quadratic radiation damage

D — Radiation dose

D_{50} — Radiation dose required to reduce cell survival to 50%

Gy — Gray; unit of absorbed radiation dose

SER — Sensitization enhancement ratio

SF — Surviving fraction

PE — Plating efficiency

$R\cdot$ — Free radical

$RO_2\cdot$ — Peroxyl radical

ROOH — Organic hydroperoxide

Z — Atomic number

°C — Degrees Celsius

% — Percent

nm — Nanometre

mV — Millivolt

mL — Millilitre

µL — Microlitre

µg/mL — Micrograms per millilitre

mg/L — Milligrams per litre

pg/cell — Picograms per cell

h — Hours

CO_2 — Carbon dioxide

Au — Gold

^{197}Au — Gold isotope measured during ICP-OES analysis

^{89}Y — Yttrium internal standard used during ICP-OES analysis

^{55}Mn — Manganese solution used for ICP-OES peaking

$HAuCl_4$ — Chloroauric acid

$HAuCl_4 \cdot 3H_2O$ — Chloroauric acid trihydrate

$Na_3C_6H_5O_7 \cdot 2H_2O$ — Sodium citrate dihydrate

HNO_3 — Nitric acid

HCl — Hydrochloric acid

Chapter 1: Introduction

1.1 The Prostate and Prostate Cancer

Prostate cancer is the most prevalent cancer among Canadian men, with 1 in 34 men expected to die from the disease in 2025 (1). Prostate cancer is a malignant cancer that forms from epithelial cells of the prostate gland (2). Cancer often arises due to dysregulated molecular signaling pathways and disrupted metabolic functions, which as a result, disrupts regulated cell growth (3). The prostate also produces PSA or prostate-specific antigen (4). PSA is a kallikrein-related serine protease widely used as a biomarker for prostate cancer detection and disease monitoring.

The prostate is an accessory gland of the male reproductive system located inferior to the bladder and anterior to the rectum. Its primary physiological role is the secretion of proteins, enzymes, and ions that contribute to seminal fluid and sperm viability (5). The prostate has three anatomical zones: peripheral, central, and transition. The transition zone surrounds the proximal urethra and is the region which grows with age (6). The transition zone accounts for 10-20% of the mass and origination of cancers. The central zone surrounds the ejaculatory ducts and is located posterior to the transition zone; it also accounts for 75% of prostate cancers (6). The peripheral zone surrounds the central zone and the distal prostatic urethra (6).

1.1.1 Diagnosis of Prostate Cancer

If a patient is suspected of having prostate cancer, the treatment protocol typically follows a diagnostic and evaluation process before any treatment begins. A diagnosis for prostate cancer begins with a serum prostate-specific antigen (PSA) test and/or a digital rectal examination (DRE). PSA is a prostate-derived serine protease that can be elevated in prostate cancer; however, PSA is not cancer-specific and may also increase due to benign prostatic hyperplasia, prostatitis, urinary tract manipulation, or increasing prostate volume. As a result, PSA testing is useful as an initial screening

tool but has limited specificity when used alone, which may contribute to unnecessary biopsies and overdiagnosis of clinically insignificant disease (7,8).

Following a high PSA test result and a suspicious DRE examination, additional tool may be used to determine the risk of prostate cancer before proceeding to a biopsy. This can include multiparametric magnetic resonance imaging (mpMRI), PSA kinetics, PSA density, the 4Kscore, Prostate Health Index (PHI), and prostate cancer antigen 3 (PCA3) score. These approaches differ from initial PSA-based screening because they are generally used as secondary risk-stratification tools rather than broad first-line screening tests. Their purpose is to improve the distinction between benign prostate conditions, low-risk prostate cancer, and clinically significant disease that is more likely to require biopsy or treatment (7,8). mpMRI combines anatomical and functional imaging sequences to identify suspicious regions within the prostate and can help guide targeted biopsy. PSA kinetics refers to changes in PSA over time, including PSA velocity and PSA doubling time, which can provide additional information about disease behaviours. PSA density adjusts the PSA value for prostate volume and is calculated by dividing serum PSA by prostate volume, helping account for PSA elevation caused by benign prostate enlargement. Blood-based biomarker tests such as the 4Kscore and PHI combine different PSA-related or kallikrein-related measurements to improve prediction of clinically significant prostate cancer compared with total PSA alone. In contrast, PCA3 is a urine-based molecular test that measures prostate cancer antigen 3 RNA, which is overexpressed in prostate cancer tissue and may assist in biopsy decision-making, particularly when PSA results are unclear (7–9).

Histopathology of prostate biopsy tissue is used to determine a definitive diagnosis of cancer. Tumour aggressiveness is described using the Gleason grading system, where each cancer is given a Gleason score based on the histopathology of prostate cancer cells. A higher Gleason score indicates

poorer differentiation and is associated with more aggressive tumour behaviour. The Gleason system is also now reported alongside Grade Groups which provide a simple prognostic scale for Grade Group 1 to Grade Group 5, where Grade Group 1 corresponds to Gleason score ≤6, while Grade Group 5 corresponds to Gleason scores 9 to 10 (10).

Below is a simplified overview adapted from Mason RJ, et al. Can Urol Assoc J 2022;6:E184-96, and Canadian Cancer Society 2026, National Cancer Institute 2024:

A. Initial Screening: For men electing to undergo PSA screening, initiate PSA testing at age 50 in most men and at age 45 in men at increased risk of prostate cancer
    a. For men with PSA <1 ng/ml, repeat PSA testing every four years
    b. For men with PSA 1–3 ng/ml, repeat PSA testing every two years
    c. For men with PSA >3 ng/ml, consider more frequent PSA testing intervals or adjunctive testing strategies (mpMRI, PSA kinetics, PSA density, 4Kscore, Prostate Health Index, and prostate cancer antigen 3 score)
B. Diagnostic Confirmation: A biopsy is often the next step to confirm the presence of cancer in the prostate. Imaging such as, MRI, CT scans, or bone scans may be used to assess the extent of the disease and the spread of cancer to areas outside of the prostate.
C. Risk Assessment: Once diagnosed, the cancer is staged using the TNM staging system (Tumor, Node, Metastasis) and graded based on the Gleason score. These evaluations help in determining the aggressiveness of the cancer and inform the treatment plan.
D. Treatment Decision: Based on the stage and grade of the cancer, overall health, and patient preferences, a treatment plan is developed. For low-risk, localized cancer, options may include active surveillance, surgery or radiation therapy. For higher risk localized cancer, a combination of radiation therapy and prostatectomy may be recommended.

E. Advanced Disease: If cancer is advanced, has metastasized or is treatment resistant, the protocol typically involves systemic therapies such as hormone therapy, chemotherapy, immunotherapy, or newer targeted therapies such as radioligand therapy, or poly(ADP-ribose) polymerase (PARP)- inhibitors.

F. Follow-Up: Regular follow-up is crucial to monitor the effectiveness of the treatment, manage side effects, quality of life, and detect any signs of recurrence or secondary cancers.

1.1.2 Types of Prostate Cancer

There are four types of prostate cancer: adenocarcinoma, transitional cell carcinoma, squamous cell carcinoma, and small cell prostate cancer. Adenocarcinoma is the most common type of prostate cancer and is further divided into two types, acinar and ductal adenocarcinoma (DAC) (11). Acinar adenocarcinoma is an epithelial-derived neoplasm of the prostate (12). Most adenocarcinomas are acinar (90%), and the remaining 10% are ductal carcinomas. Prostate adenocarcinoma cells have hyperchromatic, enlarged nuclei with prominent nucleoli and abundant cytoplasm (13). DAC arises from periurethral prostatic ducts and is found in association with acinar adenocarcinomas (14). DAC are composed of columnar cells that are arranged in two distinct patterns: papillary or cribriform pattern. This pattern is what differentiates acinar from DAC because acinar are cuboidal cells arranged in acini. Transitional cell carcinoma also known as urothelial cancer, is a rare type of prostate cancer that originates in the periurethral and prostatic ducts where the cells change from columnar to transitional (15). There are two ways urothelial cancer can spread to the prostate: the tumour cells infiltrate the lining of the epithelium and basal cells, or the tumour cells become intercalated with normal epithelial cells. Another origin of transitional cell carcinoma is from upper tract transitional cell carcinoma, which is a type of bladder cancer (15). Squamous cell carcinoma (SCC) is another rare form of prostate cancer that accounts for less than 1% of all cases

worldwide. Diagnosis of SCC of the prostate includes: 1. a malignant neoplasm, disordered growth, and cellular anaplasia; 2. definite keratinization, squamous pearls and intercellular bridges; 3. lack of glandular or acinar pattern; 4. absence of SCC in the bladder (16). Using these criteria, SCC can be differentiated from other similar tumours such as transitional cell carcinoma and adenocarcinomas. Small cell carcinomas are a rare subtype of prostate cancer that occurs in patients with a history of prostatic adenocarcinomas. This type of prostate cancer is classified as a neuroendocrine cancer because it grows more quickly than other types of prostate cancers, and it does not respond to androgen deprivation therapy. The progression of small cell carcinoma is also not associated with elevated serum PSA levels unlike the other subtypes of prostate cancers (17).

1.1.3 Stages of Prostate Cancer

Prostate cancer like all other cancers can be graded and staged based on the extent of cancer using the TNM staging system (18). Cancer staging often informs the type of treatment plan a patient receives. The figure below details the various prostate cancer stages and their key characteristics.

T	Description
T0	There is no evidence of a primary tumour.
T1	The tumour can't be felt during a DRE or seen with an imaging test. It may be found by chance during a biopsy or during surgery for another health issue related to the prostate or bladder.
T1a	Cancer is found in 5% or less of the removed tissue.
T1b	Cancer is found in more than 5% of the removed tissue.
T1c	The tumour is found by needle biopsy in one or both sides of the prostate.
T2	The tumour can be felt by your doctor during a DRE and can be seen on an imaging test. Cancer is only in the prostate.
T2a	The tumour is in one half or less of one side of the prostate.
T2b	The tumour is in one half or more of one side of the prostate.

T2c	The tumour is in both sides of the prostate.
T3	The tumour has broken through the outside layer of the prostate gland.
T3a	The tumour has grown outside the prostate but not into the seminal vesicles.
T3b	The tumour has grown outside the prostate and into the seminal vesicles
T4	The tumour has grown outside the prostate and into nearby structures such as the bladder, rectum, pelvic muscles and pelvic wall.

Table 1.1: Prostate Cancer Tumour Staging

For patients diagnosed with stage IV prostate cancer the five-year net survival in men aged 50–74 was 56.6% from 2016–2017, while net survival was 29.2% among older men. For patients with stage I-III prostate cancer the net survival was close to 100% for both age groups (18, 19).

Prostate cancer growth is strongly influenced by androgens, particularly testosterone and its more potent derivative, dihydrotestosterone (DHT) (20-23). In prostate cells, testosterone can be converted to DHT, which binds to androgen receptors and activates signaling pathways that promote prostate cancer cell survival, proliferation, and disease progression. Because of this dependence, many prostate cancer treatments aim to reduce testosterone levels or block androgen receptor signaling (22-23). However, the late stages of prostate cancer can advance to castration-resistant prostate cancer (CRPC) and metastatic CRPC (mCRPC). CRPC, also known as hormone-refractory prostate cancer, is a type of prostate cancer that continues to grow despite very low levels of circulating testosterone (24). This does not necessarily mean that the cancer is completely independent of testosterone, but rather that it can continue progressing under low-androgen conditions through mechanisms such as persistent androgen receptor signaling, increased androgen receptor sensitivity, or alternative growth pathways. mCRPC is an advanced form of CRPC in which the cancer has metastasized and spread beyond the prostate to other organs or tissues. At this stage, standard hormone therapy becomes less effective, allowing the disease to progress despite continued androgen deprivation (25).

1.2 Current Prostate Cancer Treatment Modalities

Radiation therapy and surgery are the primary treatments for prostate cancer when it is localised. However, if the cancer has metastasized, chemotherapy or hormone therapy, like androgen deprivation therapy (ADT), may be used (26,27).

1.2.1 Radiation Therapy

Radiation therapy can decrease cancer cell growth by forming ions and depositing energy into cells as it passes through, this can kill cancer cells by generating reactive oxygen species (ROS) which cause genetic changes like, double-strand breaks or base damage in the DNA (28,29). This occurs due to a mechanism known as the 'oxygen-fixation hypothesis (30). When radiation reacts with biological material free radicals (R·) are generated through water ionization (30). The free radicals then break chemical bonds and initiate a domino effect that results in biological damage either directly on DNA or other molecules. Oxygen fixation occurs when free radicals react with oxygen to produce $RO_2\cdot$, forming ROOH. ROOH can change the chemical composition of a target molecule and as a result, the damage is chemically fixed. Radiation therapy, like chemotherapy, can also harm healthy tissue cells, so when prescribing the treatment a balance between the complication rate and the tumour control rate must be achieved (31).

The hallmarks of radiobiology also known as the 6R's are used to determine the outcome of radiation therapy in practice. The 6R's are radiosensitivity, repair, redistribution, repopulation, reoxygenation, and reactivation of the immune response (31).

Radiosensitivity refers to the intrinsic radioresistance of healthy tissue cells and the acquired radioresistance of tumour cells to radiation. Repair refers to the high repair capacity of DNA damage for healthy tissues, and the low repair capacity for tumours (31). Redistribution refers to the variation of the radioresistant cell-cycle phase to the radiosensitive cell-cycle phase and vice versa after

irradiation. Repopulation refers to the growth and recovery of healthy cells after irradiation (31). Reoxygenation refers to when hypoxic tumour cells are radiosensitized when reoxygenated because of an irradiation course. Finally, reactivation of the immune response occurs when local irradiation can activate the systemic immune system to attack distant tumour niches outside of the irradiated area (31).

Radiation therapy can be prescribed as an effective palliative care, with the intent to cure and in combination with other treatment modalities like surgery, chemotherapy or immunotherapy. Radiation treatment administered before surgery, also known as neoadjuvant therapy, aims to shrink the tumour, while if used after surgery, also known as adjuvant therapy, seeks to destroy leftover microscopic tumour cells (28).

1.2.2 Types of Radiation Therapy

The two main radiation therapy delivery methods are external beam radiation therapy (EBRT) and internal radiation therapy, also known as brachytherapy.

1.2.2.1 A. External Beam Radiation Therapy

EBRT aims high-energy rays such as photons, protons or particle radiation from outside the body to the tumour's location, clinically this approach is the most common (28,32).

EBRT is often administered in a fractionated regime; given Monday to Friday, or occasionally twice daily or once weekly. A typical curative treatment regimen delivers a total dose ranging from 40 to 80 Gy given over 3 to 8 weeks. The fractionation schedule is based on the unique radiobiological properties of the cancer and healthy tissues, to amplify the survival of healthy tissue and death of cancer tissue. This is possible because compared to cancer cells, healthy cells proliferate more slowly and as a result, have time to repair DNA damage caused by radiation before replicating

(24). Current fractionation regimens are based on the linear-quadratic formula which models cancer cell survival depending on different delivered doses of radiation (29,33).

There are several EBRT techniques that incorporate advanced imaging techniques, machinery and software to deliver more dose to the tumour while sparing the surrounding healthy tissue. 3D Conformal radiotherapy (3DCRT) uses CT imaging to accurately localize the tumour and critical organ structures so the beam can be placed optimally (28). Intensity modulated radiation therapy (IMRT) uses inverse planning software and computer-controlled intensity modulation of multiple radiation beams during treatment to create irregular-shaped radiation fields that conform dose to the tumour while avoiding critical organs (28). IMRT has become common practice clinically for several tumour sites, including prostate, using linear accelerators with static or dynamic multi-leaf collimators or tomotherapy machines (34). Stereotactic body radiation therapy (SBRT) is a technique that delivers high individual doses of radiation over fewer fractions to precisely ablate small primary and oligometastatic tumours in the body. This technique has shown effectiveness for prostate cancer patients (35).

An innovation in EBRT treatment is a hypofractionation regimen. During the COVID-19 pandemic (and prior to the pandemic) trials have showcased that the total prescribed dose can be safely given in fewer fractions while achieving similar response rates. This innovation has improved resource use and has been vital in decreasing the frequency of visits to cancer centres. For example, the treatment of prostate cancer can be decreased from 7 or 8 weeks to 4 weeks (36).

1.2.2.2 B. Internal Radiation Therapy (Brachytherapy)

Internal radiation or brachytherapy is delivered from inside the body using radioactive sources. These sources are often sealed in catheters or seeds directly into the tumor site. This

modality of treatment is used in the routine treatment of prostate malignancies as well as in situations where retreatment is indicated, based on its short-range effects (28,32).

1.2.3 Chemotherapy

Chemotherapy is a combination of drugs that target cancer cells in your body and destroy those cells. Chemotherapy is currently used in three ways: primary, neoadjuvant, and adjuvant treatment (37). Primary treatment is when chemotherapy is admitted as the primary treatment method in patients. This is the main approach for treating metastatic tumours and the overall goal of primary treatment is to relieve the tumour-related symptoms, improve quality of life and prolong time to tumour progression. This type of treatment is common when treating solid tumours (37). Neoadjuvant chemotherapy is used in patients who have a localized tumour, and where surgery is an option, but it is less effective. The overall goal of neoadjuvant chemotherapy is to reduce the size of the tumour so that surgery can be done to remove the tumour completely. Adjuvant chemotherapy is used after surgical resection, and the overall goal of this is to reduce the incidence of recurrence of the tumour. This also helps increase the quality of life for patients as well as the overall survival rate (37). The current chemotherapy agents used for treating prostate cancer are docetaxel and cabazitaxel, these work by promoting tubulin polymerization with a broad-spectrum antitumor activity (38,39).

1.2.4 Hormone Therapy

In addition to traditional treatment methods, hormone therapies are commonly used to treat prostate cancer patients. For prostate cancer, hormone therapy also known as ADT is used to block testosterone, this hormone fuels the growth of prostate cancer (40). Hormone therapy is a common treatment method for mCRPC because it decreases the amount of testosterone in the body, limiting the growth of the tumour. There are currently five classes of approved therapeutic agents for prostate cancer: nonsteroidal androgen receptor antagonists (first generation), nonsteroidal androgen receptor

antagonists (second generation), which are used to treat CRPC, androgen biosynthesis inhibitors, which are used to treat mCRPC, growth hormone-releasing hormone (GnRH) antagonists, which are used to treat advanced prostate cancer and GnRH agonists, which are used to treat mCRPC (40). The target and mechanism for these agents are similar, such as both first and second-generation non-steroidal androgen receptor antagonists target androgen receptors. The mechanism in which they do so is by competitive and reversible inhibition by binding of testosterone and dihydrotestosterone (DHT) to the ligand binding domain (40).

First-generation nonsteroidal antiandrogens include bicalutamide, flutamide, and nilutamide, whereas second-generation androgen receptor inhibitors include apalutamide, darolutamide, and enzalutamide. Androgen biosynthesis inhibitors, such as abiraterone, act by targeting steroidogenic enzymes involved in androgen production. GnRH-based therapies represent another important approach to androgen deprivation therapy and include both GnRH antagonists and agonists. Although both classes target GnRH receptors, they differ in their mechanisms of action. GnRH antagonists, including degarelix and relugolix, competitively and reversibly inhibit GnRH receptors, preventing the release of follicle-stimulating hormone (FSH) and luteinizing hormone (LH) (40). Conversely, GnRH agonists, such as histrelin, goserelin, and leuprolide, continuously stimulate GnRH receptors, causing an initial surge in FSH, LH, testosterone, and dihydrotestosterone (DHT), followed by receptor desensitization and reduced androgen production (40).

1.2.5 Surgery

Surgery remains a definitive treatment option for patients with clinically localized prostate cancer who are in good general health. The primary surgical approach is radical prostatectomy, which involves complete removal of the prostate gland along with the seminal vesicles and surrounding

periprostatic tissue. In selected cases, a pelvic lymph node dissection is performed concurrently for pathological staging (41).

1.3 Cell Culture

Our current understanding of cancer growth and its response to treatment is founded on 2D monolayer cell culture, where cells are grown in single layers in plastic or glass Petri dishes. However, the environment in which cancer develops in the body differs greatly from the environment of cells grown in 2D *in vitro* culture (42). This is because adherent cells grown in 2D have a flattened morphology and minimal cell-to-cell and cell-to-extracellular matrix (ECM) interactions, which can result in different biochemical signaling, cytoskeleton remodeling, proliferation and cell death in comparison to *in vivo* and 3D cell culture phenotypes (42).

A new advancement in cell culture has resulted in 3D cell culture, which aims to bridge the gap between 2D *in vitro* and *in vivo* studies by generating spheroids or organoids using adherent cell lines or patient-derived cells (43). Spheroids are classified as 3D cell cultures that can involve one or more cell lines including patient-derived cells or tissues. They are made up of layers of heterogeneous cells that can be identified as proliferating, quiescent and necrotic and resemble 3D cellular organisation (43,44). Spheroids assume 3D organisation via self-assembly involving cell-to-cell aggregation and adhesion. Organoids on the other hand are created from embryonic stem cells, adult stem cells or induced pluripotent cells and often patient-derived tissues (45). They require an extracellular matrix and a cocktail of growth factors to form 3D structures where different cell lineages that reflect the structure and function of the organ can be identified (45). 3D cell culture can replicate the tumour microenvironment (TME) seen *in vivo*, by restoring cell-to-cell, cell-to-ECM interactions, heterogeneous cell populations and the transport gradient of oxygen, nutrients and cellular waste (43).

1.3.1 2D and 3D Cell Culture in prostate cancer research

Cell culture makes up the foundation of prostate cancer research. Three human prostate cancer cell lines, DU145, PC-3 and LNCaP, are commonly used to study prostate cancer biology, identify therapeutic targets, and perform drug testing involving prostate cancer at the cellular level (46,47). All three cell lines have been immortalized but they have different sources. PC-3 cell lines are androgen-insensitive and originated from a bone metastasis of prostatic adenocarcinoma. LNCaP is an androgen-sensitive cell line originating from lymph node metastasis of prostatic adenocarcinoma (48). The DU145 cell line is also androgen insensitive but originated from a central nervous system metastasis. DU145 cells are cited as a model cell line that can be used to better understand late-stage prostate cancer and metastasis, study androgen deprivation therapy resistance in prostate cancer, assess the efficacy of anti-tumor drugs and targeted therapy and develop better models of castration-resistant prostate cancer mechanistically at gene and protein level (47). These human prostate cancer cell lines have been used in several culture techniques including monolayer and spheroid to understand prostate cancer (49–51).

Li et al., conducted a study to investigate the role of sodium bicarbonate transporters in prostate cancer cell proliferation and viability (49). They achieved this by culturing LNCaP, PC-3 and DU145 prostate cancer cells in monolayer in hypoxic and normoxic conditions, then measuring the expression levels of sodium bicarbonate transporter 1, the pH and cell proliferation and death. They found that the sodium bicarbonate transporter 1 had an important role in acid extrusion in prostate cancer cells and affected cell proliferation and viability.

Alimirah et al., conducted a study to investigate if the DU145 and PC-3 human prostate cancer cell lines expressed androgen receptors and what implications that may have (50). They achieved this by culturing DU145 and PC-3 in monolayer, then they conducted a variety of assays to

determine the expression of androgen receptor RNA in the cells. They found that DU145 and PC-3 human prostate cancer cell lines expressed androgen receptors and can result in inhibition of cell growth.

Bromma et al., conducted a study to investigate the effects of combining gold nanoparticles and docetaxel with radiation therapy in monolayer and spheroid LNCap cell cultures (51). They achieved this by exposing cells to gold nanoparticles at 10 μg/mL and docetaxel at a dose that inhibited growth by 50%, then the cells were treated with radiation 24 hours after at 2, 5 or 10 Gy using a 6 MV beam. The researcher found that samples that received gold nanoparticles and docetaxel with 5 and 10 Gy had decreased survival and increased double-strand DNA breaks. This effect was also seen in the spheroid samples through reduced spheroid volume measurements.

Overall, much research has been completed using prostate cancer cell lines and both 2D and 3D cell culture techniques. *In vitro,* these techniques provide a foundational model needed to understand the cellular process of prostate cancer and justify the investigation of therapeutics using *in vivo* or clinical trials.

1.4 Prostate Cancer Resistance and Recurrence

Despite advancements in treatment delivery methods and techniques, prostate cancer can become tolerant or resistant to conventional treatment options like chemotherapy, radiotherapy and hormone therapies, and drastically diminish patient survival (52,53). In prostate cancer treatment resistance can commonly result in advanced prostate cancer like CRPC and mCRPC, which is considered cancer recurrence (54,55). Cancer recurrence happens when some primary tumour cells survive treatment and cannot be detected using clinical diagnostic tests. The surviving cells then can undergo genetic alterations and generate a new population of tumour cells, that may grow into a larger tumour or metastasize over a few weeks to months. The recurrence rate depends on factors

such as age, and type of cancer (56). The reason some tumour cells can survive after chemotherapy and radiation therapy is still unclear, however, scientists have discovered several factors and mechanisms that may be involved in therapy resistance and prostate cancer recurrences like the TME, and gene mutations (57–60).

1.4.1 Radiotherapy Resistance in Castration-Resistant Prostate Cancer

Radiotherapy remains a key strategy in the management of prostate cancer; however, the emergence of CRPC significantly limits its long-term efficacy. Evidence suggests that CRPC radioresistance is multifaceted, involving intrinsic tumor adaptations and influences from the tumour microenvironment (61–65).

A central driver of resistance is enhanced DNA damage repair (DDR) in prostate cancer. Ionizing radiation induces double-strand breaks (DSBs), which are lethal if unrepaired. CRPC upregulates homologous recombination (HR) and non-homologous end joining (NHEJ) pathways through activation of key molecules like ATM, ATR, CHK1/2, and DNA-PKcs, to create DNA repair complexes and enhanced DNA repair of cells after radiation. Persistent androgen receptor (AR) signaling, including splice variants such as AR-V7, can further increase DNA repair complex formation which strengthens DNA repair capacity despite androgen deprivation (61,63,64) This AR-DDR crosstalk represents another major mechanism for radioresistance.

Cell cycle dysregulation also contributes to radiotherapy resistance. The activation of the PI3K/AKT/mTOR pathway, often driven by the loss of tumour suppressor genes, promotes survival signaling and suppresses apoptosis following radiation exposure, despite DNA damage. This has been seen in radioresistant PCa cell lines (62–65).

Oxidative stress adaptation and antioxidant expression are other hallmarks of CRPC. Radiation cytotoxicity is partly mediated through reactive oxygen species (ROS), elevated ROS can increase metabolic reprogramming, activate oncogene pathways and influence the TME through immune responses and promoting the epithelial-mesenchymal transition (EMT) (62). One method CRPC adapts to oxidative stress is through upregulation of nuclear factor erythroid 2-related factor 2 (Nrf2), a key transcription factor that maintains cellular redox homeostasis and reduces ROS-mediated DNA fixation (61,62).

Beyond DNA repair mechanisms and cell cycle regulations, phenotypic diversity plays a key role in radioresistance as well. CRPC often has a complex tumour microenvironment (TME). The TME can be defined as a complex entity that is unique between tumour types and continuously evolving. It is the area surrounding and within the tumour and includes immune cells, stromal cells, blood vessels, molecules like oxygen, cancer stem cells (CSC), and the extracellular matrix or ECM (65,66). The TME is dynamic and is a key contributor to cancer progression, metastasis and therapeutic response. This is because the TME can exert and induce antitumorigenic, antimetastatic properties or fuel tumour growth, progression, metastasis and therapeutic resistance due to the influence of the tumour phenotype and environmental stressors like nutrient deprivation, hypoxia, and treatment-induced stress (67–71). For example, hypoxia, defined as a lack of oxygen, is often seen at the tumour core, and can reduce the efficacy of radiation by limiting the amount of ROS produced (61). The TME can also promote and support the growth of cancer stem-like cells (CSCs), which possess enhanced DNA repair efficiency and ROS tolerance, enabling tumor repopulation after treatment (61,62). Additionally, epithelial–mesenchymal transition (EMT) also increases invasiveness and resistance to apoptosis, resulting in tumours that can not only metastasize but are also more radioresistant (61,63).

CRPC radioresistance arises from a combination of factors including improved DNA repair, cell cycle dysregulation, redox regulation, and the TME. This further supports the investment into finding treatment strategies that can target or overcome these factors to improve the efficacy of radiotherapy in CRPC, such as radiosensitizers.

1.5 Novel approaches to improve the treatment efficacy of Prostate Cancer

1.5.1 Radiosensitizers

Radiosensitizers are chemicals or pharmaceutical agents that when combined with radiation treatment, can enhance radiation damage to tumour tissue by accelerating DNA damage (72). Modern radiosensitizers can be categorized as small molecules (tirapazamine, paclitaxel), macromolecules (proteins, RNAs) and nanomaterials (Au, Ag) (72). Some radiosensitizers that have been used in a variety of cancers like cervical, breast, colon, and bladder cancers, are common chemotherapeutic agents like cisplatin, gemcitabine, temozolomide and 5-fluorouracil (73–76). Although the mechanisms of action for radiosensitization are not completely understood, such radiosensitizers are used to enhance the effect of irradiation through a drug-sensitizing effect or by sensitizing specific cell populations, like hypoxic cells, to radiation (77). One method of radiosensitizing cancer cells is by sensitizing hypoxic tumour cells to irradiation, since these cells are often radioresistant due to the lack of oxygen (77).

Several *in vitro* and *in vivo* studies have investigated potential radiosensitizers that can act in hypoxic TME (78–81). d'Hose et al., conducted a study to determine if statins can decrease the oxygen consumption rate of cancer cells, decrease tumour hypoxia and ultimately radiosensitize tumours (78). They achieved this by measuring oxygen consumption rate, mitochondria superoxide production, and oxygen concentration in PC-3 cultured *in vivo* using nude mice models after administration of the statins and a single 6 Gy dose of Cesium-137 irradiation. d'Hose and colleagues

found that when the mice were treated with simvastatin or fluvastatin, the tumour oxygenation increased after 48 and 72 hours, however, simvastatin did not sensitize the PC-3 tumour to radiation therapy (78). The researchers concluded that although statins seemed to affect tumour metabolism and oxygenation there was a limited impact on growth with or without radiation treatment.

Sawada et al., conducted a study to examine the effects of sulfoquinovosylacy propanediol as a radiosensitizer in hypoxic TME when combined with X-ray radiation in prostate cancer (79). They achieved this by implanting DU145 and PC-3 prostate cancer cells into the legs of athymic nude mice, allowing the tumour to grow to 100-300 mm^2, then administering sulfoquinovosylacyl propanediol and 4 Gy X-ray radiation. Sawada and colleagues found that the combined treatment inhibited growth and decreased tumour vessel density in DU145 xenografts (79). They also found through pimonidazole staining that DU145 cells were positive for hypoxia at 6 and 24 hours after the first administration of combined treatment, but negative from 72 hours.

Zdrowowicz et al., conducted a study to evaluate if hypoxia influenced the radiosensitizing effects of 5-bromo-2'-deoxyuridine in MCF-7, a breast cancer cell line, and PC-3, a prostate cancer cell line (80). The researchers achieved this by culturing monolayer MCF-7 and PC-3 cancer cells in hypoxic or normoxic conditions, then treated with 5-bromo-2'-deoxyuridine and radiation, followed by monitoring for DNA incorporation, cell proliferation, and radiosensitivity. Zdrowowicz and colleagues found that the hypoxic conditions did not affect how much 5-bromo-2'-deoxyuridine was incorporated into the DNA or tumour cell proliferation, however, they also found that 5-bromo-2'-deoxyuridine had a greater radiosensitizing effect in hypoxic conditions compared to normoxic conditions (80).

Potiron et al., conducted a study to determine if PI3K/mTOR inhibitor BEZ235 could radiosensitize prostate cancer cells and reduce radioresistance due to hypoxic TME (81). They

achieved this by culturing PC-3 and DU145 cells *in vitro* and *in vivo*, using nude mice models, under normoxic and hypoxic conditions, and then exposing the cells to BEZ235 with or without radiation. Potiron and colleagues found that BEZ235 limited cell proliferation and clonogenic survival while increasing radiosensitivity in both cell lines in normoxic and hypoxic conditions (81).

1.5.2 Drug Repurposing

Drug repurposing or repositioning is a novel drug development strategy that has become popular in the last decade. Drug repurposing is the process of finding new uses for existing medications approved by regulatory agencies (82,83). This method of identifying new therapeutics is promising because the pathway of drug discovery to approval is expensive and can take 10-15 years (83). This is because repurposed drugs have already undergone safety evaluations through preclinical and human studies, so the risk of failure is lower (84). Identifying new indications for approved medications and developing molecules can be a cost- and time-efficient method to bring effective therapies to patients. This is because most of the development for the drug has already been completed and less time and money need to be invested (83,84). As a result, the actual cost of the treatment and the out-of-pocket cost for the patient can be reduced (83). Despite the benefits, drug repurposing has largely been opportunistic and serendipitous. For example, sildenafil citrate was initially developed as a potential antihypertensive drug but by 1998 it was repurposed for erectile dysfunction based on retrospective clinical experience (84). Another notable example is aspirin which has the original indication of analgesia but through retrospective clinical and pharmacological analysis by 2015, it was approved for use to help prevent colorectal cancer and cardiovascular disease (84).

Despite the benefits of drug repurposing, several challenges impede the advancement of drug repurposing including patent considerations and organizational hurdles (84). Patenting a new

indication for an approved drug is difficult since many of the potential repurposing uses are already known through literature and clinical experience. As a result, it is difficult to differentiate a patent claim for a drug repurposing with public domain information (84). In the pharmaceutical industry, drug repurposing has many challenges for several reasons. For example, a company may have stopped development and research on a compound so there is no funding and personnel able to investigate new indications. Another hurdle is that the indication a drug has been repurposed for is outside the company's disease area of interest (84). Another major challenge with predicting what new indications drugs may have, is that there is a lack of information on drug activity and annotations (85).

A variety of repurposed therapeutics and cancers have been investigated including metformin in advanced prostate cancer, and several other compounds and cancers (86–89).

Alghandour et al., conducted a randomized control study to determine if metformin in addition to standard care would improve outcomes in patients with hormone-sensitive prostate cancer (86). They achieved this by randomly assigning 62 patients to one of two conditions, metformin with standard care or standard care only. The researchers found that metformin significantly improved patient castration-resistant prostate cancer-free survival after 22 months and overall improved the outcome in locally advanced or metastatic prostate cancer patients (86).

Hegazy et al., conducted a randomized double-blind placebo-controlled study with 40 metastatic colorectal cancer patients to investigate the antitumor active and safety of mebendazole (87). They achieved this by randomly assigning patients to either the control group which received 6 cycles of bevacizumab with FOLFOX4 and placebo tablets or the mebendazole group which received 500 mg of mebendazole orally for 12 weeks and 6 cycles of bevacizumab with FOLFOX4. They

found that mebendazole enhanced tumour response to treatment, was well received by patients and significantly improved the response rate twelve weeks after intervention.

Antonarakis et al., conducted a non-comparative randomized phase two study to investigate the antitumor potential of itraconazole in patients with metastatic prostate cancer (88). The researchers achieved this by randomly assigning patients to either the low dose, 200 mg/day, or high dose, 600 mg/day of itraconazole until disease progression or toxicity was observed. They found that a high dose of itraconazole had some antitumor activity but was not associated with decreased serum testosterone.

Bibby et al., conducted an *in vitro* study to investigate if genes associated with hypoxia could be used to identify FDA-approved drugs that could be repurposed for the treatment of hypoxic prostate cancer (89). They achieved this by using connectivity mapping software to identify potential repurposing drug candidates, then testing these molecules *in vitro* in DU145, PC-3 and LNCAP prostate cancer cell lines in hypoxic and normoxic conditions. They found that menadione and gemcitabine could radiosensitize DU145 in hypoxia and PC-3 cells in normoxia, however further research needs to be completed. Menadione commonly known as vitamin K_3 can be converted into the active form vitamin K_2. Menadione has been shown to increase production of ROS via redox cycling and inhibit the transcriptional activity of hypoxia-inducible factor 1-alpha (HIF-1α) (89). Gemcitabine is a chemotherapy that is used to treat several cancers, including breast and bladder cancer (90). Gemcitabine is a nucleoside analogue that causes cell death by incorporating into the DNA and inhibiting DNA synthesis. The chemotherapeutic may potentially act as a radiosensitizer by inhibiting the repair of radiation-induced DNA damage (89).

1.6 Novel Therapeutics for Prostate Cancer

1.6.1 Nutraceuticals

Nutraceuticals refers to the foodstuffs, dietary supplements and medical foods with distinct health impact in prevention or treatment of diseases (91). Investigation into natural sources of materials or compounds for the treatment of diseases has long been an area of interest, especially for diseases that are widespread as cancer. Many nutraceuticals have been investigated as ways to complement conventional therapies due to their demonstrated anti-tumour effects such as inhibiting cell proliferation, inducing apoptosis and suppressing angiogenesis and metastasis (92–96). A key group of nutraceuticals that has shown promise over the years is polyphenolic compounds such as curcumin, resveratrol and epigallocatechin gallate (EGCG), since they have shown strong antioxidant and anticancer properties (97). Compounds such as curcumin and EGCG can sensitize cancer cells to conventional cancer treatments like chemotherapy and radiotherapy by modulating cell survival and apoptosis pathways, while also providing protection to healthy tissues through antioxidant and anti-inflammatory properties (97,98).

Despite the many advantages of nutraceuticals, they are often poorly bioavailable and so many researchers have investigated the use of nano-carriers and formulations as carriers to improve stability, absorption, enable controlled release and enhance tumour targeting (97). There have been a variety of nanoformulations of polyphenols and flavonoids investigated for cancer therapy, including curcumin-loaded Poly(lactic-co-glycolic acid) nanoparticles and theaflavin-EGCG NPs co-delivered with cisplatin (99,100).

1.6.1.1 Curcumin

Curcuma longa Linn (C. longa) commonly known as turmeric has a long history of having healing properties against many diseases. One of the major bioactive compounds in C. longa is

curcumin, a natural polyphenolic compound which is known to have anti-inflammatory and antioxidant effects (101,102). Curcumin has been shown to have potent anticancer effects through multi-targeted molecular mechanisms that regulate tumour growth, survival, and progressions, particularly in prostate cancer. These mechanisms involve the modulation of key signaling pathways like induction of apoptosis, inhibition of proliferation and suppression of metastasis (102–108).

Curcumin promotes programmed cell death in cancer cells through both intrinsic and extrinsic apoptotic pathways. This is because it can upregulate pro-apoptotic proteins like Bax, downregulate anti-apoptotic proteins like Bcl-2, and activate caspases which lead to cell death. These effects have been seen in both androgen-dependent and castration-resistant prostate cancer models (102–104). Curcumin can also suppress tumour cell growth by inducing cell cycle arrest at G1/S and G2/M phases by downregulating cyclins and cell cycle regulatory proteins. This results in reduced proliferation of prostate cancer cells (102,105). Interestingly curcumin can target several critical oncogene signaling pathways. For example, curcumin can inhibit the PI3K/Akt pathway, reduce survival and proliferation, as well as suppress NF- κB, which decreases inflammation and tumour promoting signaling (102–104). Curcumin can also impact androgen receptor signaling modulation and m6A-modified circRNA levels which can impact prostate cancer progression and growth (102,106). Additionally, curcumin reduces tumour promoting inflammation and oxidative stress by inhibiting pro-inflammatory cytokines and mediators, scavenging reactive oxygen species and reducing oxidative DNA damage. These effects contribute to prevention and inhibit cancer growth (102,104).

In addition to inhibiting cancer progression, curcumin has also been shown to enhance the effectiveness of conventional therapies by sensitizing cancer cells to chemotherapy and overcoming drug resistance mechanisms. In the context of CRPC this is extremely relevant (104,105).

1.6.2 Gold nanoparticles

Nanoparticles have been a key area of research due to their unique effects at the nanoscale and potential for use in personalized medicine. Gold is a major area of interest due to its atomic and electronic structure, [Xe] $4f^{14}$ $5d^{10}$ $6s^{1}$. Gold's 6s electron is unique because although a single outer electron usually increases reactivity, in gold this electron is inert due to relativistic effects from its heavy nucleus (109). Despite the strong nuclear attraction on the 6s orbital, the electron remains delocalized, which is why gold can be a strong conductor and chemically inert (110). Compared to other elements with one valence electron like Li, Na, and K in Group 1, which react extremely violently with water and air and readily lose their electrons, gold is virtually unreactive and stable against corrosion and oxidation; this is one of the reasons why gold is so special. Some of the unique properties of GNPs are explored below.

1.6.2.1 Quantum Size Effects

One of the reasons why GNPs are so interesting is because they exhibit unique physicochemical properties due to quantum size effects. This can alter GNPs electronic and optical behaviour due to their size. One such phenomenon, surface plasmon resonance (SPR), happens when the size of GNPs approaches the wavelength of light (111,112). This alters their interaction with electromagnetic radiation. The small size of GNPs allows the electron cloud around the NPs to oscillate and resonate at specific wavelengths. SPR lends itself to the application of GNPs in colorimetric sensing and photothermal therapy (113). For spherical GNPs this resonance is around 520-550 nm, imparts a distinct ruby red colour, and a unique optical signature resulting from these size-dependent oscillations. The SPR signal changes based on particle binding on the surface. Additionally, the shape and size of GNPs influence the electronic structure and quantum size effects, which affect catalytic activity and biological interactions (110).

1.6.2.2 Inertness and Biocompatibility

Gold is chemically inert and exhibits a high resistance to oxidation. This contributes to its favourable biocompatibility (114). GNPs are also generally considered non-toxic; however, their biological effects depend on physicochemical characteristics such as size, shape and surface chemistry. GNPs smaller than 5 nm potentially being more toxic because they can pass biological barriers like the liver sinusoids, kidney glomerulus, blood-brain barrier, nuclear envelope and excreted through the bladder, while GNPs larger than 5 nm may accumulate in the liver (115–117). Surface area also plays a role since a greater surface area may allow for more interfacial electrons, which can interact with biomolecules, contributing to toxicity. Although GNPs are considered inert the surface chemistry and size are vital in determining their impact and interactions with biological systems (114,117,118).

1.6.3 High Atomic Number

Gold has a high atomic number, Z= 79, which makes it effective at absorbing ionizing radiation. This enhances the photoelectric effect, resulting in an increased local dose deposition when exposed to radiation making it a valuable avenue of investigation for combination with radiotherapy for cancer (119).

1.6.4 Ease of Synthesis and Functionalization of GNPs

GNPs can be synthesized through a variety of reproducible and scalable methods like, chemical reduction, seed-mediated growth and green synthesis approaches (120,121). The Turkevich method can be used to synthesize spherical citrate coated GNPs, with tunable sizes ranging from 9 to 120 nm (121,122). The surface of GNPs can also be easily functionalized with biomolecules such as antibodies, peptides, and compounds to improve delivery and therapeutic effect (123,124).

There is a great diversity of methods for synthesizing GNPs due to the sensitivity of GNPs to temperature, pH, pressure, gold concentration, reducing agents and stabilizers on the size. This results in a wide array of customization to achieve specific characteristics for each unique application (120).

The synthesis of colloidal gold dates to the work of Michael Faraday in the 1850s, which established the foundation for modern nanoparticle research (125). A major advancement occurred in the 1950s with the development of the Turkevich method (Figure 2), which involves the reduction of gold chloride using citrate to produce small, spherical gold nanoparticles (GNPs). This approach is notable for its simplicity and reproducibility, enabling standardized GNP production and serving as a fundamental technique that continues to inform current synthesis strategies (121).

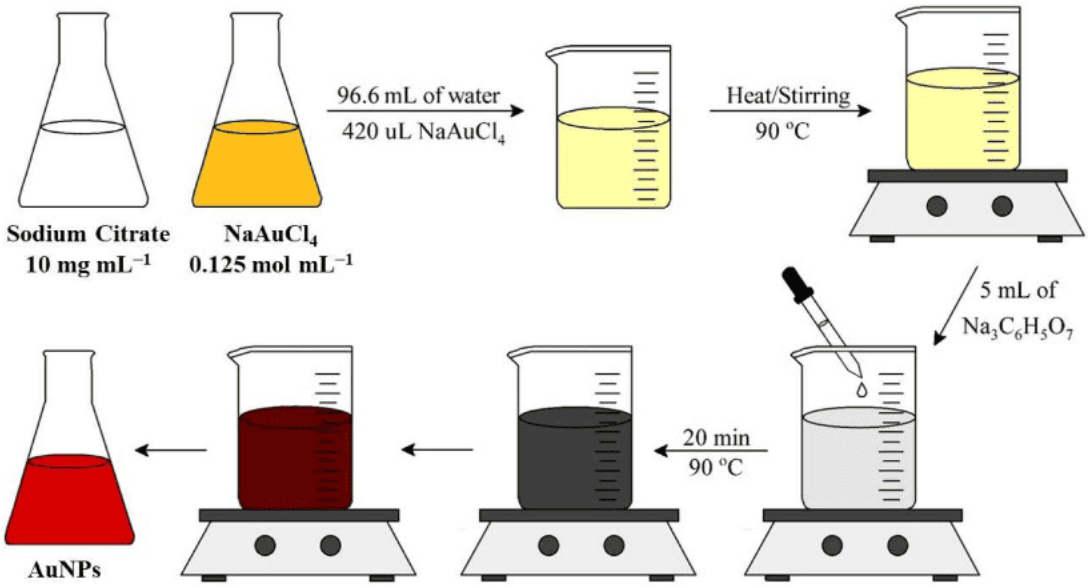


Figure 1.1: Schematic illustration of gold nanoparticles synthesis by Turkevich method (121).

Since the introduction of the Turkevich method, numerous synthesis techniques have been developed, each with distinct advantages and limitations. Broadly, these approaches are categorized into top-down and bottom-up methodologies (126). The top-down approach involves breaking down

bulk materials into nanoscale structures, whereas the bottom-up approach relies on the assembly of nanoparticles from atomic or molecular precursors. Bottom-up strategies can be further classified into physical, chemical, and biological methods. Physical methods include techniques such as laser ablation, sonication, radiation, and electrodeposition, while biological approaches utilize plant extracts, bacteria, or fungi for nanoparticle formation (127). Chemical synthesis methods include reduction reactions, condensation processes, and seed-mediated growth (120). Typically, gold nanospheres are produced through chemical reduction, nanorods through seed-mediated growth, and nanowires via electrochemical techniques.

An emerging area of interest is in vivo plant-based synthesis, where living plants absorb gold precursors from the soil and subsequently convert them into nanoparticles within their tissues. This process highlights a unique intersection between nanotechnology and plant biology, demonstrating the potential for natural systems to produce functional nanomaterials (128,129).

The concept of green synthesis gained traction in the early 2000s as a sustainable alternative to conventional methods. This approach utilizes biologically derived compounds, such as plant extracts, to both reduce gold ions and stabilize the resulting nanoparticles. A key advantage of green synthesis is that a single substance can serve dual roles as both a reducing and stabilizing agent, unlike traditional methods that require separate chemicals for each function (127,130). For example, in conventional sodium borohydride-based synthesis, sodium borohydride acts solely as the reducing agent, necessitating additional stabilizers such as citrate, polyvinyl alcohol (PVA), or polyvinylpyrrolidone (PVP) to prevent aggregation (120,131). In contrast, plant-derived compounds such as polyphenols, flavonoids, and terpenoids can simultaneously reduce gold ions and adsorb onto nanoparticle surfaces, providing inherent stabilization. This multifunctionality reflects the complex

chemical nature of biological molecules, whereas synthetic reagents are typically designed for single, specific roles.

1.6.5 Mechanistic Approach

The therapeutic effectiveness of GNPs is attributed to their interactions with biological systems through a combination of physical, chemical, and biological mechanisms. These include enhancement of radiation dose deposition, increased production of reactive oxygen species (ROS), and modulation of cellular signaling pathways, all of which contribute to their application as multifunctional agents in cancer therapy (132,133).

The mechanisms underlying GNP synthesis have been extensively investigated, with several models proposed to describe nanoparticle formation. One widely accepted model suggests a multistep process involving the rapid reduction of gold ions (Au^{3+}) to neutral gold atoms (Au^{0}), followed by nucleation into small clusters and subsequent growth into larger polycrystalline structures through aggregation (134).

In green synthesis systems, particularly those involving polyphenol-rich extracts, nanoparticle formation proceeds through three primary stages:

Nucleation:

This initial stage involves the rapid reduction of gold ions into elemental gold atoms, which then form small clusters. Bioactive molecules, such as polyphenols, play a critical role by facilitating electron transfer and reducing Au^{3+} to Au^{0}. These molecules can also bind gold ions through their hydroxyl groups, forming stable complexes that promote nucleation. Reaction conditions, including concentration, temperature, and pH, are crucial at this stage, as they determine nanoparticle size, morphology, and coating characteristics.

Growth:

Following nucleation, nanoparticle growth occurs through the accumulation of additional gold atoms or the coalescence of smaller clusters. This phase is influenced by factors such as precursor concentration and reaction conditions. The growth rate is largely governed by monomer availability, with higher concentrations of reducing agents generally leading to smaller nanoparticles due to faster stabilization. However, optimal concentrations are required, as excessively high levels may inhibit nanoparticle formation altogether (135).

Stabilization:

The final stage involves the termination of growth, which occurs due to depletion of gold ions, surface adsorption of stabilizing molecules, and thermodynamic stabilization. Biomolecules from green extracts adsorb onto the nanoparticle surface, forming a protective layer that prevents further growth and aggregation. Additionally, the negative charge imparted by these molecules induces electrostatic repulsion between particles, enhancing colloidal stability. From a thermodynamic perspective, as nanoparticles increase in size, their surface energy decreases, reducing the driving force for further growth and contributing to overall stability (127,136).

1.6.6 Uptake of GNPs in Cells

In the context of gold nanoparticle (GNP)-enhanced radiotherapy, efficient cellular uptake is a critical determinant of therapeutic success, as numerous studies have demonstrated a direct relationship between intracellular GNP accumulation and increased radiation dose enhancement (119,137–140). Although this objective appears straightforward, achieving consistent and optimal uptake remains challenging due to substantial variability across experimental systems.

A key study by Carnovale et al. systematically evaluated how physicochemical properties influence GNP uptake in PC-3 prostate cancer cells. Their findings demonstrated that nanoparticle shape plays a significant role in internalization efficiency, with gold nanospheres showing the highest uptake, followed by nanocages, nanorods, and nanoprisms. This preference for spherical particles is attributed to their geometry, which enables greater interaction with cell surface receptors and facilitates endocytosis with lower energetic requirements (116).

Despite these trends, variability in nanoparticle uptake across studies remains considerable and can be attributed to differences in size, shape, concentration, surface charge, coating, cell type, and experimental conditions such as serum presence and protein corona formation. Even minor alterations in these parameters can significantly influence nanoparticle–cell interactions (116).

Particle size is a particularly important determinant of uptake. Smaller spherical GNPs are generally internalized in greater numbers compared to larger particles; however, their total intracellular gold mass is often lower due to reduced volume (116). Across multiple studies, nanoparticles within the 25–50 nm range have demonstrated optimal uptake efficiency (141–144). Uptake mechanisms are also size-dependent, with smaller particles primarily entering cells via pinocytosis, while larger particles are more commonly internalized through receptor-mediated endocytosis. Additionally, larger GNPs tend to exhibit prolonged intracellular retention due to reduced exocytosis, whereas smaller nanoparticles may be more readily cleared (142). Cell size can also impact GNP uptake, where cells with smaller, less-spread morphologies show reduced GNP uptake, whereas larger, more-spread cells exhibit increased uptake, likely due to greater cell–substrate contact, actin organization, and membrane availability for endocytic processes (141). This is seen in

Figure 1.2 below.

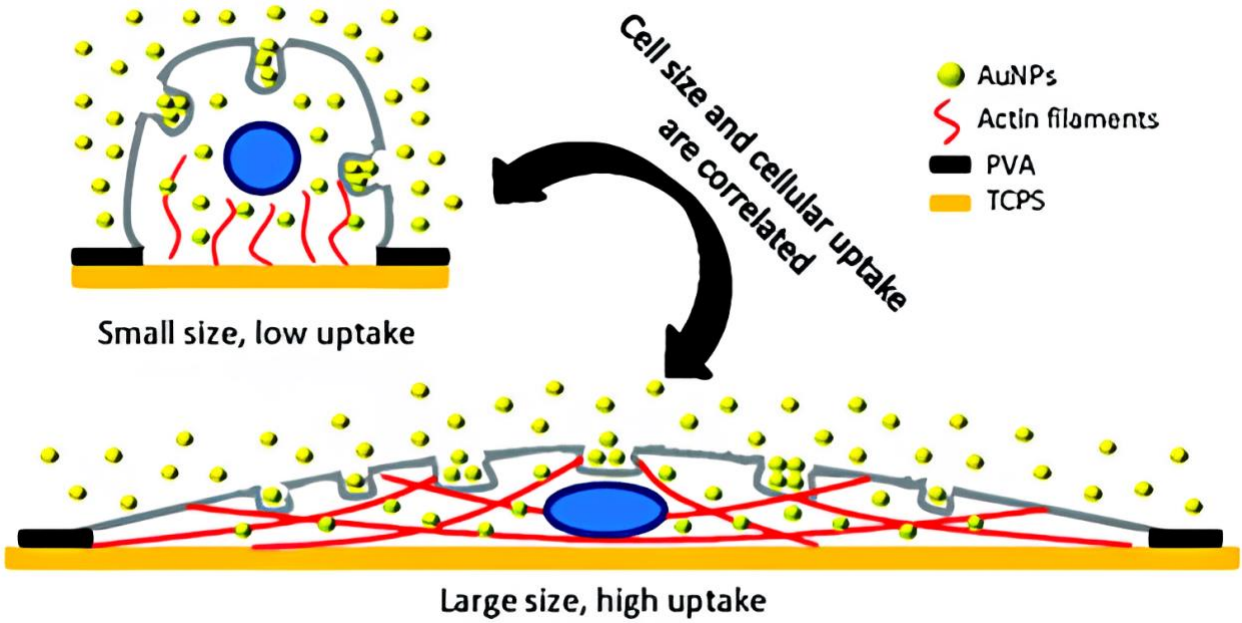


Figure 1.2: Influence of cell size on cellular uptake of GNPs.

This schematic illustrates the relationship between cell morphology and gold nanoparticle (GNP) internalization. Cells with smaller, less-spread morphologies show reduced GNP uptake, whereas larger, more-spread cells exhibit increased uptake, likely due to greater cell–substrate contact, actin organization, and membrane availability for endocytic processes. GNP uptake is also size-dependent: smaller nanoparticles are more commonly internalized through nonspecific fluid-phase uptake mechanisms such as pinocytosis, while larger nanoparticles are more often taken up through receptor-mediated endocytosis. Larger GNPs may also demonstrate greater intracellular retention because they are less readily exocytosed, whereas smaller nanoparticles may be cleared from cells more efficiently. Adapted from findings reported by (141).

The extracellular environment further modulates uptake behavior. In serum-containing conditions, proteins rapidly adsorb onto the nanoparticle surface to form a "protein corona," which alters surface characteristics and can reduce interactions with the cell membrane (116). However, the extent of this effect depends on nanoparticle surface chemistry. For instance, certain coatings, such as

aromatic amino acids, can enhance uptake by improving interactions with cellular receptors, while more conventional coatings such as citrate may show limited enhancement (116,143).

Following internalization, GNPs exhibit complex intracellular trafficking patterns that directly influence their radiosensitization potential. Nanoparticles are typically distributed throughout the cytoplasm, with some localizing near the nucleus and within organelles such as mitochondria (144). Size-dependent intracellular fate has also been observed, where smaller nanoparticles are more capable of escaping endosomal compartments and diffusing within the cytosol, while larger particles remain confined to endosomes or lysosomes (145). Importantly, smaller GNPs demonstrate an increased ability to localize within the nucleus, which is particularly advantageous for radiosensitization, as proximity to DNA enhances damage induced by short-range secondary electrons (145).

Surface functionalization strategies, including the use of cell-penetrating peptides, oligonucleotides, and nuclear localization sequences, have been shown to further enhance nuclear targeting and intracellular distribution (146). Active targeting strategies have emerged as a key approach to enhance tumor-specific uptake and radiosensitization. For example, Khoo et al., demonstrated that actively targeted GNPs significantly increased uptake in prostate cancer models, leading to enhanced radiosensitization both in vitro and in vivo when combined with orthovoltage X-ray irradiation (147). Their work highlights that ligand-mediated targeting not only improves nanoparticle accumulation within tumor cells but also translates directly into improved therapeutic response, emphasizing the importance of surface engineering in GNP design.

While much of the current understanding of GNP uptake is derived from conventional 2D cell culture systems, these models do not fully capture the complexity of tumor architecture. In 3D

tumor models, such as multicellular spheroids and co-culture systems, nanoparticle uptake and distribution are significantly altered due to the presence of diffusion barriers, extracellular matrix components, and cell–cell interactions. Studies have shown that GNP penetration in 3D systems is often heterogeneous, with higher accumulation at the outer proliferative layers and reduced penetration into the hypoxic core regions (148,149). This limited penetration can result in spatially variable radiosensitization, which is critical when considering treatment efficacy.

Furthermore, nanoparticle uptake in 3D systems is influenced by physicochemical properties like those observed in 2D models, including size, shape, and surface charge. However, these effects are often amplified in 3D environments, where smaller and neutral or slightly positively charged nanoparticles demonstrate improved penetration and distribution (149). Functional ultrasmall GNPs have also been shown to exhibit enhanced diffusion and uptake in complex 3D epithelial models, supporting their potential for improved tissue penetration (150).

Importantly, 3D models have revealed differences in biological response compared to 2D systems. For example, gene silencing and therapeutic efficacy of gold nanoparticle-based systems are often reduced in 3D spheroids due to limited penetration and altered cellular physiology (151). Similarly, studies using 3D radioresistant co-culture models have demonstrated that nanoparticle uptake and radiosensitization effects are influenced by tumor microenvironment factors such as stromal interactions and hypoxia (152). These findings highlight the importance of using physiologically relevant models when evaluating nanoparticle performance.

In addition to in vitro systems, in vivo uptake and biodistribution present further complexities. Following systemic administration, GNPs are distributed throughout the body and are often sequestered by the mononuclear phagocyte system, leading to accumulation in organs such as

the liver and spleen (118,153). Pharmacokinetic studies have demonstrated that nanoparticle size, surface chemistry, and circulation time significantly influence biodistribution, tumor accumulation, and clearance pathways (154). Tumor uptake is further governed by the enhanced permeability and retention (EPR) effect, as well as active targeting strategies that improve selective accumulation within tumor tissues (138,155). However, heterogeneous vascularization and interstitial pressure within tumors can limit uniform nanoparticle delivery.

Collectively, these findings demonstrate that GNP uptake is governed by a complex interplay of nanoparticle design parameters and biological context. While 2D studies provide foundational insights, 3D tumor models and in vivo systems reveal additional barriers to effective nanoparticle delivery, including limited penetration, heterogeneous distribution, and systemic clearance. Optimizing these factors is essential for maximizing intracellular and nuclear localization of GNPs, which remains a key determinant of enhanced radiosensitization and therapeutic efficacy (119).

1.7 GNPs in Radiation Therapy

GNPs have been an area of interest for their radiosensitization due to their ability to combine physical dose enhancement with biological targeting through the use and application of various coatings. GNPs high atomic number significantly enhances photon absorption compared to biological tissues such as water (119). This property makes GNPs effective as both contrast agents and radiosensitizers. In this context, irradiation of GNPs leads to localized energy deposition in their immediate surroundings, enhancing radiation-induced damage within tumor tissues.

The concept of radiation dose enhancement using high atomic number materials was first observed clinically in patients with metallic implants undergoing radiotherapy (119). Early attempts to exploit gold for this purpose involved bulk materials such as gold foils and microspheres; however,

these approaches were limited by inefficient delivery to tumor sites. The development of nanotechnology has since enabled the targeted delivery of GNPs to tumors and even to specific intracellular compartments, significantly improving their therapeutic potential (144–146).

A landmark study by Hainfeld et al. demonstrated the potential of GNPs as radiosensitizers in vivo, reporting substantial tumor regression and a marked increase in survival in tumor-bearing mice treated with thiol-coated GNPs in combination with X-ray irradiation (137). Subsequent investigations revealed that the extent of cell killing observed experimentally exceeded predictions based solely on physical dose enhancement models, suggesting that additional mechanisms contribute to the radiosensitization effect (132,133,156,157). This has led to the recognition that GNP-mediated radiosensitization involves a combination of physical, chemical, and biological processes (158).

1.7.1 Mechanisms of Radiosensitization

Initially, the radiosensitizing effects of GNPs were attributed primarily to physical dose enhancement resulting from increased photoelectric absorption (133). However, accumulating evidence indicates that chemical and biological mechanisms also play critical roles, suggesting that GNPs influence multiple stages of radiation interaction with biological systems (133). These mechanisms are outlined below.

1.7.2 Physical Process

The physical basis of GNP-mediated radiosensitization is well established and centers on interactions between ionizing radiation and high atomic number materials. The dominant mechanism is the photoelectric effect, in which incident photons interact with gold atoms, resulting in the ejection of inner-shell (K-shell) electrons when photon energies exceed the binding energy threshold (~80.7

keV) (132). This process produces localized ionization events that can cause significant cellular damage, particularly in regions where GNPs accumulate.

Following the ejection of a core electron, electrons from higher energy levels fill the vacancy, releasing energy either as secondary photons or through the emission of Auger electrons. Despite their low energy, Auger electrons have a very short range and high linear energy transfer, making them highly effective at inducing localized damage to DNA and other critical cellular components (132). The efficiency of this process is maximized when photon energies are near the gold K-edge.

In addition to the photoelectric effect, Compton scattering contributes to dose enhancement, particularly at higher photon energies commonly used in clinical radiotherapy (6–20 MeV). In this interaction, photons transfer part of their energy to electrons, generating secondary electrons that further propagate ionization events (159). At even higher energies, pair production may occur, where photons are converted into electron-positron pairs; however, this mechanism contributes minimally under standard therapeutic conditions (156,159).

Monte Carlo simulations have been widely used to model these physical interactions and predict dose enhancement factors. These studies demonstrate that parameters such as nanoparticle size, concentration, radiation energy, and proximity to the nucleus significantly influence radiosensitization efficiency (157). Notably, Auger electrons have been identified as key contributors to enhanced local dose deposition due to their high linear energy transfer characteristics.

1.7.3 Chemical Processes

Beyond physical interactions, chemical processes, particularly the generation of reactive oxygen species (ROS), play a central role in GNP-mediated radiosensitization. The interaction of radiation with GNPs leads to the emission of secondary electrons, which can ionize surrounding water

molecules and generate ROS such as hydroxyl radicals, superoxide anions, and hydrogen peroxide (158,160).

These ROS are major contributors to radiation-induced cytotoxicity, as they induce oxidative stress, DNA strand breaks, and damage to proteins and lipids. The presence of GNPs has been shown to amplify ROS production under irradiation, thereby enhancing cellular damage beyond that achieved with radiation alone (161). This increased oxidative stress is a key mechanism underlying the radiosensitization effect.

1.7.4 Biological Processes

The biological effects of GNP-mediated radiosensitization can be understood within the framework of the 6Rs of radiotherapy: repair, reoxygenation, repopulation, redistribution, intrinsic radiosensitivity, and reactivation of the immune response (162).

1. **Repair:**

GNPs have been shown to impair DNA repair mechanisms, leading to an accumulation of unrepaired double-strand breaks following irradiation. This is associated with downregulation of key DNA repair genes, ultimately increasing cell death (163).

2. **Reoxygenation:**

Oxygen enhances radiation-induced damage by stabilizing DNA lesions. GNP-mediated radiosensitization is more pronounced under normoxic conditions, while hypoxic environments reduce treatment efficacy. Additionally, the radiosensitization effect is diminished in the presence of radical scavengers, highlighting the importance of ROS (162).

3. **Repopulation:**

GNPs can inhibit cancer cell proliferation by inducing cell cycle arrest, thereby limiting tumor regrowth during fractionated radiotherapy. This effect has been linked to the upregulation of cell cycle regulatory proteins (162).

4. **Redistribution:**

Cellular radiosensitivity varies across the cell cycle, with cells in the G_2/M phase being more sensitive. GNPs have been shown to influence cell cycle distribution, often promoting accumulation in more radiosensitive phases, although findings are somewhat variable depending on nanoparticle characteristics (156,162).

5. **Intrinsic Radiosensitivity:**

GNPs can enhance inherent cellular sensitivity to radiation by activating apoptotic pathways, including caspase signaling, and by inhibiting antioxidant defense systems such as thioredoxin reductase (164). This may be particularly relevant in overcoming resistance in certain cancer types.

6. **Reactivation of the Immune Response:**

GNPs may contribute to radiosensitization by enhancing anti-tumour immune response by amplifying radiation-induced DNA damage and oxidative stress, thereby increasing tumour cell injury and immune-stimulatory signalling like pro-inflammatory cytokines (165,166). However, these mechanisms are still emerging and require further investigation to determine how nanoparticle formulation, tumour type, radiation dose and the tumour microenvironment influence immune reactivation during GNP-enhanced radiotherapy.

In the current clinical landscape, radiosensitization is commonly achieved using chemotherapeutic agents that interfere with DNA repair, cell cycle progression, or tumor hypoxia. For example, fluoropyrimidines disrupt DNA synthesis during the S-phase, while platinum-based agents induce DNA crosslinking and inhibit repair processes (167,168). Compared to these approaches,

GNPs offer a promising alternative by combining physical dose enhancement with chemical and biological modulation, potentially improving therapeutic efficacy while reducing systemic toxicity.

1.8 Research Gap and Rational

Gold nanoparticles (GNPs) have emerged as promising radiosensitizers due to their unique physicochemical properties, including high atomic number, ease of functionalization, and ability to enhance radiation-induced damage (119,133). These characteristics align with the broader objective of developing simple, effective, and clinically translatable interventions that can be readily incorporated into existing prostate cancer (PCa) treatment regimens. Compared to conventional pharmacological radiosensitizers, GNP-based approaches offer the advantage of localized dose enhancement with potentially reduced systemic toxicity (133).

Despite advancements in treatment, castration-resistant prostate cancer (CRPC) and metastatic CRPC (mCRPC) remain significant clinical challenges due to persistent therapeutic resistance, recurrence, and poor prognosis (169,170). A defining feature of CRPC is the presence of multiple resistance mechanisms, including enhanced DNA repair capacity, dysregulated cell cycle progression, resistance to apoptosis, and adaptation to hypoxic tumor microenvironments (67,171). These factors collectively reduce the effectiveness of radiotherapy and contribute to disease progression.

Importantly, these resistance mechanisms directly correspond to the known biological and chemical pathways through which GNPs exert radiosensitization effects, suggesting a strong mechanistic rationale for their application in CRPC. For instance, CRPC cells often exhibit upregulated DNA repair pathways that enable survival following radiation-induced damage. In contrast, GNPs have been shown to impair DNA repair processes and increase the persistence of

double-strand breaks, thereby directly counteracting this resistance mechanism (156,163,169). Similarly, CRPC tumors frequently evade apoptosis through activation of pro-survival signaling pathways; however, GNP exposure has been associated with increased apoptotic signaling and mitochondrial dysfunction, promoting cell death (158).

Tumor hypoxia represents another critical driver of radioresistance in CRPC, as reduced oxygen levels limit the generation of radiation-induced reactive oxygen species (ROS) (171). Notably, GNPs enhance ROS production during irradiation through secondary electron emission and water radiolysis, thereby partially overcoming hypoxia-mediated resistance (158,160). Furthermore, CRPC is characterized by altered cell cycle dynamics, often favoring phases that are less sensitive to radiation. GNPs have been shown to induce cell cycle redistribution, particularly promoting arrest in the radiosensitive G_2/M phase, which enhances radiation response (162).

While these complementary mechanisms suggest that GNPs are well-suited to address the biological challenges of CRPC, there remains a significant gap in the literature regarding their targeted application in CRPC-specific models. Although studies have demonstrated the radiosensitization potential of GNPs in prostate cancer broadly (137,147), few have directly investigated their ability to overcome the distinct resistance mechanisms associated with CRPC.

Additionally, there is limited research exploring the combined use of GNPs with bioactive coatings, such as phytochemicals, which may further enhance radiosensitization through complementary biological effects. Compounds such as curcumin have been shown to modulate oxidative stress, inhibit pro-survival pathways, and induce apoptosis (172). When used as nanoparticle coatings, these compounds may synergistically enhance both the physical and biological mechanisms of GNP radiosensitization. However, the extent of this synergy remains poorly understood, particularly in the context of CRPC.

Another critical limitation in the current literature is the reliance on 2D cell culture models, which do not accurately replicate the tumor microenvironment. CRPC tumors are characterized by complex structural and physiological features, including hypoxia, nutrient gradients, and limited drug penetration, all of which influence treatment response. 3D spheroid models provide a more physiologically relevant platform that captures these features and allows for more accurate assessment of nanoparticle uptake, distribution, and therapeutic efficacy. Despite this, few studies have systematically evaluated GNP-based radiosensitizers in 3D prostate cancer models.

The rationale for selecting coated GNPs is based on their enhanced stability, biocompatibility, and ability to improve cellular uptake and tumor targeting (116,146). Functional coatings such as curcumin not only facilitate nanoparticle synthesis but also introduce additional therapeutic effects, including modulation of redox balance and inhibition of signaling pathways associated with CRPC progression (172). These properties position coated GNPs as a multifunctional therapeutic platform capable of addressing both the physical and biological aspects of radioresistance.

Furthermore, GNPs are relatively accessible, cost-effective, and widely studied, with scalable synthesis methods that support their potential for clinical translation (120). Compared to traditional radiosensitizers, which often involve systemic chemotherapy or complex drug delivery systems, GNP-based approaches offer a more targeted and potentially less invasive alternative (147,160,173,174).

However, challenges remain, including size- and surface-dependent toxicity, accumulation in non-target organs, and variability in biodistribution (118,153). These limitations highlight the need for careful optimization of nanoparticle design and thorough evaluation in physiologically relevant models.

Overall, this research addresses a critical gap by investigating the combined radiosensitization potential of coated GNPs in a 3D prostate cancer model, with relevance to CRPC, to explicitly targeting the underlying mechanisms of radioresistance like DNA repair, hypoxia, oxidative stress, and cell cycle dysregulation. This study aims to advance the understanding of GNP-based therapies and contribute to the development of more effective and clinically relevant treatment strategies for prostate cancer.

The convergence between CRPC resistance mechanisms and the multifaceted radiosensitization effects of coated GNPs highlights a critical opportunity for therapeutic advancement, thereby leading to the central research question of whether curcumin-coated gold nanoparticles can effectively enhance radiosensitivity in prostate cancer within physiologically relevant 3D spheroid models.

1.9 Aim and Objectives of Research Undertaken

1.9.1 Hypothesis:

Curcumin-coated gold nanoparticles (Curc-GNPs) will be more effectively internalized by prostate cancer spheroids and act as potent radiosensitizers under clinically relevant radiation doses compared to citrate-coated gold nanoparticles (Cit-GNPs). Functionalization of GNPs with curcumin is expected to enhance cellular uptake, increase oxidative stress, and augment radiation-induced cytotoxicity in 3D DU145 prostate cancer spheroids.

1.9.2 Objective 1.1 (Synthesis & Characterization):

Synthesize curcumin-coated gold nanoparticles using a green, single-step method and characterize their physicochemical properties. This includes determining nanoparticle size (core and hydrodynamic diameter), morphology, surface charge (zeta potential), gold concentration, and

colloidal stability in biologically relevant media. The synthesized Curc-GNPs will be evaluated for consistency and suitability for biological applications.

1.9.3 Objective 1.2 (Cellular Uptake & Cytotoxicity in 3D Models):

Evaluate the interaction of citrate-GNPs and Curc-GNPs with 3D DU145 prostate cancer spheroids. This includes quantifying nanoparticle uptake using Inductively coupled plasma optical emission spectroscopy (ICP-OES) in spheroids.

1.9.4 Objective 1.3 (Radiosensitization Efficacy in 3D Spheroids):

Determine the extent of radiation dose enhancement provided by Curc-GNPs in 3D DU145 spheroids. Clonogenic survival assays will be conducted following irradiation at clinically relevant doses (0, 2, 4, and 6 Gy) to evaluate treatment efficacy. Radiosensitization will be quantified through reductions in spheroid survival and comparisons between treated and control groups. This objective will identify how much Curc-GNPs enhance radiation-induced cell killing.

1.9.5 Thesis Structure:

The remainder of this thesis is organized as follows:

- **Chapter 2:** Synthesis and Characterization of Gold Nanoparticles.
- **Chapter 3:** In Vitro Study of Gold Nanoparticles in Prostate Cancer Spheroids.
- **Chapter 4:** Conclusions and Future Directions.

Chapter 2: Synthesis and Characterization of Gold Nanoparticles

2.1 Introduction

The following chapter presents the synthesis and physicochemical characterization of the gold nanoparticles (GNPs) used in this study. Characterization is a vital first step in any nanoparticle-based biomedical application, as physicochemical properties significantly influence biological interactions such as cellular signaling, protein corona formation, membrane association, intracellular uptake, toxicity, clearance, and organ biodistribution.

Method: Two types of GNPs were evaluated Curc-GNPs and Cit-GNP. The properties analyzed included hydrodynamic size, zeta potential, shape, polydispersity index (PDI), surface coating, gold concentration, antioxidant potential and X-ray attenuation. Characterization techniques used were ultraviolet-visible (UV-Vis) spectroscopy, dynamic light scattering (DLS), and inductively coupled plasma optical emission spectrometer (ICP-OES). **Results**: All GNP formulations were monodisperse and stable in water. The green synthesis protocol yielded concentrations of 361 ± 15 μg/mL for Curc-GNPs, while the adapted Turkevich method yielded 20 ± 4 μg/mL for Cit-GNPs. Hydrodynamic diameters ranged from 18.36 ± 0.27 to 22.55 ± 0.18 nm, with Cit-GNPs being the smallest and Curc-GNPs the largest. All samples showed sharp single peaks in their size distribution histograms. All nanoparticles had negative zeta potentials, ranging from - 40.0 ± 4.6 to - 43.5 ± 1.2 mV. UV-Vis spectra revealed surface plasmon resonance (SPR) peaks between 520-525 nm for all samples.

The most common synthesis method for gold nanoparticles is the Turkevich method, first described by Turkevich in his publication in 1951 (1). The fact that it is still the most common procedure for the synthesis of GNPs is a testament to how easily the method produces stable,

spherical, and monodisperse GNPs with excellent reproducibility. The simplest description of the synthesis involves rapidly adding sodium citrate ($Na_3C_6H_5O_7$) to a boiling solution of auric acid ($HAuCl_4$). For precise control over GNP dimensions, synthesis conditions such as reactant concentrations ($HAuCl_4 + Na_3C_6H_5O_7 + H_2O$), pressure, and temperature must be carefully regulated. The main disadvantage of the Turkevich method is that it is energy intensive and produces low GNP concentrations. Many Turkevich variations have been proposed to address this, for example the addition of sodium borohydride results in reducing heat energy required to synthesize citrate capped gold nanoparticles (Cit-GNPs) (2). The other challenges with Cit-GNPs are that they are very susceptible to aggregation in salt solutions and the citrate coating provides weak steric stability. This is especially important, as weak stability against physiological buffering salts weakens the use of Cit-GNPs for biomedical applications, since blood is an ionic medium that will promote aggregation and desorption of the citrate coating (1).

The synthesis of Curcumin-GNPs was carried out through a single step, one pot, green synthesis method (3). One pot meaning the entire synthesis occurs in one vessel and "green synthesis" meaning it is an eco-friendly method that requires relatively low energy and uses naturally derived molecules as reducing and stabilizing agents. Unlike traditional synthesis methods that may involve toxic chemicals or high energy consumption, green synthesis aims to make the process safer, sustainable, and less toxic to the environment and living organisms. Another advantage of our green synthesis method is that it can be easily upsized into large scale production, and it is relatively cheap. The solvent system used in green synthesis and in our study, synthesis is ultrapure water with no chemical solvents used. Lastly, our green synthesis protocol can produce high concentrations of GNPs while still maintaining monodispersity. Having control of GNP size and the range of sizes is crucial for our *in vivo* and *in vitro* experiments. Chemically, curcumin is a diarylheptanoid composed

of two aromatic rings, each bearing methoxy and hydroxy groups, connected by a seven-carbon chain featuring two α,β-unsaturated carbonyl groups.

The synthesis of Curcumin-GNPs begins by deprotonating their multiple phenolic and enolic groups using a dilute concentration of NaOH added to an aqueous solution containing curcumin. Curcumin has numerous phenolic hydroxyl (OH) groups, and the ionization of these groups is pH dependent. Deprotonation of the hydroxyl groups enhances the nucleophilic character of the oxygen atoms, making them more reactive toward Gold(3+) ions in $HAuCl_4$ and facilitating both reduction and binding to the gold surface.

In the following sections, we provide a breakdown of the synthesis and characterization of each GNP structure. We begin with describing the step-by-step synthesis method of each GNP structure, followed by characterization using UV-Vis spectroscopy, Zetasizer analysis, and ICP-OES. In the UV-Vis spectroscopy section, we identify the surface plasmon resonance (SPR) peak for each nanostructure. The Zetasizer section will present data on the average diameter, polydispersity, mean peak intensity, and zeta potential of each GNP structure. The ICP-OES section details the yield concentration of each synthesis protocol.

2.2 Materials

For the synthesis of GNPs the following materials were used, Curcumin (≥98% purity, Alexis Biochemicals, San Diego, CA, USA), sodium citrate dihydrate (S25545-Fisher Scientific, Waltham, MA, USA), and gold(III) chloride trihydrate (520918-Aldrich, St. Louis, MO, USA). All synthesis protocols utilized ultrapure Milli-Q water derived from the Millipore Gradient A10 water purification system (Merck Millipore, MA, USA). Milli-Q water will be referred to as ultrapure water.

2.3 Synthesis

2.3.1 Citrate-coated Gold Nanoparticles

To synthesize citrate-coated GNPs the Turkevich method was used (1). To begin 50 mL of ultrapure water was heated and stirred using a stirring hot plate in an Erlenmeyer flask. A stock solution of 1 mM $HAuCl_4 \cdot 3H_2O$ was prepared in ultra-pure water. Then, 20 mL of this 1 mM $HAuCl_4 \cdot 3H_2O$ solution was transferred to the Erlenmeyer flask, heated to a rolling boil, and maintained under reflux with vigorous stirring. Separately, a 1% sodium citrate solution was prepared in ultra-pure water. Once the gold solution was boiling, 2 mL of the 1% sodium citrate solution was quickly added. Heating and stirring were continued under reflux for 15 minutes to ensure complete reaction.

During this time, the solution gradually changed color from yellow to brown to ruby red, indicating the formation of gold nanoparticles. The ruby-red solution was then allowed to cool to room temperature with continuous stirring, yielding Cit-GNPs. To remove any unreacted components, the solution was transferred, using a 0.22 um filter, into 3.5 kDa dialysis tubing and dialyzed against 2 L of ultrapure water for 48 hours, with ultrapure water changes every 12-24 hours.

2.3.2 Curcumin-coated Gold Nanoparticles

To synthesize curcumin-coated GNPs the method described in Aborig et al., and Nambiar et al., was used (3,4). A stock solution of 100 mM $HAuCl_4 \cdot 3H_2O$ was prepared in ultra-pure water. Next, 10 mL of a 1.0 mM curcumin solution was prepared, using 10 mM NaOH to promote deprotonation of the phenolic and enolic groups. The curcumin solution was then filtered using a 0.22 um filter. The curcumin solution was placed in a water bath sonicator at 44 ◦C, and 200 µL of 100 mM $HAuCl_4 \cdot 3H_2O$ was added dropwise. The formation of Curc-GNPs was indicated by a distinct color change from clear to yellow to ruby red. To remove any unreacted components, the solution

was transferred, using a 0.22 um filter, into 3.5 kDa dialysis tubing and dialyzed against 2 L of ultrapure water for 48 hours, with ultrapure water changes every 24 hours (4).

2.4 Characterization

2.4.1 UV-Vis Spectroscopy

GNP formation was confirmed using UV-Vis spectroscopy by identifying the characteristic absorbance band of spherical GNPs in the visible wavelength range (5–8). These measurements were done using the Molecular Devices SpectraMax M5 Plate Reader over the 300–750 nm range at 0.5 nm intervals, using 1 mL of GNP sample in a 1.5 mL PMMA cuvette. A single strong absorbance band between 500–550 nm indicates successful GNP formation. UV-Vis was used to identify the SPR peak for Curc-GNP and Cit-GNP, and to confirm the formation of GNPs.

2.4.2 DLS

To measure the hydrodynamic diameter, size distribution (polydispersity index, PDI), and zeta potential of the dialyzed GNP samples the Malvern Zetasizer Ultra ZS (Malvern Instruments Ltd., Malvern, UK) was used. The DLS provides information on the hydrodynamic size and size distribution of nanoparticles, as indicated by the PDI (9,10). Zeta potential was measured to estimate the apparent surface charge and colloidal stability of GNPs in aqueous suspension (9,11,12). For size and zeta potential measurements, 1.0 mL of each sample was transferred to a disposable PMMA cuvette or 0.70 mL of each sample was transferred to a DTS1070 disposable zeta potential cell respectively. These measurements were performed in triplicate at 25◦C, and the average diameter (nm), PDI, intensity-weighted mean peak and average zeta potential (in mV) were recorded. The number of significant figures was standardized by rounding the standard deviation to two significant figures and rounding the corresponding mean to the same decimal place. This was done to avoid implying greater analytical precision than supported by the replicate measurements.

2.4.3 ICP-OES

To measure the concentration of GNPs an inductively coupled plasma optical emission spectrometer (ICP-OES, Teledyne Leeman Labs, USA) was used after the completion of dialysis or centrifugation. Measurements were taken in triplicate by dividing samples into three vials, then each vial was analysed three times per ICP-OES run. To prepare the GNPs for measurement, the gold was converted back into its ionic form $HAuCl_4$ by adding 4 mL of freshly prepared aqua regia (1:3 mixture of HNO_3 to HCl) to each vial to dissolve the GNPs (4,13,14). A calibration curve for quantifying Au content was generated using a blank and five gold standards ranging from 1 to 100 µg/mL. All calibration curves had correlation coefficients > 0.995 and the calibration was verified using a standard prepared from an alternative source of gold and was considered acceptable if results were within ±10% of the expected value. The method detection limit (MDL) for Au was 1ppm, and the limit of quantitation (LOQ) was 10 ppm. Instrument analysis was performed on ^{197}Au, with ^{89}Y being used as an internal standard to correct for variations in plasma conditions. An ^{55}Mn solution was used to perform peaking to optimize the camera.

Aliquots of 0.5, 1.0, and 1.5 mL of each GNP suspension were diluted to a final volume of 50 mL with ultrapure water prior to analysis after being dissolved with aqua-regia. Dilution factors were calculated based on the ratio of final volume to aliquot volume. This method was adapted from Aborig et al., (4). The ICP-OES gold concentrations output (mg/L) were converted to final nanoparticle concentrations (µg/mL) by applying the corresponding dilution factors (DF), as seen in Equation 1, where $C_{GNP\ Final}$ is the final gold nanoparticle concentration after dilution correction, $=$ $C_{ICP-OES}$ is the gold concentration measured by ICP-OES, and DF is the dilution factor applied during sample preparation. Final concentrations were determined as the mean ± standard deviation of the three dilutions to account for instrumental variability and ensure analytical reproducibility. The

number of significant figures was standardized by rounding the standard deviation to one significant figure and rounding the corresponding mean to the same decimal place. This was done to avoid implying greater analytical precision than supported by the triplicate measurements.

$$C_{GNP\ Final} = C_{ICP-OES}\left(\frac{mg}{L}\right) \times DF \quad (1)$$

2.5 Results and Discussion

2.5.1 UV-Vis Spectroscopy

UV-Visible spectroscopy is commonly used to characterize the optical properties of gold nanoparticles because the absorbance profile is directly influenced by particle size, morphology, surface chemistry, concentration, and aggregation state (5–8,11). In GNPs, the characteristic absorbance band arises from surface plasmon resonance (SPR), which occurs when conduction electrons on the gold surface oscillate collectively in response to incident light. This optical feature is particularly useful as an efficient and cost-effective post-synthesis confirmation of nanoparticle formation. In general, small spherical GNPs exhibit a distinct SPR peak within the visible region, commonly between approximately 500 and 550 nm, while larger, aggregated, or non-spherical particles can show broader peaks and red-shifted absorbance profiles.

In this study, both Cit-GNPs and Curc-GNPs showed SPR peaks in the expected wavelength range for spherical GNPs (See Figure 2.1). The Cit-GNP spectrum showed a maximum absorbance near 520 nm, while Curc-GNPs showed a strong absorbance band within the same general region, with a peak around 525 nm (Figure 2.1). The appearance of a single SPR peak near 520 nm is consistent with successful formation of small, dispersed, spherical GNPs, since aggregation or changes in the surrounding dielectric environment can broaden or red-shift the absorbance band (15–18). The SPR peak position observed for Curc-GNPs is also comparable to Akbari et al., who

reported confirmation of Curc-AuNP synthesis by a plasmonic peak at 526 nm (19). Similarly, Aborig et al., used UV-Vis analysis to characterize Curc-GNPs developed for prostate cancer radiosensitization, where the presence of a visible-range SPR peak at 525 nm supported successful nanoparticle formation (4).

The UV-Vis spectra also showed that Curc-GNPs had a substantially higher absorbance intensity than Cit-GNPs as seen in Figure 2.1. This difference may be influenced by differences in final gold concentration since the ICP-OES results showed that Curc-GNPs had a much higher final concentration (361 ± 15 μg/mL) than Cit-GNPs (20 ± 4 μg/mL) and starting gold synthesis volume and concentration (20). Therefore, the higher absorbance intensity observed for Curc-GNPs should not be interpreted only as a difference in particle size or optical efficiency; rather, it is likely also a reflection of the higher nanoparticle concentration in the Curc-GNP suspension. This interpretation is consistent with prior work showing that absorbance intensity at the SPR peak is related to GNP concentration when particle size and aggregation state are comparable (4,5).

The Curc-GNP spectrum also showed a broader absorbance profile and higher baseline absorbance across the visible wavelength range compared with Cit-GNPs. This may be partly due to the curcumin coating, because curcumin itself absorbs strongly in the visible range and can contribute to the overall absorbance profile of the formulation (3,4,12,21). Additionally, the surface coating can alter the local dielectric environment surrounding the gold core, which can affect the SPR peak position and spectral shape slightly (3,4,7,12,21). Overall, the presence of single SPR peaks near 520 nm in both formulations supports successful spherical GNP synthesis, while the higher absorbance intensity of Curc-GNPs is likely influenced by the higher final gold concentration measured by ICP-OES, particle size, optical path length and coating (4–7,19,22,23).

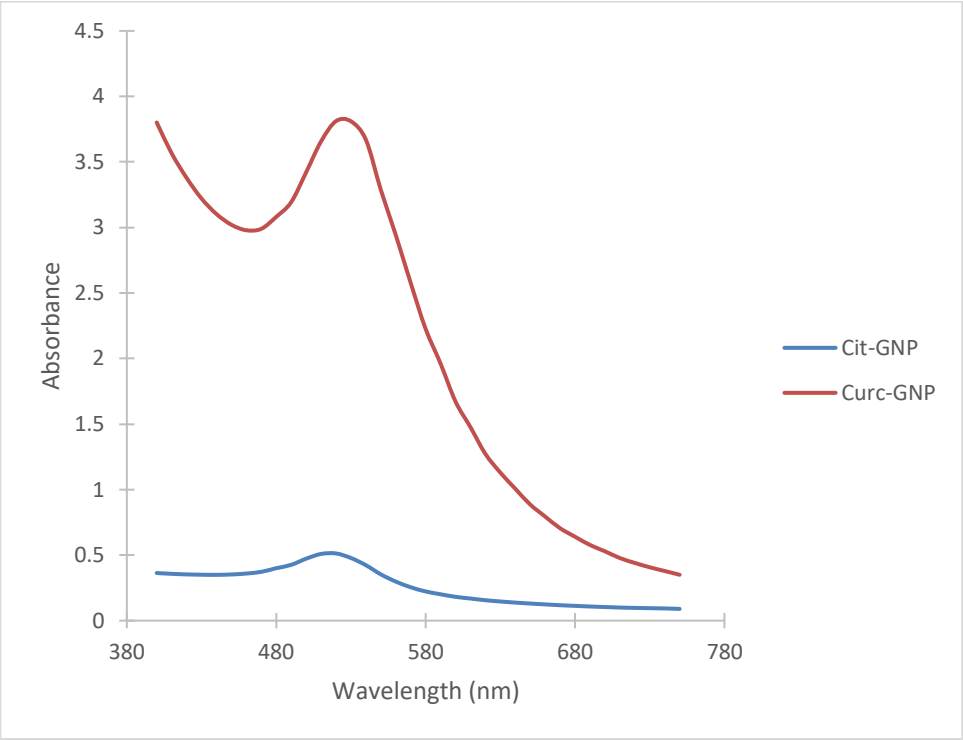


Figure 2.1: UV-Vis Spectra of Citrate- and Curcumin- GNPs

2.5.2 DLS

Dynamic light scattering (DLS) is a low-cost analytical tool used for measuring the hydrodynamic size of nanoparticles and colloids in liquid solutions. In the context of GNPs, since they have a strong light scattering at or around their plasmon resonance wavelength, DLS has been found to be an easy, high-throughput method to measure the diameter and zeta potential of various GNPs (9,10).

The DLS measurements are summarized in Table 2.1. The hydrodynamic diameters of Curc-GNPs and Cit-GNPs are 18.36 ± 0.27 and 22.55 ± 0.18 nm respectively, suggesting greater agreement between the overall average and the main intensity peak. The diameter and peak intensities for each sample are shown in Figure 2.3. The corresponding intensity-weighted peak means were 22.46 ± 0.09 nm for Curc-GNPs and 21.53 ± 0.52 nm for Cit-GNPs, this difference likely reflects slight

broadening or skewing of the size distribution. Both samples showed a single dominant intensity peak with 100% peak area. These results indicate that both synthesis approaches produced small GNPs with a single major particle population. The narrow, single-peak distributions observed in this study are important because nanoparticle size influences downstream biological behaviour, including membrane association, cellular uptake, intracellular trafficking, biodistribution, and clearance (24).

The Z-average hydrodynamic diameter and the intensity-weighted Peak 1 mean diameter were not identical because they are derived from different DLS outputs. DLS measures the hydrodynamic size of nanoparticles in suspension, rather than the dry metallic core diameter, and is influenced by the diffusion behaviour and light-scattering properties of the particles (9). The Z-average diameter represents an overall average calculated from the full DLS signal, whereas the intensity-weighted peak 1 mean diameter represents the centre of the dominant size population in the intensity-weighted distribution. Because gold nanoparticles scatter light strongly, and scattering intensity increases approximately with particle diameter to the sixth power, small differences in particle-size distribution or the presence of slightly larger particles can disproportionately affect intensity-based measurements (10). Therefore, the Z-average diameter and Intensity-weighted Peak 1 mean diameter are not expected to be identical, since the sample has some distribution width, as reflected by the PDI values.

Table 2.1: DLS Parameters for GNPs

GNPs	Diameter (nm)	PDI	Intensity-weighted Peak 1 mean diameter (nm)	Peak 1 Area Intensity	Zeta Potential (mV)
Curc-GNPs	18.36 ± 0.27	0.225 ± 0.010	22.46 ± 0.09	100.00	-43.5 ± 1.2
Cit-GNPs	22.55 ± 0.18	0.278 ± 0.005	21.53 ± 0.52	100.00	-40.0 ± 4.6

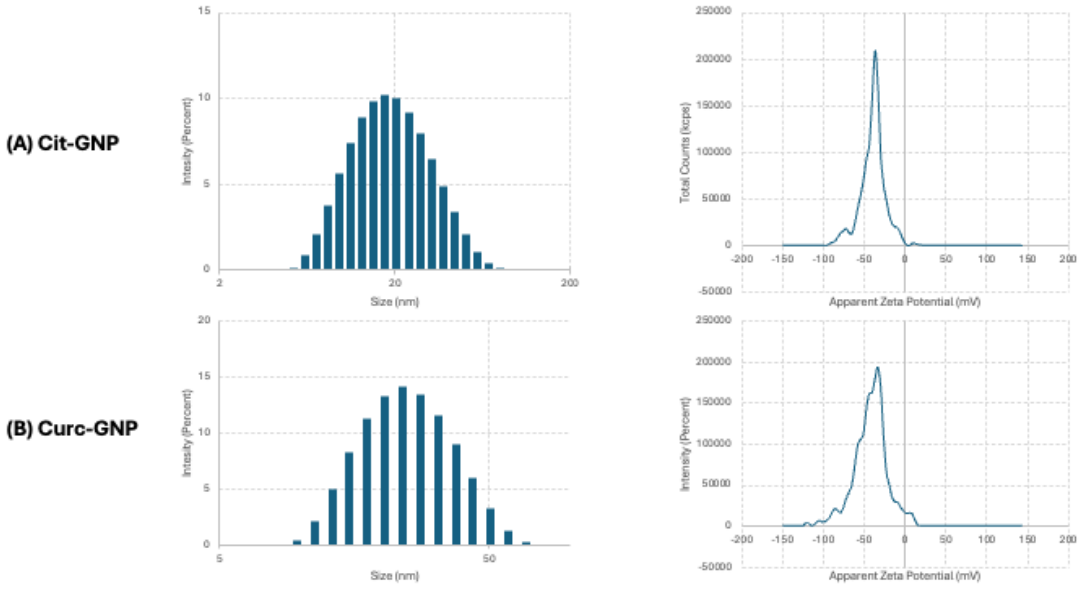


Figure 2.2: DLS Sizes and Apparent Zeta Potentials of Curc- and Cit-GNPs

The Cit-GNP diameter measured in our study is consistent with expected sizes for Turkevich-type citrate reduction. Dong et al., optimized the Turkevich method and reported that AuNPs in the 15–30 nm range can be synthesized with well-defined size and shape and relatively narrow size

distributions (1). The Cit-GNP diameter of 22.56 ± 0.18 nm obtained here falls within this expected range, supporting the reproducibility of the adapted Turkevich synthesis protocol. Although the reaction volume used in this study was lower than in larger-scale Turkevich protocols, the resulting hydrodynamic size remained within the typical range for citrate-reduced spherical GNPs.

The Curc-GNP diameter of 18.36 ± 0.27 nm was also consistent with previously reported curcumin-mediated GNP systems. The lower hydrodynamic size measured in the present study suggests that the Curc-GNP formulation remained relatively well dispersed after dialysis, since DLS is highly sensitive to aggregate formation and because increases in hydrodynamic diameter can indicate particle association or reduced colloidal stability (9,10,25). Akbari et al., synthesized Curc-AuNPs through a green synthesis procedure and reported a TEM diameter of 21.7 nm and hydrodynamic diameter of 45.1 nm (19). Sindhu et al., synthesized curcumin-coated AuNPs and reported a TEM diameter of approximately 20 nm, that demonstrated biocompatibility (26). Kalantari and Turner also compared biologically and chemically synthesized AuNPs and reported average sizes of 10 nm for curcumin-conjugated AuNPs and chemically synthesized sodium citrate AuNPs, further supporting that both curcumin- and citrate-based synthesis methods can generate small spherical AuNPs suitable for biomedical applications (12). The Curc-GNP size observed in this study falls within the small nanoparticle range reported for curcumin-conjugated GNPs, however, differences in hydrodynamic diameter and zeta potential between studies are expected because these parameters depend on synthesis conditions, coating density, purification method, and measurement medium.

A key parameter obtained from the DLS is the polydispersity index (PDI), which provides an estimate of the size uniformity or homogeneity of nanoparticles in solution. The PDI values for Curc-GNP and Cit-GNP were 0.225 ± 0.010 and 0.278 ± 0.005 respectively. The PDI is a critical parameter for our project since small variations in NP size can cause significant changes in biological

interactions, like cellular uptake and intracellular localization (24). Therefore, a narrow size distribution ensures consistency in experimental outcomes. For the pharmaceutical applications of nanoparticles, a PDI of 0.3 or less was considered acceptable, since lower PDI values indicate a narrower and more uniform particle size distribution (27). Based on these criteria, both Curc-GNPs and Cit-GNPs had acceptable polydispersity values. The slightly lower PDI observed for Curc-GNPs suggests that the curcumin-mediated green synthesis produced a somewhat narrower size distribution than the adapted citrate method under the conditions used in this study. This is important for downstream biological studies because more uniform nanoparticle populations reduce variability in uptake, cytotoxicity, and radiosensitization experiments.

The DLS was also used to measure the zeta potential to evaluate the apparent surface charge and colloidal stability of the synthesized GNPs. Both formulations had strongly negative zeta potentials, with Curc-GNPs measuring -43.5 ± 1.2 mV and Cit-GNPs measuring -40.0 ± 4.6 mV as seen in Table 2.1 and Figure 2.3. The Cit-GNP zeta potential measured in our study aligns with Ivanov et al., who reported citrate-reduced AuNPs with an average zeta potential of -39.7 ± 0.7 mV, supporting the conclusion that the surface charge obtained here is consistent with stable citrate-coated AuNPs reported in literature (28). Kalantari and Turner reported similar negative surface charges for curcumin-conjugated AuNPs and chemically synthesized citrate AuNPs, with zeta potentials of −36.3 mV and −40.4 mV, respectively (12). These values indicate that both nanoparticle suspensions had strong electrostatic repulsion in water, which would reduce particle–particle attraction and help limit aggregation (25,28,29). This interpretation is consistent with the broader caution that zeta potential values are useful for assessing surface charge and potential electrostatic stabilization, but they should not be used alone to predict nanoparticle stability across different media or storage conditions, since stability can be influenced by experimental conditions and ionic strength (29,30). Therefore, the

values obtained in our study are comparable with the literature and support the conclusion that both Curc-GNPs and Cit-GNPs were colloidally stable in our aqueous suspension.

The negative zeta potential of Cit-GNPs is expected because citrate molecules adsorb to the gold surface and provide an anionic stabilizing layer (28). Cit-GNPs are primarily stabilized by electrostatic repulsion between negatively charged citrate groups on the nanoparticle surface (28). However, this stabilization can be weakened in biological media, where salts and media components can screen surface charge and promote aggregation (11). Barbero et al., reported that sodium citrate-stabilized AuNPs can be destabilized when dispersed in cell culture media, leading to aggregation and sedimentation, although protein corona formation under certain supplemented conditions may improve colloidal stability (11). Alkilany et al., reported that citrate-capped GNPs can also be sensitive to processing stresses and aggregate irreversibly after freeze-thawing and lyophilization, highlighting that citrate stabilization may be condition dependent rather than universally robust (30). Therefore, while the Cit-GNPs synthesized in this study showed a strongly negative zeta potential in ultrapure water, their stability in biological media or storage conditions may differ from their aqueous stability (29,30). This may limit the use of Cit-GNPs in biological applications and upscale use, since aggregation can affect the size of GNPs and ultimately effect GNP uptake (24). In contrast, Curc-GNPs may derive their negative surface charge from deprotonated phenolic and enolic groups of curcumin associated with the gold surface. Curcumin contains phenolic hydroxyl and β-diketone groups that can participate in gold reduction, surface binding, and stabilization, allowing curcumin to act as both a reducing and capping agent during AuNP synthesis (21). This is consistent with the green synthesis rationale described earlier in this chapter, where curcumin acts as both a reducing and stabilizing agent.

Although both zeta potentials indicate good aqueous stability, the surface coatings may behave differently in biological media (25). Citrate coatings provide electrostatic stabilization, but this can weaken in ionic solutions because salts can screen surface charge and promote aggregation. Curcumin coating may provide additional stabilization through surface-bound organic groups and possible interactions with serum proteins under biological conditions by forming a protein corona (3,21,31–33). Similarly, curcumin has been reported to function as both a reducing and capping agent during GNP synthesis, allowing surface-bound curcumin groups to contribute to nanoparticle stabilization (21). This distinction is important for later biological applications because nanoparticle stability in aqueous synthesis conditions does not always predict stability in cell culture medium or serum-containing environments. Aborig et al., similarly emphasized that Curc-GNPs showed favourable stability characteristics relative to conventional formulations, likely due to curcumin-associated surface chemistry and protein interactions (4).

2.5.3 ICP-OES

To quantify the final gold concentration of the synthesized nanoparticle solutions after filtration ICP-OES was used. Curc-GNPs had a final average concentration of 361 ± 15 μg/mL, whereas Cit-GNPs had a final average concentration of 20 ± 4 μg/mL as seen in Tables 2.2-2.3 for each GNP sample. This indicates that the curcumin-mediated green synthesis produced a substantially more concentrated nanoparticle suspension than the adapted citrate reduction method under the experimental conditions used in this study. This makes sense since a larger starting volume and lower gold concentration was used when synthesizing Cit-GNPs. Even though Cit-GNP yielded lower concentrations they could easily be concentrated using centrifugation. Dong et al., noted that the Turkevich method is widely used because it can produce stable and reproducible spherical AuNPs, though particle size and yield are sensitive to reaction parameters including reactant ratio, batch size,

initial gold concentration, and temperature, so changing the starting synthesis parameters is risky since this could drastically change the GNP size (1).

Table 2.2: ICP-OES Parameters for Curc-GNPs

Volume (mL)	ICP Concentration (mg/L)	Dilution Factor	Final Concentration (ug/mL)
0.5	3.407	100.000	340.7167
1.0	7.453	50.000	372.635
1.5	11.175	33.333	372.504
			Avg: 361 ±15

Table 2.3:ICP-OES Parameters for Cit-GNPs

Volume (mL)	ICP Concentration (mg/L)	Dilution Factor	Final Concentration (ug/mL)
0.5	0.1662	100.000	16.620
1.0	0.3695	50.000	18.477
1.5	0.7774	33.333	25.912
			Avg: 20 ±4

2.6 Conclusion

Overall, the characterization results confirm successful synthesis of both Curc-GNPs and Cit-GNPs. UV-Vis spectra demonstrated SPR peaks consistent with spherical GNP formation (5,6). DLS showed hydrodynamic diameters within the small nanoparticle range with acceptable PDI values, zeta potential measurements indicated strong negative surface charge and aqueous colloidal stability

(9,10). ICP-OES confirmed that Curc-GNP synthesis produced a substantially higher final gold concentration than the adapted citrate method. Collectively, these findings support the use of both formulations in downstream biological assays, while also identifying Curc-GNPs as the more concentrated and slightly more monodisperse formulation under the synthesis conditions used in this study.

References:

1. Dong J, Carpinone PL, Pyrgiotakis G, Demokritou P, Moudgil BM. Synthesis of Precision Gold Nanoparticles Using Turkevich Method. KONA Powder Part J. 2020;37:224–32. doi:10.14356/kona.2020011

2. Zhao J, Friedrich B. Synthesis of Gold Nanoparticles via Chemical Reduction Method. 2015 Oct 14. doi:10.13140/RG.2.2.28933.35049

3. Nambiar S, Osei E, Fleck A, Darko J, Mutsaers AJ, Wettig S. Synthesis of curcumin-functionalized gold nanoparticles and cytotoxicity studies in human prostate cancer cell line. Appl Nanosci. 2018 Mar 1;8(3):347–57. doi:10.1007/s13204-018-0728-6

4. Aborig M, Alsefaou M, Osei E, Wettig S. Engineered dual-functional gold nanoparticles enhance radiosensitization in prostate cancer cells: synergistic action of curcumin and gold. Nanoscale Adv. 2025 Sep 24;7(19):5964–77. doi:10.1039/D5NA00376H

5. Haiss W, Thanh NTK, Aveyard J, Fernig DG. Determination of Size and Concentration of Gold Nanoparticles from UV−Vis Spectra. Anal Chem. 2007 Jun 1;79(11):4215–21. doi:10.1021/ac0702084

6. Huang X, El-Sayed MA. Gold nanoparticles: Optical properties and implementations in cancer diagnosis and photothermal therapy. J Adv Res. 2010 Jan 1;1(1):13–28. doi:10.1016/j.jare.2010.02.002

7. Amendola V, Pilot R, Frasconi M, Maragò OM, Iatì MA. Surface plasmon resonance in gold nanoparticles: a review. J Phys Condens Matter. 2017 Apr;29(20):203002. doi:10.1088/1361-648X/aa60f3

8. Jain PK, Lee KS, El-Sayed IH, El-Sayed MA. Calculated Absorption and Scattering Properties of Gold Nanoparticles of Different Size, Shape, and Composition: Applications in Biological Imaging and Biomedicine. J Phys Chem B. 2006 Apr 1;110(14):7238–48. doi:10.1021/jp057170o

9. Jans H, Liu X, Austin L, Maes G, Huo Q. Dynamic Light Scattering as a Powerful Tool for Gold Nanoparticle Bioconjugation and Biomolecular Binding Studies. Anal Chem. 2009 Nov 15;81(22):9425–32. doi:10.1021/ac901822w

10. Zheng T, Bott S, Huo Q. Techniques for Accurate Sizing of Gold Nanoparticles Using Dynamic Light Scattering with Particular Application to Chemical and Biological Sensing Based on Aggregate Formation. ACS Appl Mater Interfaces. 2016 Aug 24;8(33):21585–94. doi:10.1021/acsami.6b06903

11. Barbero F, Michelini S, Moriones OH, Patarroyo J, Rosell J, F. Gusta M, et al. Role of Common Cell Culture Media Supplements on Citrate-Stabilized Gold Nanoparticle Protein Corona Formation, Aggregation State, and the Consequent Impact on Cellular Uptake. Bioconjug Chem. 2022 Aug 17;33(8):1505–14. doi:10.1021/acs.bioconjchem.2c00232

12. Kalantari H, Turner RJ. Structural and antimicrobial properties of synthesized gold nanoparticles using biological and chemical approaches. Front Chem. 2024 Nov 13;12. doi:10.3389/fchem.2024.1482102

13. Liu J, von der Kammer F, Zhang B, Legros S, Hofmann T. Combining spatially resolved hydrochemical data with in-vitro nanoparticle stability testing: Assessing environmental behavior of functionalized gold nanoparticles on a continental scale. Environ Int. 2013 Sep 1;59:53–62. doi:10.1016/j.envint.2013.05.006

14. Oberländer J, Ayerbe R, Cabellos J, da Costa Marques R, Li B, Günday-Türeli N, et al. Higher Loading of Gold Nanoparticles in PAD Mesenchymal-like Stromal Cells Leads to a Decreased Exocytosis. Cells. 2022 Jul 28;11(15):2323. doi:10.3390/cells11152323 PubMed PMID: 35954168; PubMed Central PMCID: PMC9367297.

15. Saha K, Agasti SS, Kim C, Li X, Rotello VM. Gold Nanoparticles in Chemical and Biological Sensing. Chem Rev. 2012 May 9;112(5):2739–79. doi:10.1021/cr2001178 PubMed PMID: 22295941; PubMed Central PMCID: PMC4102386.

16. Kelly KL, Coronado E, Zhao LL, Schatz GC. The Optical Properties of Metal Nanoparticles: The Influence of Size, Shape, and Dielectric Environment. J Phys Chem B. 2003 Jan 1;107(3):668–77. doi:10.1021/jp026731y

17. Sangwan S, Seth R. Synthesis, Characterization and Stability of Gold Nanoparticles (AuNPs) in Different Buffer Systems. J Clust Sci. 2022 Mar 1;33(2):749–64. doi:10.1007/s10876-020-01956-8

18. Sudhesh P, Sruthi S, Jose M, Vyshnavi K, Aiswarya P, Manu R. Naked eye detection of hydrogen peroxide via curcumin functionalised gold nanoparticles. Sci Rep. 2025 May 15;15(1):16896. doi:10.1038/s41598-025-01613-y

19. Akbari A, Shokati Eshkiki Z, Mayahi S, Amini SM. In-vitro investigation of curcumin coated gold nanoparticles effect on human colorectal adenocarcinoma cell line. Nanomedicine Res J. 2022 Jan 1;7(1):66–72. doi:10.22034/nmrj.2022.01.006

20. Contreras-Trigo B, Díaz-García V, Guzmán-Gutierrez E, Sanhueza I, Coelho P, Godoy SE, et al. Slight pH Fluctuations in the Gold Nanoparticle Synthesis Process Influence the Performance of the Citrate Reduction Method. Sensors. 2018 Jul 12;18(7):2246. doi:10.3390/s18072246 PubMed PMID: 30002306; PubMed Central PMCID: PMC6068536.

21. Singh DK, Jagannathan R, Khandelwal P, Abraham PM, Poddar P. In situ synthesis and surface functionalization of gold nanoparticles with curcumin and their antioxidant properties: an experimental and density functional theory investigation. Nanoscale. 2013 Feb 15;5(5):1882–93. doi:10.1039/C2NR33776B

22. Bahmanyar Z, Mohammadi F, Gholami A, Khoshneviszadeh M. Effect of different physical factors on the synthesis of spherical gold nanoparticles towards cost-effective biomedical

applications. IET Nanobiotechnol. 2022 Nov 3;17(1):1–12. doi:10.1049/nbt2.12100 PubMed PMID: 36326590; PubMed Central PMCID: PMC9932436.

23. Aborig M, Malik PRV, Nambiar S, Chelle P, Darko J, Mutsaers A, et al. Biodistribution and Physiologically-Based Pharmacokinetic Modeling of Gold Nanoparticles in Mice with Interspecies Extrapolation. Pharmaceutics. 2019 Apr;11(4):179. doi:10.3390/pharmaceutics11040179

24. Liu X, Huang N, Li H, Jin Q, Ji J. Surface and Size Effects on Cell Interaction of Gold Nanoparticles with Both Phagocytic and Nonphagocytic Cells. Langmuir. 2013 Jul 23;29(29):9138–48. doi:10.1021/la401556k

25. Shaabani E, Amini SM, Kharrazi S, Tajerian R. Curcumin coated gold nanoparticles: synthesis, characterization, cytotoxicity, antioxidant activity and its comparison with citrate coated gold nanoparticles. Nanomedicine J. 2017 Apr 1;4(2):115–25. doi:10.22038/nmj.2017.8413

26. Sindhu K, Rajaram A, Sreeram KJ, Rajaram R. Curcumin conjugated gold nanoparticle synthesis and its biocompatibility. RSC Adv. 2013 Dec 2;4(4):1808–18. doi:10.1039/C3RA45345F

27. Danaei M, Dehghankhold M, Ataei S, Hasanzadeh Davarani F, Javanmard R, Dokhani A, et al. Impact of Particle Size and Polydispersity Index on the Clinical Applications of Lipidic Nanocarrier Systems. Pharmaceutics. 2018 Jun;10(2):57. doi:10.3390/pharmaceutics10020057

28. Ivanov MR, Bednar HR, Haes AJ. Investigations of the Mechanism of Gold Nanoparticle Stability and Surface Functionalization in Capillary Electrophoresis. ACS Nano. 2009 Feb 24;3(2):386–94. doi:10.1021/nn8005619 PubMed PMID: 19236076; PubMed Central PMCID: PMC2707777.

29. Pochapski DJ, Carvalho dos Santos C, Leite GW, Pulcinelli SH, Santilli CV. Zeta Potential and Colloidal Stability Predictions for Inorganic Nanoparticle Dispersions: Effects of Experimental Conditions and Electrokinetic Models on the Interpretation of Results. Langmuir. 2021 Nov 16;37(45):13379–89. doi:10.1021/acs.langmuir.1c02056

30. Alkilany AM, Abulateefeh SR, Mills KK, Bani Yaseen AI, Hamaly MA, Alkhatib HS, et al. Colloidal Stability of Citrate and Mercaptoacetic Acid Capped Gold Nanoparticles upon Lyophilization: Effect of Capping Ligand Attachment and Type of Cryoprotectants. Langmuir. 2014 Nov 25;30(46):13799–808. doi:10.1021/la504000v

31. Patra D, El Kurdi R. Curcumin as a novel reducing and stabilizing agent for the green synthesis of metallic nanoparticles. Green Chem Lett Rev. 2021 Jul 3;14(3):474–87. doi:10.1080/17518253.2021.1941306

32. Baruah K, Singh AK, Kumari K, Nongbri DL, Jha AN, Singha Roy A. Interactions of Turmeric- and Curcumin-Functionalized Gold Nanoparticles with Human Serum Albumin: Exploration of Protein Corona Formation, Binding, Thermodynamics, and Antifibrillation Studies. Langmuir. 2024 Jan 16;40(2):1381–98. doi:10.1021/acs.langmuir.3c03032

33. Bashiri G, Padilla MS, Swingle KL, Shepherd SJ, Mitchell MJ, Wang K. Nanoparticle protein corona: from structure and function to therapeutic targeting. Lab Chip. 2023 Mar 14;23(6):1432–66. doi:10.1039/D2LC00799A

Chapter 3: In Vitro Study of Gold Nanoparticles in Prostate Cancer Spheroids

3.1 Introduction

Gold nanoparticles (GNPs) have been widely investigated as potential radiosensitizers because their physicochemical properties allow them to enhance the biological effects of ionizing radiation. In radiotherapy, GNP-mediated radiosensitization has been associated with both physical and chemical mechanisms, including increased local radiation interaction, secondary electron production, reactive oxygen species (ROS) generation, oxidative stress, DNA damage, mitochondrial injury, and altered cellular recovery after irradiation (1). These mechanisms suggest that GNPs may increase radiation-induced cancer cell death and reduce the radiation dose required to achieve comparable therapeutic effects. Previous prostate cancer (PCa) studies have shown that GNPs can enhance radiation response; however, the extent of radiosensitization depends on factors such as radiation energy, nanoparticle size, surface coating, concentration, cell type, and intracellular localization (2–6).

The surface chemistry of GNPs is especially important because the coating influences colloidal stability, cellular uptake, intracellular distribution, and interaction with biological membranes (1,7). Conventional Cit-GNPs are commonly used as comparison formulations because citrate can act as both a reducing and capping/stabilizing agent during Turkevich-style synthesis. Citrate also provides electrostatic stabilization of the gold nanoparticle surface, helping to maintain particle dispersion in aqueous suspension (8-10). However, the uptake and biological effects of Cit-GNPs may be limited by their surface properties, as nanoparticle internalization and radiosensitization depend strongly on physicochemical properties, coating chemistry, cellular localization, and biological targets (1,6). In contrast, functionalized GNPs can be designed to improve nanoparticle–

cell interactions and enhance radiosensitization, as shown by glucose-bound GNPs in DU145 cells and Curc-GNPs in PC-3 prostate cancer cells (2,11). Several studies using surface-modified or targeted GNPs have shown that functionalization can improve nanoparticle internalization and increase radiation sensitivity in prostate cancer models (2,4,5,12). These findings support the rationale for comparing conventional Cit-GNPs with bioactive Curc-GNPs in PCa spheroids.

Curcumin is a bioactive compound of interest because it has been reported to affect several cellular processes relevant to cancer treatment. At the membrane level, curcumin can interact with lipid bilayers and alter membrane structure, which may influence how effectively curcumin-coated nanoparticles can associate with the plasma membrane and enter cells (13,14). Curcumin has also been reported to influence intracellular pathways associated with proliferation, apoptosis, cytoskeletal organization, oxidative stress, autophagy, cell-cycle arrest, and senescence (15–21). These biological effects are relevant to radiosensitization because reduced proliferative capacity, increased oxidative stress, impaired recovery, and senescence or apoptosis induction may decrease the ability of irradiated cells to retain clonogenic survival. Clinically this has implications in preventing how fast and if tumours proliferate after radiation treatment, as well as how much radiation needs to be delivered to achieve an effective therapeutic dose.

Therefore, Curc-GNPs may function as dual-action nanoparticles by combining gold-mediated radiation enhancement with curcumin-associated biological effects. Aborig et al., demonstrated that Curc-GNPs enhanced radiosensitization in prostate cancer cells, likely through the combined effects of gold and curcumin, including increased ROS production and improved radiation response compared with conventional formulations (11). Similarly, Yadav et al., supported the rationale for gold-curcumin nanoformulations by suggesting that these types of nanoparticles may enhance radiation response through complementary gold-mediated and curcumin-mediated

mechanisms (22). Despite the promising literature, most nanoparticle uptake and radiosensitization studies are performed in two-dimensional monolayer cultures, which do not fully reproduce the structural and transport barriers present in tumour tissue *in vivo*.

Three-dimensional tumour spheroids provide a more physiologically relevant *in vitro* model than conventional two-dimensional monolayers because they can better incorporate tumour-like features such as compact cell-cell interactions, nutrient and oxygen gradients, diffusion limitations, and treatment resistance. These characteristics can influence nanoparticle penetration, uptake, and radiation response (23-26). In spheroids, nanoparticle delivery is affected by extracellular matrix interactions, spheroid architecture, incubation time, nanoparticle size, charge, and surface chemistry (23,24,27,28). These factors are important to consider in radiosensitization studies because for GNPs to be effective radiosensitizers, they must be sufficiently internalized or localized near intracellular targets, like the nucleus (3). The use of DU145 spheroids is relevant to advanced prostate cancer research because DU145 cells are androgen-insensitive and are derived from a metastatic prostate cancer site (29,30). Therefore, while this model does not completely model CRPC, it provides a useful platform for evaluating Curc-GNP uptake and radiosensitization in an androgen-insensitive, tumour-like prostate cancer system.

Previous studies have shown that GNP uptake is strongly influenced by nanoparticle physicochemical properties. Chithrani et al., demonstrated that GNP uptake depends on nanoparticle size and shape, while Chithrani and Chan further showed that protein-coated GNP internalization and removal are size dependent (31,32). Huang et al., also showed that smaller GNPs can have improved penetration and localization in cancer cells, multicellular spheroids, and tumours *in vivo* (33). More recently, Bilgi et al., used machine learning to identify predictors of GNP uptake, and found that particle size, zeta potential, nanoparticle concentration, and exposure duration were the most

important drivers of cellular uptake (34). Together, these studies indicate that nanoparticle uptake in spheroids is not determined by only the gold core alone, but through a combination of coating type, size, charge, concentration, incubation time, and three-dimensional tumour structure.

Although Curc-GNPs have shown promise as radiosensitizers in PCa monolayer models, it remains important to determine whether they can be effectively taken up and retain radiosensitizing activity in 3D PCa spheroids. This is especially relevant because spheroid architecture can restrict nanoparticle diffusion and contribute to greater treatment resistance than monolayer cultures. As a result, spheroid-based radiosensitivity testing represents a key translational step between simplified *in vitro* studies and future *in vivo* applications, as it evaluates whether GNP-mediated radiosensitization is maintained under more tumour-like conditions. Therefore, evaluating Curc-GNPs in DU145 spheroids provides a more rigorous model for assessing their potential as radiosensitizing agents.

The aim of this chapter was to investigate the uptake and radiosensitizing effects of Curc-GNPs in DU145 PCa spheroids. Cellular uptake of Curc-GNPs was compared with conventional Cit-GNPs using inductively coupled plasma optical emission spectroscopy (ICP-OES) following exposure to different nanoparticle concentrations and incubation times. The radiosensitizing effect of Curc-GNPs was then assessed using clonogenic survival analysis after exposure to megavoltage photon radiation. Together, these experiments were designed to determine whether functionalizing GNPs with curcumin improved uptake in 3D PCa spheroids and whether Curc-GNPs enhance radiation-induced cell killing in a concentration-dependent manner.

3.2 Materials

Reagents for GNP synthesis were as follows: Curcumin (≥98% purity; Alexis Biochemicals, San Diego, CA, USA), sodium citrate dihydrate (S25545; Fisher Scientific, Waltham, MA, USA), and gold(III) chloride trihydrate ($HAuCl_4 \cdot 3H_2O$, 520918; Sigma-Aldrich, St. Louis, MO, USA). All

synthesis protocols utilized ultrapure Milli-Q water from a Millipore Gradient A10 water purification system (Merck Millipore, Burlington, MA, USA). Reagents for in vitro studies included RPMI 1640 medium (R8758; Sigma-Aldrich), fetal bovine serum (FBS; A3160702; Fisher Scientific), penicillin-streptomycin (15140122; Fisher Scientific), Dulbecco's phosphate buffered saline (PBS; SH30028.02; Fisher Scientific), trypsin-EDTA (25200072; Fisher Scientific), glutaraldehyde (ca. 50% in water, ca. 5.6 mol/L; G0068500ML; Fisher Scientific), and crystal violet (C0775-100G; Sigma-Aldrich). Tools and reagents used to create the DU145 spheroids were the MicroTissues® 3D Petri Dish® micro-mold spheroids, size L, 9 × 9 array (Z764019; Sigma-Aldrich), UltraPure™ agarose (16500100; Thermo Fisher Scientific), sodium chloride (S-2830; ACP Chemicals).

3.3 Methods

3.3.1 Spheroid Culture

DU145 cells were harvested from a donor culture in RPMI-1640 (Sigma-Aldrich, USA) culture medium supplemented with 10% fetal bovine serum (FBS) (Thermo Fisher Scientific, USA) and 1% penicillin (Thermo Fisher Scientific, USA) and incubated in a humidified atmosphere at 37 ◦C and 5% CO_2. Prostate tumor spheroids were seeded and cultured in 2% agarose 3D Petri Dish (MicroTissues Inc., USA) gels. The 9×9 array of wells contained in each agarose gel was seeded with a suspension of DU145 cells such that spheroids of approximately 1,000 cells formed in each well. The prostate tumour spheroids were allowed to settle and proliferate for one day prior to treatment. This process is visualized in Figure 3.1, which was adapted from Swanson et al., (35).

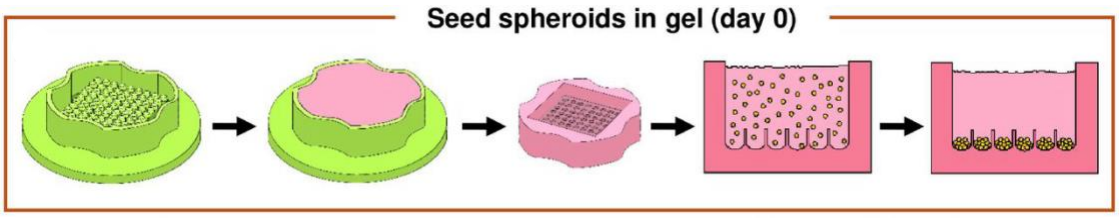


Figure 3.1: Process of seeding spheroids in gels.

Cells (yellow) seeded into agarose gels (pink) created from molds (green) self-assemble into prostate tumor spheroids in the bottom of wells. Adapted from Swanson et al., (35).

3.3.2 GNP Treatment

24 hours post-seeding, spheroid cultures were exposed to five different Curc-GNP concentrations: 0, 24, 50, 100, and 200 μg/mL suspended in supplemented RPMI-1640 for 24 hours. The 500 µL gel was included in the culture medium volume for calculating treatment concentration. To keep the spheroids intact prior to irradiation, while removing the GNPs a serial dilution was performed: all liquid was carefully removed from around and inside the gel and replaced dropwise with 5 mL of RPMI, then gels were left to soak for 30 minutes. The process was repeated four times so that the GNP in each 500 µL gel was diluted by a factor of 10,000. In the final dilution before irradiation, spheroid gels received supplemented culture medium. This method was adapted from Swanson et al., (35) and can be seen in Figure 3.2.

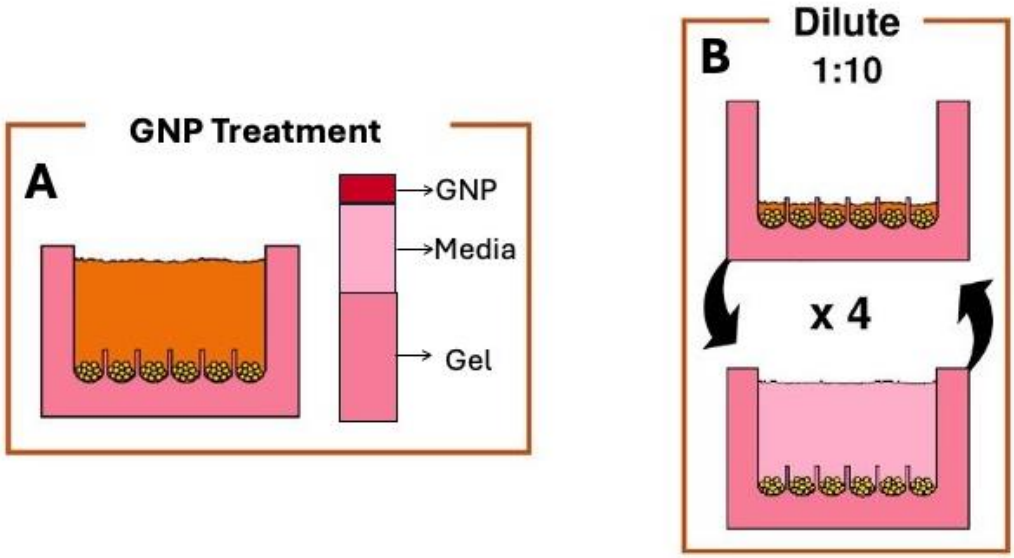


Figure 3.2: GNP treatment of spheroids and preparation for radiation.

(A) Spheroids were exposed to 0, 25, 50, 100, and 200 μg/mL of Curc-GNP diluted in supplemented media for 24 hours. GNP were removed by (B) serial dilution of spheroid-containing gels prior to radiation treatment. Adapted from Swanson et al., (35).

3.3.3 Radiation Treatment

Radiation treatment was then administered at Waterloo Regional Health Network (WRHN) with a 6 MV photon beam delivered by Varian TrueBeam clinical linear accelerator (Varian LINAC). The following radiation doses were administered: 0, 2, 4, 6, Gy. Each GNP concentration was performed in triplicate gels for consistency and to ensure enough cells for clonogenic assay. 12 well plates were used to store gels, with one well containing one gel. The control group (0 Gy) was only treated with GNPs and not irradiated; however, it was transported to WHRN to ensure no differences were present other than radiation and GNP concentration.

3.3.4 Disaggregating Spheroids

Following treatment, 3D tumour spheroids were disaggregated into a single-cell suspension prior to clonogenic plating. Spheroids were first flushed from the agarose gel by repeatedly pipetting the medium over the gel surface, and the recovered medium was transferred into a Falcon tube, with one tube used per experimental condition. The gel was then washed three additional times with 500 µL of complete culture medium, and each wash was collected into the same tube. The suspension was mixed thoroughly by pipetting up and down to reduce cellular clumping, vortexed for approximately 1 minute, and visually inspected to confirm that no large clumps remained. The suspension was then centrifuged for 5 minutes at 1000 rpm and 25°C. The supernatant was removed carefully, and 200 µL trypsin was added. The suspension was pipetted repeatedly to promote disaggregation, vortexed again for approximately 1 minute, and incubated for approximately three minutes. Incomplete medium was then added at a 1:2 ratio relative to trypsin to inactivate the enzyme, and the suspension was centrifuged for 5 minutes at 1000 rpm and 25°C. The supernatant was removed carefully, and the final pellet was resuspended in complete medium.

3.3.5 Clonogenic Assay

A clonogenic assay was conducted following the procedure outlined by Franken et al., (36) 12-hours after the irradiation treatment. The resulting cell suspensions were prepared for plating in the clonogenic assay. Samples were seeded at least in triplicate for both control and treated conditions at each radiation dose. Cells were irradiated while in the exponential growth phase, approximately 24 to 48 hours after initial plating. Delayed plating was used; cells were incubated for 6 to 24 hours following treatment before further processing. After disaggregation, the number of cells in each suspension was counted using the Countess 3 Automated Cell Counter (Thermo Fisher Scientific, USA). and the suspensions were diluted so that approximately 100 to 10,000 cells could be plated

into new wells as a 2D monolayer, again at least in triplicate. Seeding densities were selected empirically for the DU145 cell line and treatment condition, based on data from literature and toxicity assessments (37,38). To ensure that individual colonies could be clearly distinguished, multiple seeded densities were chosen depending on treatment severity.

Following plating, the cells were incubated for 10 to 16 days to allow colony formation. The incubation period was sufficient for surviving cells to generate colonies containing at least 50 cells. At the end of the incubation period, the medium was removed and the wells were rinsed with PBS. The PBS was then removed, and the cells were fixed by adding 2 to 3 mL of a 6% (v/v) glutaraldehyde, 0.5% (w/v) crystal violet in DI water solution for 1 hour. The fixing-staining solution was then removed carefully, and the plates were rinsed by immersion in water rather than placing them directly under running tap water. The plates were then left to dry in normal air at room temperature. After drying, colonies were imaged and counted, with only wells containing distinguishable, non-overlapping colonies considered suitable for analysis. Colonies were defined as groups containing at least 50 cells.

Images of each clonogenic assay well were captured using a camera with the corresponding cell type, culture method, radiation dose, and number of cells seeded written adjacent to the well or in the file name for identification. Each image was then opened in ImageJ and labeled using the format *culture type_dose_number of cells seeded_well number*. Colonies were counted manually using the multi-point tool, and only colonies judged to contain more than 50 cells were included. Where necessary, counted colonies were cross-checked under a compound microscope to confirm that colonies were not missed and that only colonies exceeding the 50-cell threshold were recorded. The final colony counts were entered into a spreadsheet with the experimental date, cell culture method, number of cells plated, well number and the number of colonies counted.

Using the control, the **Plating Efficiency (PE)** was calculated using the equation seen in Equation 3.1, using the treated cells, the **Survival Fraction (SF)** was calculated using the equation seen in Equation 3.2. The PE and SF were calculated to evaluate the effects of GNPs and radiation treatment on DU145 cells.

Plating Efficiency was determined as the ratio of the number of colonies formed to the number of cells originally seeded. This metric reflects the proportion of cells capable of adhering to the plate and forming colonies following GNP exposure in the absence of radiation treatment. In this study, plating efficiency was calculated for each GNP concentration (0, 25, 50, 100, and 200 μg/mL) using control plates that did not receive any radiation. The formula used for PE was:

$$PE = \left(\frac{Number\ of\ Colonies}{Number\ of\ Cells\ Seeded}\right) \times 100\% \quad (3.1)$$

This calculation was the baseline for subsequent analysis for the effect of radiation treatment on colony formation and survival.

Surviving Fraction (SF) was calculated to determine the proportion of cells that retained their ability to form colonies after exposure to radiation treatment. This metric is essential for evaluating the combined effect of GNPs and radiation therapy in inhibiting DU145 spheroid proliferation and survival. Surviving Fraction was computed using the formula:

$$SF = \left(\frac{Number\ of\ Colonies\ after\ radiotherapy}{Number\ of\ Cells\ Seeded\ \times\ PE}\right) \times 100\% \quad (3.2)$$

Once the PE and SF for each treatment group was determined radiation survival curves were created. These curves plot the radiation dose on the x-axis and the surviving fraction, in logarithmic form, on the y-axis. This analysis was repeated for all doses and treatment conditions and data are fit

by a weighted, stratified, linear regression according to the **linear–quadratic (LQ) model**, described by Equation 3.3.

$$SF = e^{-(\alpha D + \beta D^2)} \quad (3.3)$$

Where:

- SF: Surviving Fraction.
- D: Radiation dose.
- α: Represents the linear component of cell killing (single-track DNA damage).
- β: Represents the quadratic component of cell killing (double-track DNA damage).

The non-linear regression model allowed for trends in radiation sensitivity, synergistic effects of GNPs and radiation, and cell viability to be determined. Fitting the survival curves to the LQ model allowed for determination of α, β, and dose-response relationships to be quantified for each treatment condition.

To analyze the data and determine the α, and β parameters, a revised linear-quadratic (LQ) workflow was implemented in R using the CFAssay, CellSurvAssay and supporting tidyverse packages. The raw data was imported and cleaned so variables were renamed into a standardized format, converted to the appropriate data types and missing data excluded from analysis. In the final analysis table, each nanoparticle concentration was treated as a separate survival curve, the cline variable, while each well was defined as an experimental replicate, the Exp variable, within that curve.

Initial quality-control checks were performed before model fitting. These checks confirmed that radiation dose, plating density and colony counts were numeric and free of missing values after

cleaning and summary tables were generated to document the number of observations, dose levels, seeding densities and replicate wells available for each nanoparticle concentration. Additionally, each concentration group was screened for analytical eligibility. A concentration was considered suitable for fitting into the LQ model if it contained at least two observations, at least two distinct radiation dose levels, at least two replicate wells, replicate wells available for each nanoparticle concentration and at least one 0 Gy condition. This step was included to ensure that plating efficiencies and radiation-response parameters could be stable and reproducible. The CFAcoop framework was used before fitting to model the seeded cell to colony relationship, since conventional plating-efficiency-based survival analysis can be compromised when colony formation departs from the non-cooperative case (39).

Once the dataset was cleaned survival-curve fitting was done using the CFAssay::cellsurvLQfit() function in R, while CellSurvAssay was used for plotting and visualization. For each nanoparticle concentration, several fitting strategies were attempted sequentially, including maximum-likelihood, Franken, and least-squares methods, each with either fitted or fixed plating efficiency. The first successful fit was retained for that concentration, and unsuccessful attempts were recorded in individual text log files to preserve a traceable record of fitting behavior. For the final analysis, all concentrations were successfully modeled using the maximum-likelihood method with fitted plating efficiency. This approach is appropriate since replicate wells are maintained as unique experimental units. This methodology is also consistent with clonogenic assay analysis frameworks described in literature (40–42)

The LQ survival model was used to describe the relationship between radiation dose and clonogenic survival. Model coefficients, α and β, were extracted from the fitted curves. From these values the median lethal dose (D_{50}) was calculated by solving the LQ equation at a surviving fraction

of 0.5 (50% survival). The α/β ratio was determined for each concentration, and the sensitization enhancement ratio (SER) was calculated relative to the untreated control as the ratio of the control D_{50} to the treatment D_{50}. This method is consistent with the approach seen commonly in literature (40,41).

Sensitizer Enhancement Ratio (SER): Quantifies the radiosensitizing effect of GNPs at 50% survival and is calculated according to equation 3.4.

$$SER = \frac{D_{50}\ without\ GNP}{D_{50}\ with\ GNP} \quad (3.4)$$

Radiation survival curves were visualized using CellSurvAssay::ggplotCSCurve() function, which produced survival plots in R and allows direct comparison of fitted survival curves across multiple treatment conditions. A combined panel containing all fitted curves was first generated, followed by separate pairwise plots comparing the untreated control with each nanoparticle-treated condition. Statistical comparison of fitted curves was then performed using the CFAssay::cellsurvLQdiff() function on paired control-treatment datasets. This methodology allowed for the raw clonogenic data to be cleaned, screened, modeled, visualized and summarized in a reproducible manner (42).

3.3.6 ICP-OES Cellular Uptake

The uptake of Curc-GNP, and Cit-GNPs was measured using ICP-OES, (ICP-OES, Teledyne Leeman Labs, USA) where DU-145 cells cultured in 3D were exposed to two GNP concentrations (50 μg/mL and 100 μg/mL) for a 5-, 10-or 24-hour incubation period, in supplemented media. This experiment was designed to determine the effect of 3D culture, incubation time and supplemented media on Curc-GNPs and Cit-GNPs uptake in DU-145 cells.

Spheroids were seeded and treated with Cit-GNPs or Curc-GNPs in triplicate, as previously described, for 5-, 10-or 24-hour incubation period. To prepare spheroids for ICP-OES analysis they

were disaggregated using the previously described procedure in section 3.3.2 Disaggregating Spheroids. To ensure there was minimal extracellular GNPs, the cell solution was washed with PBS. This was done by resuspending the cell pellet in PBS with 3 mL of PBS, then centrifuging the suspension for 5 minutes at 1000 rpm and 25°C. This was repeated five times. After the final wash the cells were suspended in 5 mL of sterilized MQ water. The resuspended cells were then transferred to a DigiTUBE acid digestion tube. 4 mL of aqua regia, 1:3 mixture of HNO_3 and HCL, was added for acid digestion. The tubes were then placed on an EHD36 Digiblock Digester at 150°C for 20 minutes. After digestion the solution was diluted to 50 mL of Milli-Q water, thoroughly mixed, then filtered using a vacuum before analysis.

To determine the gold concentrations in the digested samples, ICP-OES (Agilent Technologies) was used. Measurements were performed for ^{197}Au, with ^{89}Y being used as an internal standard to correct for variations in plasma conditions. An ^{55}Mn solution was used to perform peaking to optimize the camera. A calibration curve for quantifying Au content was generated using a blank and seven gold standards ranging from 0.05 to 20 μg/mL. All calibration curves had correlation coefficients > 0.995 and the calibration was verified using a standard prepared from an alternative source of gold and was considered acceptable if results were within ±10% of the expected value. The method detection limit (MDL) for Au was 1ppm, and the limit of quantitation (LOQ) was 10 ppm. To calculate gold uptake the following formula was used.

$$Au\ per\ cell = \frac{Total\ Au\ concetration\ (from\ 3\ gels)}{Total\ cell\ count\ (from\ 3\ gels)} \quad (3.6)$$

To analyze the data obtained from ICP-OES R and the following packages were used: readxl, tidyverse, ggpubr, rstatix, car, FSA, ARTool, and emmeans. The Raw uptake values were imported from excel, and gold uptake per cell, expressed as Au/cell (pg/cell), was used as the primary response

variable. The experimental factors, including nanoparticle coating condition (Curc-GNP or Cit-GNP), dose (50 or 100 μg/mL), and incubation time (5, 10, or 24 h), were coded as categorical variables prior to analysis. Summary visualizations were then generated in R by calculating the mean uptake for each treatment group, with standard deviation used to define the error bars shown on the final bar plots and time-course plots. The main uptake figure was arranged as a faceted plot with incubation time and dose as paneling variables and coating type on the x-axis. The normality, variance, and effect size was assessed using Shapiro-Wilk tests, Q-Q plots and histograms, Levene's test, and by calculating Cohen's d respectively. The uptake data did not consistently satisfy normality assumptions, so nonparametric methods were applied. The experiment involved three fixed and potential interaction effects, so an aligned rank transform (ART) ANOVA model was used. The model Au_pg_cell ~ Condition * Dose * Time_h was used to test the main effects of coating condition, dose, and incubation time, together with all two-way and three-way interactions. This nonparametric factorial approach was selected because it permits analysis of interaction terms while accommodating non-normal data. Post-hoc contrasts were then performed using ART-based pairwise comparisons with Bonferroni adjustment, and the biologically relevant comparisons between Curc-GNP and Cit-GNP within matched dose and time conditions were summarized in a reduced post-hoc table.

3.4 Results and Discussion

3.4.1 ICP-OES Cellular Uptake

The uptake of Curc-GNP, and Cit-GNPs was measured using ICP-OES, (ICP-OES, Teledyne Leeman Labs, USA) where DU-145 spheroids were exposed to two GNP concentrations (50 μg/mL and 100 μg/mL) for a 5-, 10-or 24-hour incubation period, in supplemented media.

The uptake analysis of citrate-coated gold nanoparticles (Cit-GNPs) and curcumin-coated gold nanoparticles (Curc-GNPs) demonstrated that nanoparticle internalization in DU145 spheroids was dependent on coating type, dose, and incubation time. Overall, Curc-GNPs produced greater gold uptake than Cit-GNPs across most treatment conditions, with the most pronounced difference observed after 24 h of exposure. At 5 h, Curc-GNP uptake was significantly higher than Cit-GNP uptake at both 50 μg/mL and 100 μg/mL as seen in Figure 3.3. Specifically, at 50 μg/mL, Curc-GNP uptake was 0.51 ± 0.07 pg/cell compared with 0.17 ± 0.02 pg/cell for Cit-GNPs, while at 100 μg/mL Curc-GNP uptake was 0.345 ± 0.039 pg/cell compared with 0.09 ± 0.06 pg/cell for Cit-GNPs (Figure 3.3). At 10 h, Curc-GNPs remained significantly higher than Cit-GNPs at 50 μg/mL, but the difference was not significant at 100 μg/mL, suggesting that uptake in spheroids may not increase in a strictly linear dose-dependent manner at early time points. By 24 h, Curc-GNP uptake increased substantially, reaching 2.4 ± 0.1 pg/cell at 50 μg/mL and 4.81 ± 0.60 pg/cell at 100 μg/mL, compared with 1.60 ± 0.21 and 1.01 ± 0.06 pg/cell for Cit-GNPs, respectively (Figure 3.3). These findings indicate that curcumin functionalization improved GNP uptake in DU145 spheroids, particularly after longer incubation periods.

The statistical analysis further supports the conclusion that uptake was influenced by multiple interacting variables. The ART ANOVA demonstrated significant effects of condition, dose, time, and their interactions, including a significant condition:dose:time interaction. This indicates that Curc-GNP and Cit-GNP uptake should not be interpreted only as a simple coating effect, but rather as the result of coating-dependent uptake that changes with both nanoparticle dose and exposure duration (Table 3.1). The post hoc analysis also showed that Curc-GNP uptake was significantly higher than Cit-GNP uptake at 50 μg/mL after 5 h and 10 h, while no significant difference was observed at 24 h for this dose (Table 3.2). At 100 μg/mL, Curc-GNP uptake was significantly higher

at 5 h and 24 h, but not at 10 h. This pattern suggests that nanoparticle uptake in spheroids is influenced by dynamic transport and redistribution processes that may differ between early and later time points.

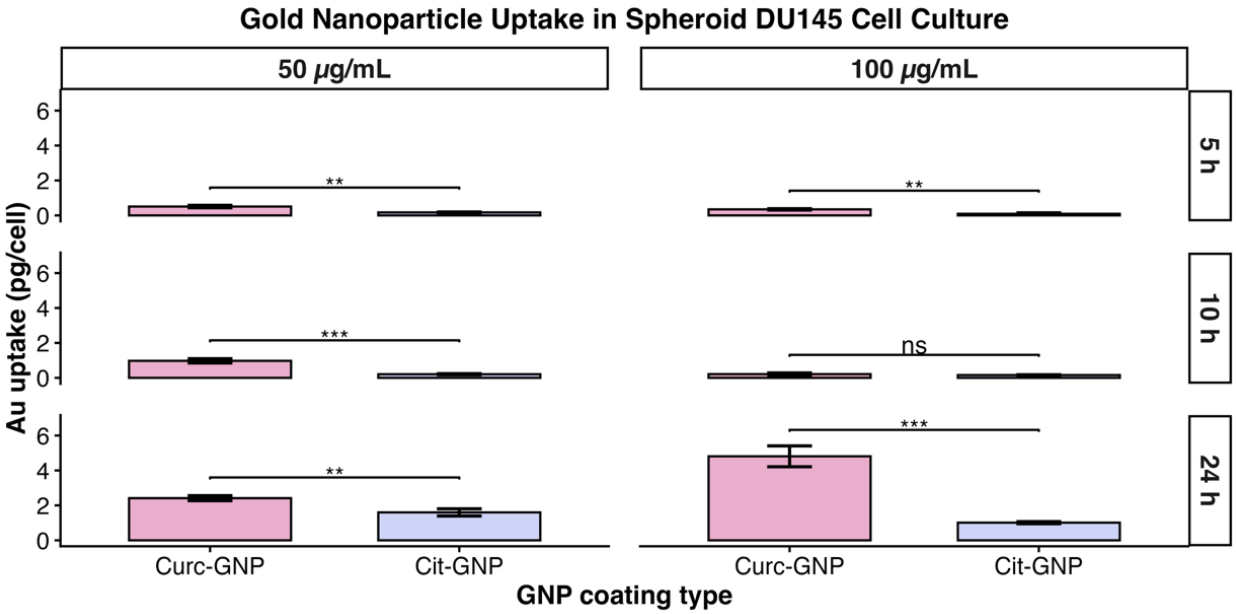


Figure 3.3: Gold nanoparticle uptake in DU145 spheroids following treatment with citrate-coated and curcumin-coated GNPs.

Gold uptake in DU145 spheroids following treatment with citrate-coated gold nanoparticles (Cit-GNPs) or curcumin-coated gold nanoparticles (Curc-GNPs) at 50 and 100 µg/mL for 5, 10, and 24 h. Uptake was quantified as pg Au/cell. Curc-GNPs generally demonstrated higher uptake than Cit-GNPs, with the greatest uptake observed after 24 h. Statistical annotations indicate significant differences between coating types within each dose and time condition, where statistical significance is indicated as *$p < 0.05$, **$p < 0.01$, and ***$p < 0.001$.

Table 3.1: Aligned rank transform ANOVA summary for the effects of coating type, dose, and incubation time on gold nanoparticle uptake in DU145 spheroids.

Effect	Df	F value	p-value	Partial η^2
Condition	1	75.09	<0.001	0.758
Dose	1	12.90	0.001	0.350
Time	2	67.83	<0.001	0.850
Condition × Dose	1	35.84	<0.001	0.599
Condition × Time	2	103.15	<0.001	0.896
Dose × Time	2	46.63	<0.001	0.795
Condition × Dose × Time	2	140.48	<0.001	0.921

Condition refers to GNP coating type: Curc-GNP or Cit-GNP. Dose refers to 50 or 100 µg/mL. Time refers to 5, 10, or 24 h. Partial η^2 represents effect size. Df represents the degrees of freedom associated with each model term, while F represents the F-statistic, which compares between-group variation to within-group variation to determine whether each factor significantly influenced clonogenic survival. p-values < 0.05 were considered statistically significant.

Table 3.2: Post hoc comparisons of Curc-GNP and Cit-GNP uptake in DU145 spheroids across dose and incubation time.

Dose	Time	Comparison	p-value	Significance
50 µg/mL	5 h	Curc-GNP vs Cit-GNP	0.0007	***

Dose	Time	Comparison	p-value	Significance
50 µg/mL	10 h	Curc-GNP vs Cit-GNP	0.0003	***
50 µg/mL	24 h	Curc-GNP vs Cit-GNP	1.0000	ns
100 µg/mL	5 h	Curc-GNP vs Cit-GNP	0.0001	***
100 µg/mL	10 h	Curc-GNP vs Cit-GNP	1.0000	ns
100 µg/mL	24 h	Curc-GNP vs Cit-GNP	0.0049	**

*Post hoc comparisons were performed between Curc-GNP and Cit-GNP uptake within each dose and time condition. ns = not significant; **$p < 0.01$; **$p < 0.001$.

Several studies have demonstrated that nanoparticle uptake in 3D tumour models is strongly influenced by spheroid architecture, extracellular matrix interactions, diffusion barriers, nanoparticle size, and surface chemistry. Rane and Armani showed that GNP uptake in 3D spheroids differs from uptake in 2D monolayers and that penetration into spheroids is affected by nanoparticle physicochemical properties, including size and surface functionalization (23). Their study supports the interpretation that the DU145 spheroid model used in our study may limit or delay nanoparticle internalization compared to monolayer models because cells are organized into a compact three-dimensional structure. This is important because 3D spheroids contain cell–cell contacts, nutrient and oxygen gradients, and diffusion barriers that more closely mimic *in vivo* tumour architecture than 2D cultures (23,24).Therefore, the lower uptake observed at earlier time points in our study may reflect the time required for GNPs to penetrate the spheroid structure before reaching internal cell populations.

The time-dependent increase in uptake observed in our study is consistent with Petrovic et al., who used 3D tumour models to show that GNP localization changes over time (24). Their study reported that GNPs were initially associated with extracellular matrix compartments and only gradually accumulated in cancer cells over multiple days (24). This supports the interpretation that the higher uptake observed at 24 h in DU145 spheroids may reflect the progressive redistribution of GNPs from the extracellular spheroid environment into cellular compartments. The timing of nanoparticle localization is particularly important for radiosensitization because GNPs must be sufficiently close to biologically relevant targets at the time of irradiation to enhance damage through secondary electron production, reactive oxygen species generation, or local chemical effects (24,27). Therefore, the increased Curc-GNP accumulation at 24 h suggests that longer incubation times may be necessary for GNPs to penetrate the spheroid and be effective radiosensitizers.

The coating-dependent differences observed between Curc-GNPs and Cit-GNPs may also be explained by differences in surface chemistry. Tchoryk et al., showed that nanoparticle penetration and uptake in 3D tumour spheroids are governed by physicochemical properties, including particle size, surface characteristics, and uptake kinetics (27). Similarly, Kim et al., demonstrated that gold nanoparticles with different surface charges moved and localized differently in 3D tumour cylindroid models, showing that surface properties can strongly influence nanoparticle transport through tumour-like tissue (28). More recently in a landmark study, Bilgi et al., used machine learning models to identify the factors controlling cellular uptake of GNPs and found that particle size, zeta potential, GNP concentration, and exposure duration were among the most important predictors of uptake (34). This is consistent with the present findings, where uptake differed according to coating type, dose, and incubation time in DU145 spheroids. Together, these studies support the interpretation that the

higher Curc-GNP uptake observed in DU145 spheroids was likely influenced by the altered surface properties of the curcumin-coated formulation rather than by the gold core alone.

These findings are directly relevant to the present study because Curc-GNPs and Cit-GNPs share a gold core but differ in their surface coating. The citrate coating provides a conventional negatively charged stabilizing surface, whereas the curcumin coating may alter nanoparticle interaction with serum proteins, cell membranes, and spheroid extracellular components. This interpretation is supported by studies showing that curcumin can directly interact with lipid membranes. Hung et al., demonstrated that curcumin can induce a membrane-thinning effect, while Barry et al., used solid-state NMR spectroscopy to show that curcumin inserts into lipid bilayers and alters membrane structure (13,43). These membrane-related effects suggest that curcumin on the nanoparticle surface may modify how Curc-GNPs interact with the plasma membrane, potentially promoting stronger membrane association or internalization compared with citrate-coated particles. Therefore, the higher uptake of Curc-GNPs may reflect enhanced interaction between the curcumin-coated nanoparticle surface and DU145 spheroid cells.

In addition to membrane-level effects, curcumin has been reported to influence several intracellular pathways related to proliferation, apoptosis, and cytoskeletal organization. Giommarelli et al., showed that curcumin enhanced the antiproliferative and proapoptotic activity of histone deacetylase inhibitors through Hsp90 inhibition, while Jackson et al., reported that curcumin binds tubulin, induces mitotic catastrophe, and disrupts normal endothelial cell proliferation (15,16). Li et al., also showed that curcumin downregulated constitutively active NF-κB and IκB kinase signaling in pancreatic cancer cells, which was associated with suppressed proliferation and induction of apoptosis (17). Although these pathways were not directly measured in our study, they provide biological support for the idea that Curc-GNPs may have additional functional relevance as a

therapeutic beyond improved gold delivery. In the context of DU145 spheroids, the curcumin coating may therefore contribute both to altered nanoparticle–cell interactions at the membrane and to downstream biological effects that could become important in later radiosensitization experiments.

The importance of nanoparticle size and shape in cellular uptake has also been well established. Chithrani et al., demonstrated that gold nanoparticle uptake into mammalian cells depends strongly on size and shape, with uptake kinetics and saturation concentration varying according to particle dimensions (31). In a later study, Chithrani and Chan observed that protein-coated GNPs entered cells primarily through clathrin-mediated endocytosis and that nanoparticle removal from cells was also size-dependent (32). Although the present study compared coating type rather than particle size, these studies support the broader conclusion that small changes in nanoparticle physicochemical properties can significantly alter uptake behaviour and provide context for how the Curc-GNPs in this study may have been internalized in DU145 spheroids. Huang et al., further demonstrated that ultrasmall GNPs smaller than 10 nm showed advantages in penetration and localization within cancer cells, multicellular spheroids, and tumours in vivo (33). This agrees with the results we observed since the GNPs used for this study ranged from 15-25 nm. Together, these studies indicate that nanoparticle uptake in DU145 spheroids likely depends on a combination of surface coating, size, endocytic uptake, spheroid penetration, and time-dependent redistribution.

The present findings are also consistent with prostate cancer studies showing that surface modification can improve GNP internalization and radiosensitizing potential. Bennie et al., investigated RALA/Au nanocomplexes in prostate cancer models and reported that peptide complexation improved AuNP internalization and increased prostate tumour cell sensitivity to radiation (12). This is relevant because it supports the idea that modifying the surface of GNPs can enhance uptake in prostate cancer cells. Similarly, Khoo et al., demonstrated that actively targeted

gold nanorods enhanced radiosensitization in prostate cancer models by improving tumour and cellular delivery (4). Wolfe et al., also showed that targeted GNPs enhanced sensitization of prostate tumours, further supporting the role of nanoparticle surface design in improving therapeutic response (5). In the present study, Curc-GNPs were not actively targeted to a prostate-specific receptor; however, the increased uptake compared with Cit-GNPs suggests that curcumin coating may still improve nanoparticle–cell interactions in DU145 spheroids.

The findings of Bromma et al., further support the use of 3D spheroids for evaluating GNP uptake and radiosensitization. They reported that 3D tumour spheroids provide a more reliable platform than 2D monolayers for studying combined GNP and radiotherapy responses because spheroids better represent tumour microenvironmental barriers (25). In a later study, Bromma et al., compared nanoparticle accumulation in 2D monolayer, 3D spheroid, and xenograft mouse cancer models and showed that spheroids can better reflect *in vivo*-like nanoparticle behaviour than monolayers (26). This is highly relevant to our study because DU145 spheroids likely represent a more treatment-resistant and diffusion-limited model of prostate cancer than DU145 or other PCa cells grown in monolayers. The difference in culture technique, and the resulting *in vivo*-like environment may also be why higher uptake at both incubation times and doses was seen in PC3 monolayers grown in in serum supplemented media by Aborig et al., compared to our study (11). Therefore, the observation that Curc-GNPs still achieved greater uptake than Cit-GNPs under these 3D conditions strengthens the rationale for Curc-GNPs as a potentially useful radiosensitizing formulation.

The enhanced uptake of Curc-GNPs may also have biological significance because curcumin is not only a surface coating but also a bioactive compound with reported anticancer and radiosensitizing properties. Aborig et al., examined Curc-GNPs in PC-3 prostate cancer cells and

reported that Curc-GNPs enhanced radiation response are most likely through the combined effects of gold and curcumin, including increased ROS production and improved radiosensitization compared with conventional formulations (11). The present DU145 spheroid uptake results extend those findings by demonstrating that Curc-GNPs can also achieve enhanced gold accumulation in a 3D PCa model. This is important because DU145 spheroids are expected to be more resistant to nanoparticle penetration than monolayer cultures due to compact spheroid architecture and diffusion gradients.

Yadav et al., also support the rationale for combining gold and curcumin in a nanoformulation, reporting that gold-curcumin nanoparticles may improve radiation response through complementary gold-mediated and curcumin-mediated mechanisms (22). Although their study focused on cervical cancer rather than prostate cancer, it supports the broader concept that gold-curcumin nanoparticles may provide dual functionality: physical dose enhancement from gold and biological pathway modulation from curcumin.

Overall, the uptake results from the present study show that Curc-GNPs were internalized more effectively than Cit-GNPs in DU145 spheroids, particularly after 24 h. The strongest uptake was observed with 100 μg/mL Curc-GNPs at 24 h (Figure 3.4), suggesting that longer exposure may be required for maximal nanoparticle accumulation in 3D prostate cancer spheroids. These results are consistent with previous studies showing that GNP uptake in 3D tumour models is controlled by time-dependent penetration, extracellular matrix interactions, surface chemistry, size, charge, and endocytic internalization (23,24,27,28,31–33). The findings are also supported by PCa nanoparticle studies showing that surface modification can improve GNP internalization and radiosensitization (4,5,12,11,25,26). Therefore, the increased Curc-GNP uptake observed in DU145 spheroids suggests that curcumin functionalization may improve GNP delivery in 3D prostate cancer models and may contribute to enhanced radiosensitization if paired with radiation treatment.

3.4.2 Clonogenic Assay

The analysis of Curc-GNPs radiosensitizing effects demonstrated a clear dose-dependent radiosensitizing effect seen through SER, and radiation-induced cell death (Table 3.3). The D_{50} decreased with increasing GNP concentration from 2.012 Gy at 0 μg/mL to 1.295 Gy at 200 μg/mL. Comparing the D_{50} at 100 μg/mL (1.352) and 200 μg/mL (1.295) there is a shift in the trend. This suggests that there may be minimal difference in radiation dose required to achieve 50% cell survival between 100 and 200 μg/mL. Overall, this trend suggests that higher concentrations of Curc-GNPs significantly reduce the radiation dose required to achieve comparable therapeutic outcomes, as well as greater radiosensitivity at with increasing Curc-GNP concentrations. The SER increased with increasing GNP concentration from 1.000 at 0 μg/mL to 1.554 at 200 μg/mL. This trend indicates that higher concentrations of GNP can act as an effective radiosensitizer, with the strongest effect seen at 100-200 μg/mL.

The α parameter from the linear-quadratic model, which represents the linear single track DNA damage component, increased from 0.292 at 0 μg/mL to 0.527 at 200 μg/mL. This indicates an enhanced direct DNA damage effect as Curc-GNP concentration increases. The β parameter, which represents the quadratic double track DNA damage component, decreased from 0.026 at 0 μg/mL to 0.007 at 200 μg/mL. This trend is associated with limited accumulation of sublethal DNA damage and reduction of DNA damage repair interactions. The α/β ratio increased significantly across concentrations from 11.191at 0 μg/mL to 78.717 at 200 μg/mL. This suggests a greater dominance of the α component over β, which also aligns with the trend of increasing α and decreasing β parameters. These trends suggest that increasing Curc-GNPs concentration may cause more linear single track DNA damage from radiation, while decreasing the contribution of accumulated DNA damage.

Overall, the results from this study show that Curc-GNPs include a concentration-dependent radiosensitization effect in DU145 prostate cancer spheroids, as seen by the changes in clonogenic survival (Figure 3.4 A-E) and linear-quadratic (LQ) model parameters (Table 3.3). Increasing Curc-GNP resulted in enhanced cell killing at all radiation doses with the most pronounced divergence from control was observed at 100 and 200 μg/mL. These findings are quantitatively supported by shifts in all LQ-derived parameters, including increased α, decreased β, reduced D_{50}, elevated SER, and a rise in the α/β ratio, as seen in Table 3.3.

Table 3.3: Curc-GNP radiosensitization parameters derived from linear-quadratic model fitting. Including α, β, median lethal dose (D_{50}), sensitization enhancement ratio (SER), and α/β ratio across increasing nanoparticle concentrations.

Concentration	α	β	D_{50}	*SER*	α/β
0 μg/ml	0.292	0.026	2.012	1.000	11.191
25 μg/ml	0.339	0.022	1.824	1.103	15.286
50 μg/ml	0.388	0.018	1.661	1.212	22.044
100 μg/ml	0.505	0.006	1.352	1.489	82.250
200 μg/ml	0.527	0.007	1.295	1.554	78.717

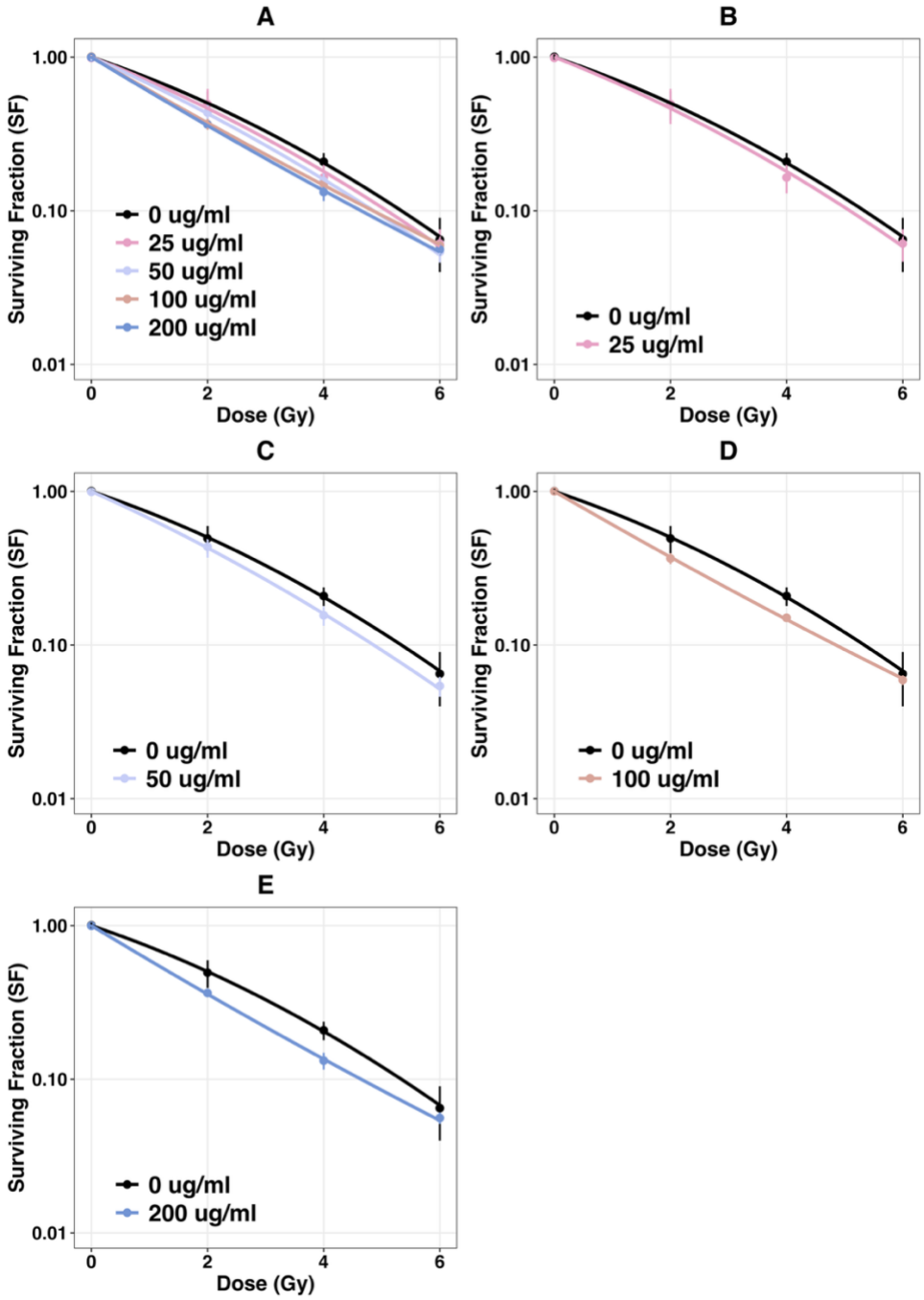


Figure 3.4: Survival Curves of DU145 Spheroids exposed to Curc-GNPs and radiation.

The greater the separation between the black line (control) and the colored lines (treatment), the higher the SER. Graph (E) shows a significant gap, corresponding to the 200 µg/mL concentration.

Several studies have demonstrated comparable radiosensitizing effects of gold nanoparticles (GNPs) in prostate cancer and other cancer models. In the present study, the survival curves shown in Figure 3.4 demonstrated a progressive downward shift with increasing Curc-GNP concentration, indicating enhanced radiation-induced cell death. This trend was quantified by the sensitization enhancement ratio (SER), which increased from 1.00 in the control condition to 1.554 at 200 μg/mL Curc-GNPs. These results fall within the range reported for effective nanoparticle-mediated radiosensitization in prostate cancer. Zhang et al., first demonstrated that functionalized GNPs could enhance radiation sensitivity in radiation-resistant DU145 prostate cancer cells, showing that glucose-bound GNPs enhanced radiation sensitivity and toxicity compared with irradiation alone (2). Similarly, Aborig et al., examined the cytotoxicity, cellular uptake, and radiosensitizing potential of Curc-GNPs in PC-3 prostate cancer cells grown in monolayer and reported SER values of approximately 1.82 at high Curc-GNP concentrations (11). Soares et al. assessed the biological interaction of amine-PEGylated GNPs of different sizes and shapes with ionizing radiation in PC-3, DU145, and LNCaP prostate cancer cell lines (6). They found that spherical PEG-GNPs produced SER values ranging from 0.84 to 1.23 in DU145 monolayer cultures. However, it is important to note that Soares et al., used 0.1 mM GNPs, which is approximately equivalent to 20 μg/mL, in combination with radiation doses of 0, 2.5, 5, and 7.5 Gy (6). These differences in nanoparticle concentration, radiation dose range, and culture model limit direct comparison with the present study.

The lower maximum SER observed in this study compared with Aborig et al., may be attributed to the use of a 3D spheroid model, which more closely mimics in vivo tumour architecture and is known to exhibit greater resistance to radiation and nanoparticle penetration (11). Bennie et al., similarly reported that 3D prostate tumour models contain diffusion barriers and oxygen gradients that can influence nanoparticle penetration and radiosensitization (12). Despite these barriers, the

concentration-dependent downward shift in the DU145 spheroid survival curves suggests that Curc-GNPs enhanced radiation response under more treatment-resistant 3D culture conditions.

The progressive downward shift of the survival curves can be explained by the combined physical, chemical, and biological effects of Curc-GNPs. The gold core likely enhanced local photon absorption and secondary electron emission, while the nanoparticle surface may have promoted reactive oxygen species (ROS) generation. Howard et al., described that nanoparticle-mediated radiosensitization is influenced not only by physical dose effects, but also by chemical mechanisms involving ROS generation, nanoparticle–water interactions, and redox-related biological damage (1). These mechanisms may explain the lower surviving fraction observed at each radiation dose, as cells exposed to Curc-GNPs likely experienced greater oxidative stress, increased DNA damage, mitochondrial and membrane injury, and reduced clonogenic recovery after irradiation. Nanoparticle radiosensitization is also highly dependent on physicochemical properties and cellular fate because ROS effects depend on nanoparticle localization and the biological targets affected after irradiation (1).

This interpretation is consistent with Aborig et al., who found that Curc-GNPs leveraged both the photoelectric properties of gold and the radiosensitizing effects of curcumin to produce significant radiosensitization in PC-3 monolayer cells (11). Aborig et al., also reported a biphasic Curc-GNP dose response, with minimal cytotoxicity up to 100 μg/mL but greater cytotoxicity above 100 μg/mL, along with increased ROS production and elevated α after irradiation (11). Yadav et al., further supported the rationale for gold-curcumin nanoformulations, reporting that gold-curcumin nanoparticles may enhance radiation response through the combined radiosensitizing properties of gold and curcumin-associated biological pathway modulation (22). Zhang et al., also support the importance of nanoparticle functionalization, as their study showed that glucose-bound GNPs

enhanced radiation sensitivity in DU145 prostate cancer cells (2). In contrast, Jain et al., found no significant radiosensitization when DU145 cells were exposed to spherical GNPs, Aurovist, and radiation, with SER values of only 0.97 to 1.08 (3). This contrast supports the interpretation that nanoparticle coating and surface chemistry strongly influence radiosensitization and that the curcumin coating likely contributed to the stronger SER response through chemical and biological mechanisms, rather than the gold core acting alone.

In the present study, D_{50} decreased from 2.012 Gy in the control condition to 1.295 Gy at 200 μg/mL Curc-GNPs. This suggests that a lower radiation dose was required to reduce survival to 50%, indicating increased radiosensitivity following exposure to Curc-GNPs. The decline in D_{50} was likely due to the combined effect of increased α and reduced β. As Curc-GNP concentration increased, each radiation dose likely produced greater ROS generation, DNA damage, and mitochondrial stress. ROS can cause lipid peroxidation, DNA double-strand breaks, protein misfolding, mitochondrial disruption, and apoptosis signaling (1). As these cellular injuries occurred at lower radiation doses, the survival curves shifted downward and D_{50} decreased. These LQ trends, including increasing α and SER with decreasing β and D_{50}, are summarized in Table 3.3.

The decrease in D_{50} is also supported by curcumin-specific biological mechanisms. Wang et al., showed that curcumin induced ROS accumulation, apoptosis, autophagy, G2/M cell-cycle arrest, and cellular senescence, accompanied by increased p53 and p21 expression in cervical cancer cells (17). These effects would reduce the ability of irradiated cells to maintain clonogenic survival after treatment, helping to explain why a lower radiation dose was required to achieve the same level of cell killing. Liu et al., studied colorectal cancer rather than prostate cancer, their findings support the broader conclusion that curcumin can induce ROS-linked, p53-independent apoptosis and senescence pathways, which may be relevant to DU145 cells given their altered p53 status (18). Li et al., further

reviewed curcumin's anticancer mechanisms in colorectal cancer, including its effects on inflammatory, proliferative, and survival-related pathways, while also noting translational limitations such as poor bioavailability and pharmacokinetic challenges (44). Together, these studies support the interpretation that the curcumin coating may have contributed to reduced clonogenic recovery and decreased D_{50} after irradiation.

One of the key findings from this study was the progressive increase in the α parameter from 0.292 in the control condition to 0.527 at 200 μg/mL Curc-GNPs, as shown in Table 3.1. The α parameter represents the linear component of radiation-induced cell killing and is commonly associated with single-event, irreparable damage. The observed increase in α suggests that Curc-GNPs enhanced the probability of lethal radiation-induced injury per unit dose. In other words, when prostate cancer cells were exposed to Curc-GNPs and radiation, the same delivered radiation dose produced more irreversible biological injury than radiation alone.

This increase in α can be explained by several mechanisms. Gold nanoparticles can increase local secondary electron production after irradiation, promoting dense ionization near the nanoparticle surface and enhancing local ROS formation. Nanoparticles can also enhance ROS production through physical dose effects, secondary electron emission, and catalytic effects at the nanoparticle–water interface (1). Excessive ROS can damage DNA, proteins, lipids, and mitochondria, leading to oxidative stress and ultimately cell death (1). These mechanisms would increase α because radiation-induced damage becomes more immediately lethal rather than requiring the accumulation of multiple sublethal events.

The curcumin coating may have further contributed to the increase in α by promoting cancer-cell stress responses that reduced post-irradiation survival. Wang et al., reported that curcumin induced ROS generation, apoptosis, autophagy, G2/M arrest, and senescence (18). G2/M arrest is

particularly relevant because cells in this phase of the cell cycle are generally more radiosensitive. The curcumin coating may have further contributed to the increase in α by promoting cancer-cell stress responses that reduced post-irradiation survival. Wang et al., also reported that curcumin induced ROS generation, apoptosis, autophagy, G2/M arrest, and senescence in cervical cancer cells (18). Although G2/M arrest is relevant because cells in this phase are generally more radiosensitive, cell-cycle distribution was not directly assessed in the present DU145 spheroid study. Therefore, Curc-GNP-mediated G2/M redistribution remains a possible but unconfirmed mechanism that could be evaluated in future work using flow cytometry or immunostaining for cell-cycle markers. In addition, Xu et al., showed that, in colon cancer cells, curcumin promoted senescence by inhibiting early growth response 1 (EGR1) transcriptional activity and altering the expression of senescence-related gene targets, including telomerase reverse transcriptase, (TERT), and sirtuin 6, (SIRT6); however, this pathway was not directly assessed in the present DU145 spheroid model (20). This pathway is biologically plausible in DU145 cells because EGR1 is present and functionally relevant in DU145 prostate cancer cells, where EGR1 has been implicated in cyclin D2 regulation, IL-8 transcription, and radiation-related signaling (45–47). DU145 cells also have documented hTERT/telomerase-related biology and SIRT6 expression, suggesting that curcumin-mediated effects on senescence-associated pathways may be relevant in this model, although EGR1, TERT, and SIRT6 were not directly measured in the present study (48,49). Therefore, this mechanism should be interpreted as supportive mechanistic rationale rather than a confirmed pathway in the current work.

Since clonogenic assays measure long-term reproductive survival, any curcumin-mediated induction of permanent growth arrest or senescence would appear as increased cell killing and may have contributed to the observed rise in α. These observations are consistent with Aborig et al., who found that exposure to Curc-GNPs elevated the α parameter, likely due to heightened ROS production

and enhanced radiation-induced damage (11). Bennie et al., also found that RALA/Au nanocomplexes increased prostate cancer radiosensitivity and that mechanistic studies supported nuclear accumulation and increased DNA damage (12). Zhang et al., further support the broader interpretation that functionalized GNPs can enhance radiation sensitivity in DU145 cells, reinforcing the importance of nanoparticle design and surface chemistry in determining radiosensitizing efficacy (2).

Another major finding was the decrease in β from 0.026 in the control condition to 0.006–0.007 at 100–200 μg/mL Curc-GNPs. This suggests that the quadratic component of cell killing contributed less as Curc-GNP concentration increased. The β parameter is commonly understood as reflecting damage accumulation through sublethal lesions and repair-dependent processes that result in double-track events. The decrease in β alongside the increase in α suggests that Curc-GNPs may have converted otherwise repairable or sublethal injury into more immediate lethal injury. This interpretation is supported by literature showing that nanoparticle-mediated ROS can overwhelm redox equilibrium, causing oxidative stress, biomolecular damage, and ultimately cell death (1). The decrease in β with increasing Curc-GNP concentration could also reflect delayed repair of radiation-induced damage through inhibition or overwhelming of DNA repair pathways.

Curcumin related studies provide further biological support for this interpretation. Hendrayani et al., reported that curcumin triggered p16-dependent senescence in active cancer-associated fibroblasts and suppressed their pro-carcinogenic paracrine effects (21). Wang et al., similarly linked curcumin exposure to ROS accumulation, autophagy, apoptosis, G2/M arrest, and senescence, while Liu et al., provided evidence that curcumin can induce apoptosis and senescence through ROS-linked, p53-independent mechanisms in colorectal cancer cells (18,19). Therefore, the

observed decrease in β may reflect a shift away from repair-dependent survival and toward loss of clonogenic capacity through oxidative stress, senescence, apoptosis, and impaired recovery.

The α/β ratio increased sharply from 11.191 in controls to 82.250 at 100 μg/mL and 78.717 at 200 μg/mL Curc-GNPs. This large increase occurred because α increased while β decreased. Since the DU145 spheroids were treated once with Curc-GNPs, exposed once at each radiation dose, and then plated for clonogenic assay, this α/β trend should not be interpreted as direct evidence of altered clinical fractionation sensitivity or inter-fraction repair. Instead, the high α/β ratio at higher Curc-GNP concentrations suggests that, following a single radiation exposure, DU145 spheroid cell killing became increasingly dominated by the linear α component rather than the quadratic β component. This indicates that Curc-GNPs may have enhanced immediate or irreparable radiation-induced damage, reducing the relative contribution of sublethal lesion interaction or repair-associated survival within the clonogenic assay.

The sharp increase in the α/β ratio at 100 μg/mL suggests that there may have been a threshold in the radiosensitizing response. Below 100 μg/mL, Curc-GNPs appeared to enhance radiosensitivity gradually. However, at and above 100 μg/mL, nanoparticle uptake, ROS generation, and curcumin-mediated biological stress may have become sufficient to shift cells toward more linear, irreparable cell death. This is consistent with Aborig et al., who found that Curc-GNPs showed minimal cytotoxicity up to 100 μg/mL but became more cytotoxic above 100 μg/mL, while also increasing α and ROS after radiation in PC-3 monolayer cells (11). Curcumin-specific studies further support this interpretation because curcumin can promote ROS accumulation, apoptosis, autophagy, G2/M arrest, and senescence, apoptosis and senescence in a p53-independent manner, p16-dependent senescence, and EGR1/TERT/SIRT6-related senescence signaling in colon cancer cells (18–21). Li et al., also described curcumin's ability to modulate multiple cancer-related pathways, including

proliferative, inflammatory, and survival-associated signaling pathways, which may further reduce clonogenic recovery after irradiation (44). These pathways help explain why the curcumin coating may have contributed to a shift toward α-dominated radiosensitization rather than acting only as a passive stabilizing surface.

In summary, the progressive downward shift of the survival curves in Figure 3.3 with increasing Curc-GNP concentration indicates that DU145 spheroids became more sensitive to radiation, with lower survival fractions observed at equivalent radiation doses. This trend is supported by the LQ parameters shown in Table 3.1, where α, SER, and the α/β ratio increased, while β and D_{50} decreased with increasing Curc-GNP concentration. Mechanistically, these trends suggest that Curc-GNPs enhanced radiation response by increasing ROS production, localized secondary electron effects, mitochondrial and membrane damage, DNA damage, apoptosis, autophagy, senescence, cell-cycle arrest, and inhibition or overwhelming of repair mechanisms. These mechanisms are consistent with the nanoparticle radiosensitization literature, the direct Curc-GNP prostate cancer study by Aborig et al., and additional curcumin studies showing ROS accumulation, apoptosis, senescence, p53/p21 signaling, p16-dependent senescence, EGR1/TERT/SIRT6-associated senescence, p53-independent anticancer effects, and broader modulation of cancer survival pathways (1,11,18–21,44). The computational and pathway-based work by Yadav et al., further supports the rationale that gold-curcumin nanoformulations may enhance radiation response through complementary gold-mediated and curcumin-mediated mechanisms (22). The findings of Zhang et al., also support the importance of surface functionalization in prostate cancer GNP radiosensitization, as glucose-bound GNPs enhanced radiation sensitivity in DU145 cells (2).

3.5 Conclusion:

This study aimed to evaluate the effects of Curc-GNPs and Cit-GNPs *in vitro* using DU145 PCa spheroid models. The results showcase the potential of these nanoparticles as effective radiosensitizers through clonogenic assay and cellular uptake analysis respectively. The key findings from these studies show that Curc-GNPs demonstrate dose-depended radiosensitization, with enhancements in SER and reductions in radiation dose (D_{50}) seen in Figure 3.4 and Table 3.3. At 24 hours the uptake of 100 μg/ml Curc-GNPs by DU145 spheroids was 4.76-fold higher than Cit-GNPs, highlighting the enhanced internalization efficiency of Curc-GNPs. At this concentration Curc-GNPs also resulted in a SER of 1.489, which was the second greatest radiosensitization effect observed, while the strongest radiosensitizing effect at the highest tested Curc-GNP concentration, 200 µg/mL with SER of 1.554.

The implications of these results are significant because they provide the foundation for designing GNP therapeutics that can enhance the effect of radiotherapy. Curc-GNP enhanced radiation-induced damage in DU145 spheroid models, providing a strong bridge for *in vivo* studies where dosage, surface coating, size and route of administration can be further optimized.

While this study provides important insights into GNP effects on PCa cells, there are several limitations that should be addressed. First although clonogenic assay was used to determine the radiosensitization effect of Curc-GNPs in DU145 spheroids, the mode of action was not measured and therefore the biological mechanisms like ROS production, cannot be confirmed with this study alone. Second, this study only measured gold uptake, not localization of the GNPs in the spheroid layers. Since the location of GNPs intracellular can greatly affect the amount of radiation-induced cell death, this is an important area to investigate in the future (3). To measure GNP localization and penetration in spheroids confocal microscopy with a Z stack could be used (23).

References

1. Howard D, Sebastian S, Le QVC, Thierry B, Kempson I. Chemical Mechanisms of Nanoparticle Radiosensitization and Radioprotection: A Review of Structure-Function Relationships Influencing Reactive Oxygen Species. Int J Mol Sci. 2020 Jan;21(2):579. doi:10.3390/ijms21020579

2. Zhang X, Xing JZ, Chen J, Ko L, Amanie J, Gulavita S, et al. Enhanced radiation sensitivity in prostate cancer by gold-nanoparticles. Clin Investig Med Med Clin Exp. 2008;31(3):E160-167. doi:10.25011/cim.v31i3.3473 PubMed PMID: 18544279.

3. Jain S, Coulter JA, Hounsell AR, Butterworth KT, McMahon SJ, Hyland WB, et al. CELL-SPECIFIC RADIOSENSITIZATION BY GOLD NANOPARTICLES AT MEGAVOLTAGE RADIATION ENERGIES. Int J Radiat Oncol Biol Phys. 2011 Feb 1;79(2):531–9. doi:10.1016/j.ijrobp.2010.08.044 PubMed PMID: 21095075; PubMed Central PMCID: PMC3015172.

4. Khoo AM, Cho SH, Reynoso FJ, Aliru M, Aziz K, Bodd M, et al. Radiosensitization of Prostate Cancers In Vitro and In Vivo to Erbium-filtered Orthovoltage X-rays Using Actively Targeted Gold Nanoparticles. Sci Rep. 2017 Dec 22;7(1):18044. doi:10.1038/s41598-017-18304-y

5. Wolfe T, Chatterjee D, Lee J, Grant JD, Bhattarai S, Tailor R, et al. Targeted Gold Nanoparticles Enhance Sensitization of Prostate Tumors to Megavoltage Radiation Therapy in vivo. Nanomedicine Nanotechnol Biol Med. 2015 Jul;11(5):1277–83. doi:10.1016/j.nano.2014.12.016 PubMed PMID: 25652893; PubMed Central PMCID: PMC4476911.

6. Soares S, Faria I, Aires F, Monteiro A, Pinto G, Sales MG, et al. Application of Gold Nanoparticles as Radiosensitizer for Metastatic Prostate Cancer Cell Lines. Int J Mol Sci. 2023 Jan;24(4):4122. doi:10.3390/ijms24044122

7. Alkilany AM, Abulateefeh SR, Mills KK, Bani Yaseen AI, Hamaly MA, Alkhatib HS, et al. Colloidal stability of citrate and mercaptoacetic acid capped gold nanoparticles upon lyophilization: effect of capping ligand attachment and type of cryoprotectants. *Langmuir*. 2014 Nov 25;30(46):13799–808. doi:10.1021/la504000v

8. Dong J, Carpinone PL, Pyrgiotakis G, Demokritou P, Moudgil BM. Synthesis of Precision Gold Nanoparticles Using Turkevich Method. KONA Powder Part J. 2020;37:224–32. doi:10.14356/kona.2020011

9. Gao Y, Torrente-Murciano L. Mechanistic insights of the reduction of gold salts in the Turkevich protocol. Nanoscale. 2020;12(5):2740–51. doi:10.1039/C9NR08877F

10. Park JW, Shumaker-Parry JS. Structural study of citrate layers on gold nanoparticles: role of intermolecular interactions in stabilizing nanoparticles. J Am Chem Soc. 2014 Feb 5;136(5):1907–21. doi:10.1021/ja4097384

11. Aborig M, Alsefaou M, Osei E, Wettig S. Engineered dual-functional gold nanoparticles enhance radiosensitization in prostate cancer cells: synergistic action of curcumin and gold. Nanoscale Adv. 2025 Sep 24;7(19):5964–77. doi:10.1039/D5NA00376H

12. Bennie LA, Feng J, Emmerson C, Hyland WB, Matchett KB, McCarthy HO, et al. Formulating RALA/Au nanocomplexes to enhance nanoparticle internalisation efficiency, sensitising prostate tumour models to radiation treatment. J Nanobiotechnology. 2021 Sep 19;19(1):279. doi:10.1186/s12951-021-01019-8

13. Hung WC, Chen FY, Lee CC, Sun Y, Lee MT, Huang HW. Membrane-Thinning Effect of Curcumin. Biophys J. 2008 Jun 1;94(11):4331–8. doi:10.1529/biophysj.107.126888 PubMed PMID: 18310254.

14. Barry J, Fritz M, Brender JR, Smith PES, Lee DK, Ramamoorthy A. Determining the Effects of Lipophilic Drugs on Membrane Structure by Solid-State NMR Spectroscopy: The Case of the Antioxidant Curcumin. J Am Chem Soc. 2009 Apr 1;131(12):4490–8. doi:10.1021/ja809217u

15. Giommarelli C, Zuco V, Favini E, Pisano C, Dal Piaz F, De Tommasi N, et al. The enhancement of antiproliferative and proapoptotic activity of HDAC inhibitors by curcumin is mediated by Hsp90 inhibition. Cell Mol Life Sci. 2010 Mar 1;67(6):995–1004. doi:10.1007/s00018-009-0233-x

16. Jackson SJT, Murphy LL, Venema RC, Singletary KW, Young AJ. Curcumin binds tubulin, induces mitotic catastrophe, and impedes normal endothelial cell proliferation. Food Chem Toxicol. 2013 Oct 1;60:431–8. doi:10.1016/j.fct.2013.08.008

17. Li L, Aggarwal BB, Shishodia S, Abbruzzese J, Kurzrock R. Nuclear factor-κB and IκB kinase are constitutively active in human pancreatic cells, and their down-regulation by curcumin (diferuloylmethane) is associated with the suppression of proliferation and the induction of apoptosis. Cancer. 2004 Nov 15;101(10):2351–62. doi:10.1002/cncr.20605

18. Wang T, Wu X, Al rudaisat M, Song Y, Cheng H. Curcumin induces G2/M arrest and triggers autophagy, ROS generation and cell senescence in cervical cancer cells. J Cancer. 2020 Sep 25;11(22):6704–15. doi:10.7150/jca.45176 PubMed PMID: 33046993; PubMed Central PMCID: PMC7545669.

19. Liu C, Rokavec M, Huang Z, Hermeking H. Curcumin activates a ROS/KEAP1/NRF2/miR-34a/b/c cascade to suppress colorectal cancer metastasis. Cell Death Differ. 2023 Jul;30(7):1771–85. doi:10.1038/s41418-023-01178-1 PubMed PMID: 37210578; PubMed Central PMCID: PMC10307888.

20. Xu D, Li L, Yu Z. Effect and mechanism of curcumin on colon cancer cell senescence through early growth response 1 (EGR1). Transl Cancer Res. 2024 Jul 31;13(7). doi:10.21037/tcr-24-26

21. Hendrayani SF, Al-Khalaf HH, Aboussekhra A. Curcumin Triggers p16-Dependent Senescence in Active Breast Cancer-Associated Fibroblasts and Suppresses Their Paracrine Procarcinogenic Effects. Neoplasia N Y N. 2013 Jun;15(6):631–40. doi:10.1593/neo.13478 PubMed PMID: 23730211; PubMed Central PMCID: PMC3664995.

22. Yadav P, Bandyopadhyay A, Sarkar K. Enhancement of gold-curcumin nanoparticle mediated radiation response for improved therapy in cervical cancer: a computational approach and predictive pathway analysis. Discov Nano. 2024 Sep 18;19(1):153. doi:10.1186/s11671-024-04104-7 PubMed PMID: 39292302; PubMed Central PMCID: PMC11410751.

23. Rane TD, Armani AM. Two-Photon Microscopy Analysis of Gold Nanoparticle Uptake in 3D Cell Spheroids. PLoS ONE. 2016 Dec 9;11(12):e0167548. doi:10.1371/journal.pone.0167548 PubMed PMID: 27936027; PubMed Central PMCID: PMC5147918.

24. Petrovic LZ, Oumano M, Hanlon J, Arnoldussen M, Koruga I, Yasmin-Karim S, et al. Image-Based Quantification of Gold Nanoparticle Uptake and Localization in 3D Tumor Models to Inform Radiosensitization Schedule. Pharmaceutics. 2022 Mar;14(3):667. doi:10.3390/pharmaceutics14030667

25. Bromma K, Alhussan A, Perez MM, Howard P, Beckham W, Chithrani DB. Three-Dimensional Tumor Spheroids as a Tool for Reliable Investigation of Combined Gold Nanoparticle and Docetaxel Treatment. Cancers. 2021 Mar 23;13(6):1465. doi:10.3390/cancers13061465 PubMed PMID: 33806801; PubMed Central PMCID: PMC8004664.

26. Bromma K, Dos Santos N, Barta I, Alexander A, Beckham W, Krishnan S, et al. Enhancing nanoparticle accumulation in two dimensional, three dimensional, and xenograft mouse cancer cell models in the presence of docetaxel. Sci Rep. 2022 Aug 5;12:13508. doi:10.1038/s41598-022-17752-5 PubMed PMID: 35931743; PubMed Central PMCID: PMC9356051.

27. Tchoryk A, Taresco V, Argent RH, Ashford M, Gellert PR, Stolnik S, et al. Penetration and Uptake of Nanoparticles in 3D Tumor Spheroids. Bioconjug Chem. 2019 May 15;30(5):1371–84. doi:10.1021/acs.bioconjchem.9b00136

28. Kim B, Han G, Toley B, Kim C kyu, Rotello VM, Forbes NS. Tuning Payload Delivery in Tumour Cylindroids using Gold Nanoparticles. Nat Nanotechnol. 2010 Jun;5(6):465–72. doi:10.1038/nnano.2010.58 PubMed PMID: 20383126; PubMed Central PMCID: PMC2881185.

29. Stone KR, Mickey DD, Wunderli H, Mickey GH, Paulson DF. Isolation of a human prostate carcinoma cell line (DU 145). Int J Cancer. 1978;21(3):274–81. doi:10.1002/ijc.2910210305

30. Alimirah F, Chen J, Basrawala Z, Xin H, Choubey D. DU-145 and PC-3 human prostate cancer cell lines express androgen receptor: Implications for the androgen receptor functions and regulation. FEBS Lett. 2006;580(9):2294–300. doi:10.1016/j.febslet.2006.03.041

31. Chithrani BD, Ghazani AA, Chan WCW. Determining the Size and Shape Dependence of Gold Nanoparticle Uptake into Mammalian Cells. Nano Lett. 2006 Apr 1;6(4):662–8. doi:10.1021/nl052396o

32. Chithrani BD, Chan WCW. Elucidating the Mechanism of Cellular Uptake and Removal of Protein-Coated Gold Nanoparticles of Different Sizes and Shapes. Nano Lett. 2007 Jun 13;7(6):1542–50. doi:10.1021/nl070363y

33. Huang K, Ma H, Liu J, Huo S, Kumar A, Wei T, et al. Size-Dependent Localization and Penetration of Ultrasmall Gold Nanoparticles in Cancer Cells, Multicellular Spheroids, and Tumors in Vivo. ACS Nano. 2012 May 22;6(5):4483–93. doi:10.1021/nn301282m PubMed PMID: 22540892; PubMed Central PMCID: PMC3370420.

34. Bilgi E, Winkler DA, Oksel Karakus C. Identifying factors controlling cellular uptake of gold nanoparticles by machine learning. J Drug Target. 2024 Jan 2;32(1):66–73. doi:10.1080/1061186X.2023.2288995 PubMed PMID: 38009690.

35. Swanson S, McKenna CB, Cheraghi E, Osei E. Post-treatment recovery of docetaxel-treated prostate cancer monolayer and spheroid culture [Internet]. bioRxiv; 2025 [cited 2026 Apr 23]. p. 2025.11.17.688723. Available from: https://www.biorxiv.org/content/10.1101/2025.11.17.688723v1 doi:10.1101/2025.11.17.688723

36. Franken NAP, Rodermond HM, Stap J, Haveman J, Van Bree C. Clonogenic assay of cells in vitro. Nat Protoc. 2006 Dec;1(5):2315–9. doi:10.1038/nprot.2006.339

37. Cho YM, Kim YS, Kang MJ, Farrar WL, Hurt EM. Long-Term Recovery of Irradiated Prostate Cancer Increases Cancer Stem Cells. Prostate. 2012 Dec 1;72(16):1746–56. doi:10.1002/pros.22527 PubMed PMID: 22513891; PubMed Central PMCID: PMC7417080.

38. Nezamtaheri MS, Khoei S, Nikoofar AR, Goliaei B. Comparison of radiosensitizing effect of Resveratrol on monolayer and spheroid culture of DU145 prostatic cell line. International Journal of Radiation Research. 2012 Dec 10;10(3):177–81.

39. Brix N, Samaga D, Hennel R, Gehr K, Zitzelsberger H, Lauber K. The clonogenic assay: robustness of plating efficiency-based analysis is strongly compromised by cellular cooperation. Radiat Oncol. 2020 Oct 29;15(1):248. doi:10.1186/s13014-020-01697-y

40. Braselmann H, Michna A, Heß J, Unger K. CFAssay: statistical analysis of the colony formation assay. Radiat Oncol Lond Engl. 2015 Nov 4;10:223. doi:10.1186/s13014-015-0529-y PubMed PMID: 26537797; PubMed Central PMCID: PMC4634140.

41. Zhang Y, Hu K, Beumer JH, Bakkenist CJ, D'Argenio DZ. RAD-ADAPT: software for modelling clonogenic assay data in radiation biology. DNA Repair. 2017 Apr;52:24–30. doi:10.1016/j.dnarep.2017.02.004 PubMed PMID: 28254357; PubMed Central PMCID: PMC5396547.

42. Sarkar A, Pickering C. CellSurvAssay: Clonogenic Survival Analysis in R made easy! [Internet]. 2022 [cited 2026 Apr 22]. CellSurvAssay: Clonogenic Survival Analysis in R made easy! Available from: https://pickeringlab.github.io/CellSurvAssay/

43. Barry J, Fritz M, Brender JR, Smith PES, Lee DK, Ramamoorthy A. Determining the Effects of Lipophilic Drugs on Membrane Structure by Solid-State NMR Spectroscopy: The Case of the Antioxidant Curcumin. J Am Chem Soc. 2009 Apr 1;131(12):4490–8. doi:10.1021/ja809217u

44. Li SQ, Zhu XR, Qin BC, Chen MB. Curcumin in colorectal cancer: mechanistic insights, pharmacological limitations, and translational perspectives. Front Pharmacol. 2025 Sep 29;16:1667731. doi:10.3389/fphar.2025.1667731 PubMed PMID: 41089849; PubMed Central PMCID: PMC12515899.

45. Ma J, Ren Z, Ma Y, Xu L, Zhao Y, Zheng C, et al. Targeted Knockdown of EGR-1 Inhibits IL-8 Production and IL-8-mediated Invasion of Prostate Cancer Cells through Suppressing EGR-1/NF-κB Synergy. J Biol Chem. 2009 Dec 11;284(50):34600–6. doi:10.1074/jbc.M109.016246 PubMed PMID: 19837667; PubMed Central PMCID: PMC2787322.

46. Virolle T, Krones-Herzig A, Baron V, Gregorio GD, Adamson ED, Mercola D. Egr1 Promotes Growth and Survival of Prostate Cancer Cells: IDENTIFICATION OF NOVEL Egr1 TARGET GENES *. J Biol Chem. 2003 Apr 4;278(14):11802–10. doi:10.1074/jbc.M210279200

47. Zagurovskaya M, Shareef MM, Das A, Reeves A, Gupta S, Sudol M, et al. EGR-1 forms a complex with YAP-1 and upregulates Bax expression in irradiated prostate carcinoma cells. Oncogene. 2009 Feb 26;28(8):1121–31. doi:10.1038/onc.2008.461 PubMed PMID: 19137013.

49. Brambilla C, Folini M, Gandellini P, Daprai L, Daidone MG, Zaffaroni N. Oligomer -mediated modulation of hTERT alternative splicing induces telomerase inhibition and cell growth decline in human prostate cancer cells. Cell Mol Life Sci CMLS. 2004 Jul;61(14):1764–74. doi:10.1007/s00018-004-4062-7 PubMed PMID: 15241552; PubMed Central PMCID: PMC11138665.

50. Liu X, Huang N, Li H, Jin Q, Ji J. Surface and Size Effects on Cell Interaction of Gold Nanoparticles with Both Phagocytic and Nonphagocytic Cells. Langmuir. 2013 Jul 23;29(29):9138–48. doi:10.1021/la401556k.

Chapter 4: Conclusions and Future Directions

4.1 Conclusions

The research presented in this thesis provide insight into the synthesis and characterization and application of phytochemical-coated gold nanoparticles, specifically Curc-GNPs, as novel therapeutics for prostate cancer. The aim of this research was to synthesize and assess these nanoparticles for their radiosensitizing potential and uptake using 3D DU145 spheroids models, to bridge the gap between *in vitro* and *in vivo* radiosensitization and uptake studies.

In Chapter 2, titled "Synthesis and Characterization of Gold Nanoparticles" two distinct gold nanoparticle formulations, Curc-GNPs and Cit-GNPs were successfully synthesized and characterized. The eco-friendly, single pot green synthesis method used for Curc-GNPs resulted in nanoparticles with higher yield, stability and beneficial physiochemical properties compared to Cit-GNPs. Characterization using Dynamic Light Scattering (DLS) revealed that the synthesis resulted in hydrodynamic diameter of Cit- and Curc-GNPS ranging from 18 – 25 nm with Cit-GNPs being on the smaller end of the range. Colloidal analysis indicated negative zeta potentials from both Cit- and Curc-GNPs, and UV-Vis analysis indicated a SPR peak ranging from 520-530 nm for both GNPs.

In Chapter 3, titled "In Vitro Study of Gold Nanoparticles in Prostate Cancer Spheroids" the therapeutic potential of Curc-GNPs as radiosensitizers were investigated using DU145 prostate cancer spheroids. The use of DU145 spheroids provided a more stringent and translationally relevant model than conventional monolayer culture, as DU145 cells are androgen-insensitive and derived from a metastatic prostate cancer site (50, 175). Therefore, while this model does not fully recapitulate the clinical and molecular heterogeneity of castration-resistant prostate cancer, it provides a useful in

vitro platform for evaluating Curc-GNP uptake and radiosensitization in an advanced, treatment-resistant prostate cancer context (50,176).

Cellular uptake of Curc-GNPs in DU145 prostate cancer spheroids was quantified using ICP-OES, which highlighted that multiple interacting variables influenced cellular uptake. This includes GNP-coating, GNP-dose, incubation time and their interactions. The post hoc analysis showed that Curc-GNP uptake was significantly higher than Cit-GNP uptake at 50 μg/mL after 5 h and 10 h, while no significant difference was observed at 24 h for this dose (Table 3.2). At 100 μg/mL, Curc-GNP uptake was significantly higher at 5 h and 24 h, but not at 10 h. This trend suggests that nanoparticle uptake in spheroids is influenced by dynamic transport and redistribution processes that may differ between early and later time points. Clonogenic assay revealed that Curc-GNPs have a concentration-dependent radiosensitization effect in DU145 prostate cancer spheroids, where the highest Sensitization Enhancement Ratio (SER) of 1.554 was observed at 200 μg/mL. This was supported by the shift in all LQ parameters which suggested that increasing Curc-GNPs may cause more linear single track DNA damage from radiation, while decreasing the contribution of accumulated DNA damage. This study also found that the radiosensitizing effect and cellular uptake was more moderate compared to *in vitro* studies that used monolayer cell cultures. This further supports the importance of using 3D spheroid models to test therapeutic efficacy before progressing to *in vivo* studies.

4.2 Challenges and Future Directions

Based on the results presented in Chapters 2 and 3, several challenges and future directions have emerged. These challenges are mainly related to, colloidal stability in biologically relevant environments, nanoparticle penetration into three-dimensional tumour spheroids, investigation and optimization of Curc-GNP-mediated radiosensitization. Addressing these challenges will be

important for improving the reliability of Curc-GNPs as a radiosensitizing platform and for advancing this work toward more physiologically relevant in vitro and future in vivo models.

4.2.1 Improving Nanoparticle Penetration and Uptake in 3D Spheroids

A key challenge identified in Chapter 3 is the complexity of nanoparticle uptake in three-dimensional spheroid models. Unlike monolayer cultures, spheroids contain compact cell-cell interactions, diffusion barriers, and nutrient and oxygen gradients. These properties make spheroids more physiologically relevant, but they also limit nanoparticle penetration and make uptake more difficult to interpret. Chapter 3 showed that Curc-GNPs were taken up more effectively than Cit-GNPs in DU145 spheroids, particularly at 24 hours, with the strongest uptake observed for 100 μg/mL Curc-GNPs at 24 hours.

This suggests that longer incubation times may be required for Curc-GNPs to penetrate the spheroid structure and accumulate within cells. However, ICP-OES measures total gold content and does not distinguish between nanoparticles bound to the spheroid surface, trapped in extracellular spaces, or internalized by cells. Therefore, a major future direction is to determine where Curc-GNPs localize within the spheroid.

Future studies should incorporate imaging-based approaches such as confocal microscopy, dark-field microscopy with hyperspectral imaging, or TEM of spheroid sections to determine whether GNPs are distributed throughout the spheroid or mainly retained in outer cell layers (177-179). Spheroids of different sizes should also be tested to determine how spheroid diameter influences GNP penetration. This would help identify the optimal incubation time and treatment concentration needed to achieve sufficient nanoparticle accumulation before irradiation.

4.2.2 Linking GNP Uptake to Radiosensitization

Another challenge is that uptake and radiosensitization were evaluated as related but separate endpoints. Chapter 3 showed that Curc-GNP uptake increased with incubation time and that Curc-GNPs produced concentration-dependent radiosensitization in DU145 spheroids. The clonogenic assay results showed that D_{50} decreased from 2.012 Gy in the untreated control to 1.295 Gy at 200 μg/mL Curc-GNPs, while SER increased from 1.000 to 1.554. These results support the radiosensitizing potential of Curc-GNPs in spheroids.

However, it remains unclear whether the degree of radiosensitization is directly proportional to intracellular gold concentration. For example, the difference between the 100 and 200 μg/mL Curc-GNP groups appeared smaller than the difference between lower concentrations, suggesting a possible plateau in radiosensitization. This may indicate that once sufficient gold accumulation is reached, additional nanoparticle exposure produces only modest further enhancement.

Future work should directly pair uptake and clonogenic survival experiments under the same treatment conditions. For example, spheroids could be treated with Curc-GNPs at all the concentrations and used for radiosensitization, with one set analyzed for gold uptake and another set irradiated for clonogenic survival. This would allow gold content per cell to be correlated with D_{50}, SER, α, β, and α/β values. Establishing this relationship would help determine whether a minimum intracellular gold threshold is required for radiosensitization and whether higher concentrations provide meaningful additional benefit.

4.2.3 Investigating the Mechanisms of Curc-GNP-Mediated Radiosensitization

The LQ modelling results in Chapter 3 suggest that Curc-GNPs may enhance radiation-induced cell killing by increasing the linear component of damage. The α parameter increased with Curc-GNP concentration, while β decreased, suggesting that Curc-GNPs may increase direct or single-track lethal damage while reducing the relative contribution of accumulated sublethal damage. However, clonogenic survival analysis alone cannot confirm the biological mechanisms responsible for this effect.

Future work should investigate whether Curc-GNP-mediated radiosensitization is associated with increased ROS generation, DNA double-strand breaks, mitochondrial dysfunction, apoptosis, senescence, or impaired DNA repair. This could be assessed using assays such as γ-H2AX staining for DNA double-strand breaks, DCFDA fluorescence for ROS production, Annexin V/propidium iodide staining for apoptosis, and markers of DNA repair pathway activation (180–184). Since curcumin has been reported to affect oxidative stress, apoptosis, cell cycle regulation, and proliferation, these assays would help determine whether the observed radiosensitization is due to gold-mediated physical dose enhancement, curcumin-mediated biological effects, or a combination of both (185–188).

In addition, the possible role of Curc-GNPs in cell-cycle redistribution should be investigated directly. In Chapter 3, the increase in the α parameter suggests that Curc-GNPs may have enhanced the linear component of radiation-induced cell killing, however the current study did not measure whether Curc-GNP treatment altered the distribution of DU145 spheroids across G_0/G_1, S, or G_2/M phases. Therefore, any proposed contribution of G_2/M arrest remains speculative based on the findings from existing literature (189). The effect of Curc-GNPs on the cell cycle redistribution could be tested experimentally by treating DU145 spheroids with Curc-GNPs, dissociating them into single-cell

suspensions before irradiation, and performing flow cytometry using DNA-content staining with propidium iodide, DAPI or phosphor-histone H3, a mitotic marker, to quantify the proportion of cells in each cell-cycle phase (190,191). This would allow future studies to determine whether Curc-GNP treatment increases the proportion of cells in radiosensitive cell-cycle phases before irradiation. If an increase in G_2/M-phase cells were observed, this would provide experimental support for the hypothesis that cell-cycle redistribution contributes to the increased α parameter and enhanced clonogenic radiosensitization observed in this study. However, if no change were observed, the increase in the α parameter would be more likely attributable to other mechanisms, like ROS generation, persistence of DNA damage, mitochondrial dysfunction, or impaired repair.

A future direction would also be to include free curcumin and a physical mixture of free curcumin plus Cit-GNPs as comparison groups. This would help determine whether the curcumin coating provides a unique advantage compared with curcumin and gold delivered separately.

4.2.4 Future In Vitro Evaluation of Curc-GNPs

Although the DU145 spheroids we used in this study provide a more physiologically relevant model than monolayer cultures, they still do not fully replicate the complexity of prostate cancer in vivo. This is because, conventional tumour spheroids do not fully replicate the complexity of prostate cancer *in vivo* because they lack key features like vascularization, immune cells, stromal components, and systemic clearance mechanisms (43,192). In addition, although DU145 cells are androgen-insensitive and originate from a metastatic prostate cancer, they should not be interpreted as a complete model of CRPC (50, 175). CRPC is biologically heterogeneous and influence by androgen receptor signalling, prior therapy exposure, the TME, and patient-specific molecular alterations (176).

Therefore, while the results from Chapter 3 provide an important translational step, additional models are required before Curc-GNPs can be advanced toward *in vivo* testing.

Future studies should evaluate Curc-GNP uptake and radiosensitization in spheroids generated from additional prostate cancer cell lines, such as LNCaP, and other CRPC-relevant models, to determine whether the observed effects are specific to DU145 cells or more broadly applicable across prostate cancer phenotypes. Including both androgen-sensitive and androgen-insensitive models would help determine whether Curc-GNP-mediated uptake and radiosensitization are influenced by androgen receptor status, metastatic phenotype, or treatment-resistant biology (50,176). Normal or healthy prostate epithelial cells should also be included to assess whether Curc-GNPs preferentially radiosensitize cancer cells over non-malignant cells. This is important because an ideal radiosensitizer should increase tumour cell killing without increasing toxicity to surrounding healthy tissue.

Future spheroid studies could also incorporate hypoxic conditions, larger spheroids or more complex *in vitro* models to better model radioresistant tumour regions. Since hypoxia is a major contributor to radioresistance, testing Curc-GNPs under hypoxic or oxygen-gradient conditions would help determine whether these nanoparticles remain effective in more resistant tumour-like environments (67,193-197). More advanced *in vitro* models including co-culture spheroids, patient-derived organoids, and organ-on-a-chip systems, would further strengthen the translational relevance of this work by incorporating additional components of the TME, improving patient-specific disease modelling, and in microfluidic platforms, allow nanoparticle transport, toxicity, and tissue-level responses to be assed under more physiologically relevant conditions (19,198–201).

4.2.5 Future In Vivo Evaluation of Curc-GNPs

Although the DU145 spheroid model using in this study provides a more physiologically relevant model than monolayer culture, future *in vivo* studies are required to determine whether Curc-GNPs can achieve sufficient tumour accumulation, maintain radiosensitizing activity and avoid systemic toxicity. The translation from *in vitro* spheroid models to *in vivo* systems is challenging because nanoparticle behaviour is strongly influenced by circulation time, biodistribution, organ clearance, biological barriers, protein corona formation, particle size, surface charge and coating (116-118, 153-155). Studies have also shown that GNP biodistribution after intravenous administration, accumulation is commonly observed in organs of the mononuclear phagocyte system, like the liver and spleen (118, 155). Therefore, while the present study demonstrated enhanced Curc-GNP uptake and radiosensitization in DU145 spheroids, these findings do not guarantee efficient delivery *in vivo*.

Future studies could further investigate biodistribution, tumour accumulation and clearance profile of Curc-GNPs in prostate cancer animal models. For example, Aborig et al., completed foundational work using mice models and pharmacokinetic modeling to evaluate GNP behaviour and extrapolate nanoparticle kinetics (154). Similarly, Khlebtsov and Dykman emphasized that GNP biodistribution and toxicity are influenced by physicochemical properties, including particle size, coating, aggregation state, and administration route (153). These studies suggest that future Curc-GNP work should include pharmacokinetic analysis, organ-level gold quantification, tumour-to-organ accumulation ratios, and histological assessment of potential toxicity.

Before *in vivo* testing is done the size and surface chemistry of Curc-GNPs should be optimized. Vedantam et al., demonstrated that cellular uptake and toxicity of colloidal GNPs in

DU145 cells are size dependent, supporting the need to carefully evaluate whether the particle size range used in this thesis is optimal for both tumour uptake and safety (117). Carnovale et al. further showed that GNP toxicity and cellular uptake are affected by size, shape, capping ligand, and biological corona formation, suggesting that Curc-GNP behaviour in serum and biological fluids may differ from behaviour observed in simplified in vitro systems (116). Therefore, future studies should assess Curc-GNP hemocompatibility, organ toxicity, and immune response before moving toward therapeutic *in vivo* studies.

The optimal timing and dosing for Curc-GNP administration alongside irradiation should also be evaluated through *in vivo* radiosensitization studies. The uptake results from Chapter 3 showed that Curc-GNP accumulation in DU145 spheroids was time and dose dependent, with greater uptake observed after longer incubation and higher doses. *In vivo*, the timing of irradiation would need to be matched to the period of maximum tumour accumulation and dose with acceptable normal-organ clearance. Future studies should therefore combine biodistribution studies with radiation-response experiments, using tumour-bearing animal models to determine whether Curc-GNPs improve tumour control at clinically relevant radiation doses and at what Curc-GNP doses and treatment regimens. This would help establish whether the enhanced uptake and radiosensitization observed in DU145 spheroids can be translated into meaningful therapeutic benefit *in vivo*.

Overall, future *in vivo* studies should focus on determining whether Curc-GNPs can selectively accumulate in prostate tumours, enhance radiation response, and maintain an acceptable safety profile. These studies would represent an important next step in translating Curc-GNPs from a promising *in vitro* radiosensitizing platform toward a clinically relevant nanoparticle-based therapeutic strategy.

References:

1. Canadian Cancer Statistics Advisory Committee in collaboration with the Canadian Cancer Society, Statistics Canada and the Public Health Agency of Canada. Canadian Cancer Statistics 2025. [Internet]. Toronto, ON: Canadian Cancer Society; 2025 Nov. Available from: cancer.ca/Canadian-Cancer-Statistics-2025-EN.

2. Frydenberg M, Stricker PD, Kaye KW. Prostate cancer diagnosis and management. The Lancet. 1997 Jun 7;349(9066):1681–7. doi:10.1016/S0140-6736(96)07393-X PubMed PMID: 9186395.

3. Thakur N, Singh P, Bagri A, Srivastava S, Dwivedi V, Singh A, et al. Therapy resistance in prostate cancer: mechanism, signaling and reversal strategies. Explor Target Anti-Tumor Ther. 2024;5(5):1110–34. doi:10.37349/etat.2024.00266 PubMed PMID: 39351434; PubMed Central PMCID: PMC11438573.

4. Dunn MW, Kazer MW. Prostate Cancer Overview. Semin Oncol Nurs. 2011 Nov 1;Current Issues in Prostate Cancer27(4):241–50. doi:10.1016/j.soncn.2011.07.002

5. Hayward SW, Cunha GR. THE PROSTATE: DEVELOPMENT AND PHYSIOLOGY. Radiol Clin North Am. 2000 Jan 1;38(1):1–14. doi:10.1016/S0033-8389(05)70146-9

6. Vargas HA, Akin O, Franiel T, Goldman DA, Udo K, Touijer KA, et al. Normal Central Zone of the Prostate and Central Zone Involvement by Prostate Cancer: Clinical and MR Imaging Implications. Radiology. 2012 Mar;262(3):894–902. doi:10.1148/radiol.11110663 PubMed PMID: 22357889; PubMed Central PMCID: PMC3285222.

7. Loeb S, Lilja H, Vickers A. Beyond PSA: Utilizing Novel Strategies to Screen Men for Prostate Cancer. Curr Opin Urol. 2016 Sep;26(5):459–65. doi:10.1097/MOU.0000000000000316 PubMed PMID: 27262138; PubMed Central PMCID: PMC5035435.

8. Descotes JL. Diagnosis of prostate cancer. Asian J Urol. 2019 Apr 1;Prostate Cancer : On the Road of Progress6(2):129–36. doi:10.1016/j.ajur.2018.11.007

9. Liu Y, Hatano K, Nonomura N. Liquid Biomarkers in Prostate Cancer Diagnosis: Current Status and Emerging Prospects. World J Mens Health. 2025 Jan 1;43(1):8–27. doi:10.5534/wjmh.230386

10. Montironi R, Cheng L, Cimadamore A, Mazzucchelli R, Scarpelli M, Santoni M, et al. Narrative review of prostate cancer grading systems: will the Gleason scores be replaced by the Grade Groups? Transl Androl Urol. 2021 Mar;10(3):1530–40. doi:10.21037/tau-20-853 PubMed PMID: 33850787; PubMed Central PMCID: PMC8039597.

11. Seipel AH, Delahunt B, Samaratunga H, Egevad L. Ductal adenocarcinoma of the prostate: histogenesis, biology and clinicopathological features. Pathology (Phila). 2016 Aug 1;48(5):398–405. doi:10.1016/j.pathol.2016.04.001

12. Cheng HH, Sokolova AO, Schaeffer EM, Small EJ, Higano CS. Germline and Somatic Mutations in Prostate Cancer for the Clinician. J Natl Compr Canc Netw. 2019 May 1;17(5):515–21. doi:10.6004/jnccn.2019.7307

13. Lavery A, Kirby RS, Chowdhury S. Prostate cancer. Medicine (Baltimore). 2016 Jan 1;Oncology44(1):47–51. doi:10.1016/j.mpmed.2015.10.001

14. Baig FA, Hamid A, Mirza T, Syed S. Ductal and Acinar Adenocarcinoma of Prostate: Morphological and Immunohistochemical Characterization. Oman Med J. 2015 May;30(3):162–6. doi:10.5001/omj.2015.36 PubMed PMID: 26171121; PubMed Central PMCID: PMC4459157.

15. Matzkin H, Soloway MS, Hardeman S. Transitional Cell Carcinoma of the Prostate. J Urol. 1991 Nov 1;146(5):1207–12. doi:10.1016/S0022-5347(17)38047-3

16. Malik RD, Dakwar G, Hardee ME, Sanfilippo NJ, Rosenkrantz AB, Taneja SS. Squamous Cell Carcinoma of the Prostate. Rev Urol. 2011;13(1):56–60. PubMed PMID: 21826130; PubMed Central PMCID: PMC3151589.

17. Nadal R, Schweizer M, Kryvenko ON, Epstein JI, Eisenberger MA. Small cell carcinoma of the prostate. Nat Rev Urol. 2014 Apr;11(4):213–9. doi:10.1038/nrurol.2014.21

18. Stages of prostate cancer | Canadian Cancer Society [Internet]. [cited 2026 Mar 23]. Available from: https://cancer.ca/en/cancer-information/cancer-types/prostate/staging

19. Wilkinson AN, Ellison LF, Zhang SX, Ong M, Morgan SC, Goldenberg SL, et al. Canadian Prostate Cancer Trends in the Context of PSA Screening Guideline Changes. Curr Oncol. 2025 Dec;32(12):669. doi:10.3390/curroncol32120669

20. Dai C, Heemers H, Sharifi N. Androgen signaling in prostate cancer. Cold Spring Harb Perspect Med. 2017 Sep 1;7(9):a030452. doi:10.1101/cshperspect.a030452 PubMed PMID: 28389515; PubMed Central PMCID: PMC5580512.

21. Green SM, Mostaghel EA, Nelson PS. Androgen action and metabolism in prostate cancer. Mol Cell Endocrinol. 2012 Sep 5;360(1–2):3–13. doi:10.1016/j.mce.2011.09.046 PubMed PMID: 22453214; PubMed Central PMCID: PMC4124858.

22. Watson PA, Arora VK, Sawyers CL. Emerging mechanisms of resistance to androgen receptor inhibitors in prostate cancer. Nat Rev Cancer. 2015 Dec;15(12):701–11. doi:10.1038/nrc4016 PubMed PMID: 26563462; PubMed Central PMCID: PMC4771416.

23. Senapati D, Kumari S, Heemers HV. Androgen receptor co-regulation in prostate cancer. Asian J Urol. 2020 Jul;7(3):219–32. doi:10.1016/j.ajur.2019.09.005 PubMed PMID: 32742924; PubMed Central PMCID: PMC7385509.

24. Chandrasekar T, Yang JC, Gao AC, Evans CP. Mechanisms of resistance in castration-resistant prostate cancer (CRPC). Transl Androl Urol. 2015 Jun;4(3):365–80. doi:10.3978/j.issn.2223-4683.2015.05.02 PubMed PMID: 26814148; PubMed Central PMCID: PMC4708226.

25. Ferretti S, Mercinelli C, Marandino L, Litterio G, Marchioni M, Schips L. Metastatic Castration-Resistant Prostate Cancer: Insights on Current Therapy and Promising Experimental Drugs. Res Rep Urol. 2023 Jun 26;15:243–59. doi:10.2147/RRU.S385257 PubMed PMID: 37396015; PubMed Central PMCID: PMC10312338.

26. Litwin MS, Tan HJ. The Diagnosis and Treatment of Prostate Cancer: A Review. JAMA. 2017 Jun 27;317(24):2532. doi:10.1001/jama.2017.7248

27. Chaiswing L, Weiss HL, Jayswal RD, Clair DKSt, Kyprianou N. Profiles of Radioresistance Mechanisms in Prostate Cancer. Crit Rev Oncog. 2018;23(1–2):39–67. doi:10.1615/CritRevOncog.2018025946

28. Baskar R, Lee KA, Yeo R, Yeoh KW. Cancer and Radiation Therapy: Current Advances and Future Directions. Int J Med Sci. 2012;9(3):193–9. doi:10.7150/ijms.3635

29. Brenner DJ. The linear-quadratic model is an appropriate methodology for determining isoeffective doses at large doses per fraction. Semin Radiat Oncol. 2008 Oct;18(4):234–9. doi:10.1016/j.semradonc.2008.04.004 PubMed PMID: 18725109; PubMed Central PMCID: PMC2750078.

30. Stewart GD, Ross JA, McLaren DB, Parker CC, Habib FK, Riddick ACP. The relevance of a hypoxic tumour microenvironment in prostate cancer. BJU Int. 2010 Jan 1;105(1):8–13. doi:10.1111/j.1464-410X.2009.08921.x

31. Sminia P, Guipaud O, Viktorsson K, Ahire V, Baatout S, Boterberg T, et al. Clinical Radiobiology for Radiation Oncology. In: Baatout S, editor. Radiobiology Textbook [Internet]. Cham: Springer International Publishing; 2023 [cited 2024 Jul 21]. p. 237–309. Available from: https://doi.org/10.1007/978-3-031-18810-7_5 doi:10.1007/978-3-031-18810-7_5

32. Bortfeld T, Jeraj R. The physical basis and future of radiation therapy. Br J Radiol. 2011 Jun;84(1002):485–98. doi:10.1259/bjr/86221320

33. McMahon SJ. The linear quadratic model: usage, interpretation and challenges. Phys Med Biol. 2018 Dec;64(1):01TR01. doi:10.1088/1361-6560/aaf26a

34. Barney BM, Lee RJ, Handrahan D, Welsh KT, Cook JT, Sause WT. Image-Guided Radiotherapy (IGRT) for Prostate Cancer Comparing kV Imaging of Fiducial Markers With Cone Beam Computed Tomography (CBCT). Int J Radiat Oncol. 2011 May 1;80(1):301–5. doi:10.1016/j.ijrobp.2010.06.007

35. Freeman DE, King CR. Stereotactic body radiotherapy for low-risk prostate cancer: five-year outcomes. Radiat Oncol. 2011 Jan 10;6(1):3. doi:10.1186/1748-717X-6-3

36. Chaput G, Regnier L. Radiotherapy: Clinical pearls for primary care. Can Fam Physician Med Fam Can. 2021 Oct;67(10):753–7. doi:10.46747/cfp.6710753 PubMed PMID: 34649900; PubMed Central PMCID: PMC8516179.

37. Chu E, Jr VTD, Jr VTD. Physicians' Cancer Chemotherapy Drug Manual 2024. Jones & Bartlett Learning; 2023. 971 p.

38. Catimel G, Verweij J, Mattijssen V, Hanauske A, Piccart M, Wanders J, et al. Docetaxel (Taxotere®): An active drug for the treatment of patients with advanced squamous cell carcinoma of the head and neck. Ann Oncol. 1994 Jul 1;5(6):533–7. doi:10.1093/oxfordjournals.annonc.a058908

39. Ruiz de Porras V, Font A, Aytes A. Chemotherapy in metastatic castration-resistant prostate cancer: Current scenario and future perspectives. Cancer Lett. 2021 Dec 28;523:162–9. doi:10.1016/j.canlet.2021.08.033

40. Desai K, McManus JM, Sharifi N. Hormonal Therapy for Prostate Cancer. Endocr Rev. 2021 Jan 22;42(3):354–73. doi:10.1210/endrev/bnab002 PubMed PMID: 33480983; PubMed Central PMCID: PMC8152444.

41. Prostate Cancer Treatment - NCI [pdqCancerInfoSummary] [Internet]. 2026 [cited 2026 Mar 23]. Located at: nciglobal,ncienterprise. Available from: https://www.cancer.gov/types/prostate/patient/prostate-treatment-pdq

42. Hoffman RM. In vitro sensitivity assays in cancer: A review, analysis, and prognosis. J Clin Lab Anal. 1991 Jan;5(2):133–43. doi:10.1002/jcla.1860050211

43. Jubelin C, Muñoz-Garcia J, Griscom L, Cochonneau D, Ollivier E, Heymann MF, et al. Three-dimensional in vitro culture models in oncology research. Cell Biosci. 2022 Sep 11;12(1):155. doi:10.1186/s13578-022-00887-3

44. Fontana F, Marzagalli M, Sommariva M, Gagliano N, Limonta P. In Vitro 3D Cultures to Model the Tumor Microenvironment. Cancers. 2021 Jun 13;13(12):2970. doi:10.3390/cancers13122970

45. Gunti S, Hoke ATK, Vu KP, London NR. Organoid and Spheroid Tumor Models: Techniques and Applications. Cancers. 2021 Feb 19;13(4):874. doi:10.3390/cancers13040874

46. Rhim JS. In vitro human cell culture models for the study of prostate cancer. Prostate Cancer Prostatic Dis. 2000 Dec;3(4):229–35. doi:10.1038/sj.pcan.4500470

47. Ahmed K, Omarova Z, Sheikh A, Abuova G, Ghias K, Abidi SH. Comparison of baseline global gene expression profiles of prostate cancer cell lines LNCaP and DU145. BMC Res Notes. 2024 Dec 31;17:398. doi:10.1186/s13104-024-07050-w PubMed PMID: 39741355; PubMed Central PMCID: PMC11689513.

48. Russell PJ, Kingsley EA. Human Prostate Cancer Cell Lines. In: Russell PJ, Jackson P, Kingsley EA, editors. Prostate Cancer Methods and Protocols [Internet]. Totowa, NJ: Springer New York; 2003 [cited 2024 Jul 17]. p. 21–39. Available from: https://doi.org/10.1385/1-59259-372-0:21 doi:10.1385/1-59259-372-0:21

49. Li JM, Lee S, Zafar R, Shin E, Choi I. Sodium bicarbonate transporter NBCe1 regulates proliferation and viability of human prostate cancer cells LNCaP and PC3. Oncol Rep. 2021 Jul;46(1):129. doi:10.3892/or.2021.8080 PubMed PMID: 34013380; PubMed Central PMCID: PMC8144930.

50. Alimirah F, Chen J, Basrawala Z, Xin H, Choubey D. DU-145 and PC-3 human prostate cancer cell lines express androgen receptor: implications for the androgen receptor functions and regulation. FEBS Lett. 2006 Apr 17;580(9):2294–300. doi:10.1016/j.febslet.2006.03.041 PubMed PMID: 16580667.

51. Bromma K, Beckham W, Chithrani DB. Utilizing two-dimensional monolayer and three-dimensional spheroids to enhance radiotherapeutic potential by combining gold nanoparticles and docetaxel. Cancer Nanotechnol. 2023;14(1):80. doi:10.1186/s12645-023-00231-5 PubMed PMID: 37867929; PubMed Central PMCID: PMC10587262.

52. Sekhoacha M, Riet K, Motloung P, Gumenku L, Adegoke A, Mashele S. Prostate Cancer Review: Genetics, Diagnosis, Treatment Options, and Alternative Approaches. Molecules. 2022 Jan;27(17):5730. doi:10.3390/molecules27175730

53. Nakazawa M, Paller C, Kyprianou N. Mechanisms of Therapeutic Resistance in Prostate Cancer. Curr Oncol Rep. 2017 Feb;19(2):13. doi:10.1007/s11912-017-0568-7

54. Shayegan B, Wallis CJD, Malone S, Cagiannos I, Hamilton RJ, Ferrario C, et al. Real-world use of systemic therapies in men with metastatic castration resistant prostate cancer (mCRPC) in Canada. Urol Oncol Semin Orig Investig. 2022 May 1;40(5):192.e1-192.e9. doi:10.1016/j.urolonc.2022.01.009

55. Housman G, Byler S, Heerboth S, Lapinska K, Longacre M, Snyder N, et al. Drug Resistance in Cancer: An Overview. Cancers. 2014 Sep;6(3):3. doi:10.3390/cancers6031769

56. Esmatabadi MJD, Bakhshinejad B, Motlagh FM, Babashah S, Sadeghizadeh M. Therapeutic resistance and cancer recurrence mechanisms: Unfolding the story of tumour coming back. J Biosci. 2016 Sep 1;41(3):497–506. doi:10.1007/s12038-016-9624-y

57. Mansoori B, Mohammadi A, Davudian S, Shirjang S, Baradaran B. The Different Mechanisms of Cancer Drug Resistance: A Brief Review. Adv Pharm Bull. 2017 Sep 25;7(3):3. doi:10.15171/apb.2017.041

58. Harris KS, Kerr BA. Prostate Cancer Stem Cell Markers Drive Progression, Therapeutic Resistance, and Bone Metastasis. Stem Cells Int. 2017 Jan 1;2017(1):8629234. doi:10.1155/2017/8629234

59. Aramini B, Masciale V, Grisendi G, Bertolini F, Maur M, Guaitoli G, et al. Dissecting Tumor Growth: The Role of Cancer Stem Cells in Drug Resistance and Recurrence. Cancers. 2022 Jan;14(4):4. doi:10.3390/cancers14040976

60. Khan SU, Fatima K, Aisha S, Malik F. Unveiling the mechanisms and challenges of cancer drug resistance. Cell Commun Signal. 2024 Feb 12;22(1):109. doi:10.1186/s12964-023-01302-1

61. Lyu F, Shang SY, Gao XS, Ma MW, Xie M, Ren XY, et al. Uncovering the Secrets of Prostate Cancer's Radiotherapy Resistance: Advances in Mechanism Research. Biomedicines. 2023 Jun 3;11(6):1628. doi:10.3390/biomedicines11061628 PubMed PMID: 37371723; PubMed Central PMCID: PMC10296152.

62. Wang M, Xing R, Wang L, Pan M, Zhang R, Li T, et al. Mechanisms underlying prostate cancer sensitivity to reactive oxygen species: overcoming radiotherapy resistance and recent clinical advances. Cancer Biol Med. 2025 Jul 15;22(7):747–61. doi:10.20892/j.issn.2095-3941.2024.0584

63. King L, Bernaitis N, Christie D, Chess-Williams R, Sellers D, McDermott C, et al. Drivers of Radioresistance in Prostate Cancer. J Clin Med. 2022 Sep 24;11(19):5637. doi:10.3390/jcm1119563

64. Sosa GA, Crosswhite B, Kirschner AN. Cellular signaling and radioresistance in prostate cancer. Cell Signal. 2026 May 1;141:112367. doi:10.1016/j.cellsig.2026.112367

65. Nair SS, Weil R, Dovey Z, Davis A, Tewari AK. The Tumor Microenvironment and Immunotherapy in Prostate and Bladder Cancer. Urol Clin North Am. 2020 Nov 1;Cancer Immunotherapy in Urology (Supplement)47(4, Supplement):e17–54. doi:10.1016/j.ucl.2020.10.005

66. Bożyk A, Wojas-Krawczyk K, Krawczyk P, Milanowski J. Tumor Microenvironment—A Short Review of Cellular and Interaction Diversity. Biology. 2022;11(6). doi:10.3390/biology11060929

67. Milosevic M, Warde P, Ménard C, Chung P, Toi A, Ishkanian A, et al. Tumor Hypoxia Predicts Biochemical Failure following Radiotherapy for Clinically Localized Prostate Cancer. Clin Cancer Res. 2012 Apr 1;18(7):2108–14. doi:10.1158/1078-0432.CCR-11-2711

68. Brown M, Rébillard A, Hart NH, O'Connor D, Prue G, O'Sullivan JM, et al. Modulating Tumour Hypoxia in Prostate Cancer Through Exercise: The Impact of Redox Signalling on Radiosensitivity. Sports Med - Open. 2022 Apr 8;8:48. doi:10.1186/s40798-022-00436-9 PubMed PMID: 35394236; PubMed Central PMCID: PMC8993953.

69. Zhong X, He X, Wang Y, Hu Z, Huang H, Zhao S, et al. Warburg effect in colorectal cancer: the emerging roles in tumor microenvironment and therapeutic implications. J Hematol OncolJ Hematol Oncol. 2022 Nov 1;15(1):160. doi:10.1186/s13045-022-01358-5

70. Arneth B. Tumor Microenvironment. Medicina (Mex). 2019 Dec 30;56(1):15. doi:10.3390/medicina56010015

71. Quail DF, Joyce JA. Microenvironmental regulation of tumor progression and metastasis. Nat Med. 2013 Nov;19(11):1423–37. doi:10.1038/nm.3394

72. Gong L, Zhang Y, Liu C, Zhang M, Han S. Application of Radiosensitizers in Cancer Radiotherapy. Int J Nanomedicine. 2021 Feb 12;16:1083–102. doi:10.2147/IJN.S290438 PubMed PMID: 33603370; PubMed Central PMCID: PMC7886779.

73. Pauwels B, Korst AEC, Pattyn GGO, Lambrechts HAJ, Van Bockstaele DR, Vermeulen K, et al. Cell cycle effect of gemcitabine and its role in the radiosensitizing mechanism *in vitro*. Int J Radiat Oncol. 2003 Nov 15;57(4):1075–83. doi:10.1016/S0360-3016(03)01443-3

74. Theodore S. Lawrence MD, Avraham Eisbruch MD, Cornelius J. Mcginn MD, Marc T. Fields MD, Donna S. Shewach P. Radiosensitization by Gemcitabine [Internet]. Vol. 13. 1999 Oct 1 [cited 2024 Jul 14];ONCOLOGY Vol 13 No 1013. Available from: https://www.cancernetwork.com/view/radiosensitization-gemcitabine

75. Candelaria M, Garcia-Arias A, Cetina L, Dueñas-Gonzalez A. Radiosensitizers in cervical cancer. Cisplatin and beyond. Radiat Oncol. 2006 May 8;1(1):15. doi:10.1186/1748-717X-1-15

76. Ojima E, Inoue Y, Watanabe H, Hiro J, Toiyama Y, Miki C, et al. The optimal schedule for 5-fluorouracil radiosensitization in colon cancer cell lines. Oncol Rep. 2006 Nov 1;16(5):1085–91. doi:10.3892/or.16.5.1085

77. Zeman EM, Schreiber EC, Tepper JE. 27 - Basics of Radiation Therapy. In: Niederhuber JE, Armitage JO, Kastan MB, Doroshow JH, Tepper JE, editors. Abeloff's Clinical Oncology (Sixth Edition) [Internet]. Philadelphia: Elsevier; 2020 [cited 2024 Jul 21]. p. 431-460.e3. Available from: https://www.sciencedirect.com/science/article/pii/B978032347674400027X doi:10.1016/B978-0-323-47674-4.00027-X

78. d'Hose D, Mignion L, Hamelin L, Sonveaux P, Jordan BF, Gallez B. Statins Alleviate Tumor Hypoxia in Prostate Cancer Models by Decreasing Oxygen Consumption: An Opportunity for Radiosensitization? Biomolecules. 2022 Oct 3;12(10):1418. doi:10.3390/biom12101418

79. Sawada Y, Omoto K, Kohei N, Sakaguchi K, Miura M, Tanabe K. Sulfoquinovosylacylpropanediol is a novel potent radiosensitizer in prostate cancer. Int J Urol. 2015 Jun;22(6):590–5. doi:10.1111/iju.12753

80. Zdrowowicz M, Spisz P, Hać A, Herman-Antosiewicz A, Rak J. Influence of Hypoxia on Radiosensitization of Cancer Cells by 5-Bromo-2′-deoxyuridine. Int J Mol Sci. 2022 Jan 27;23(3):1429. doi:10.3390/ijms23031429

81. Potiron VA, Abderrhamani R, Giang E, Chiavassa S, Di Tomaso E, Maira SM, et al. Radiosensitization of prostate cancer cells by the dual PI3K/mTOR inhibitor BEZ235 under normoxic and hypoxic conditions. Radiother Oncol. 2013 Jan;106(1):138–46. doi:10.1016/j.radonc.2012.11.014

82. Langedijk J, Mantel-Teeuwisse AK, Slijkerman DS, Schutjens MHDB. Drug repositioning and repurposing: terminology and definitions in literature. Drug Discov Today. 2015 Aug 1;20(8):1027–34. doi:10.1016/j.drudis.2015.05.001

83. Parvathaneni V, Kulkarni NS, Muth A, Gupta V. Drug repurposing: a promising tool to accelerate the drug discovery process. Drug Discov Today. 2019 Oct 1;24(10):2076–85. doi:10.1016/j.drudis.2019.06.014

84. Pushpakom S, Iorio F, Eyers PA, Escott KJ, Hopper S, Wells A, et al. Drug repurposing: progress, challenges and recommendations. Nat Rev Drug Discov. 2019 Jan;18(1):41–58. doi:10.1038/nrd.2018.168

85. Corsello SM, Bittker JA, Liu Z, Gould J, McCarren P, Hirschman JE, et al. The Drug Repurposing Hub: a next-generation drug library and information resource. Nat Med. 2017 Apr 7;23(4):405–8. doi:10.1038/nm.4306 PubMed PMID: 28388612; PubMed Central PMCID: PMC5568558.

86. Alghandour R, Ebrahim MA, Elshal AM, Ghobrial F, Elzaafarany M, ELbaiomy MA. Repurposing metformin as anticancer drug: Randomized controlled trial in advanced prostate cancer (MANSMED). Urol Oncol. 2021 Dec;39(12):831.e1-831.e10. doi:10.1016/j.urolonc.2021.05.020 PubMed PMID: 34167872.

87. Hegazy SK, El-Azab GA, Zakaria F, Mostafa MF, El-Ghoneimy RA. Mebendazole; from an anti-parasitic drug to a promising candidate for drug repurposing in colorectal cancer. Life Sci. 2022 Jun 15;299:120536. doi:10.1016/j.lfs.2022.120536 PubMed PMID: 35385794.

88. Antonarakis ES, Heath EI, Smith DC, Rathkopf D, Blackford AL, Danila DC, et al. Repurposing itraconazole as a treatment for advanced prostate cancer: a noncomparative randomized phase II trial in men with metastatic castration-resistant prostate cancer. The Oncologist. 2013;18(2):163–73. doi:10.1634/theoncologist.2012-314 PubMed PMID: 23340005; PubMed Central PMCID: PMC3579600.

89. Bibby BAS, Thiruthaneeswaran N, Yang L, Pereira RR, More E, McArt DG, et al. Repurposing FDA approved drugs as radiosensitizers for treating hypoxic prostate cancer. BMC Urol. 2021 Dec;21(1):96. doi:10.1186/s12894-021-00856-x

90. Toschi L, Finocchiaro G, Bartolini S, Gioia V, Cappuzzo F. Role of gemcitabine in cancer therapy. Future Oncol Lond Engl. 2005 Mar 1;1:7–17. doi:10.1517/14796694.1.1.7

91. Introduction to Nutraceuticals and Pharmaceuticals. In: Nutraceuticals and Natural Product Pharmaceuticals [Internet]. Academic Press; 2019 [cited 2026 Mar 23]. p. 1–31. Available from: https://www.sciencedirect.com/science/chapter/edited-volume/abs/pii/B9780128164501000015 doi:10.1016/B978-0-12-816450-1.00001-5

92. Calvani M, Pasha A, Favre C. Nutraceutical Boom in Cancer: Inside the Labyrinth of Reactive Oxygen Species. Int J Mol Sci. 2020 Mar 12;21(6):1936. doi:10.3390/ijms21061936 PubMed PMID: 32178382; PubMed Central PMCID: PMC7139678.

93. Puri V, Nagpal M, Singh I, Singh M, Dhingra GA, Huanbutta K, et al. A Comprehensive Review on Nutraceuticals: Therapy Support and Formulation Challenges. Nutrients. 2022 Nov

3;14(21):4637. doi:10.3390/nu14214637 PubMed PMID: 36364899; PubMed Central PMCID: PMC9654660.

94. Fatima G, Khan S, Shukla V, Awaida W, Li D, Gushchina YS. Nutraceutical formulations and natural compounds for the management of chronic diseases. Front Nutr. 2025 Oct 15;12. doi:10.3389/fnut.2025.1682590

95. Garza-Juárez A, Pérez-Carrillo E, Arredondo-Espinoza EU, Islas JF, Benítez-Chao DF, Escamilla-García E. Nutraceuticals and Their Contribution to Preventing Noncommunicable Diseases. Foods. 2023 Jan;12(17):3262. doi:10.3390/foods12173262

96. AlAli M, Alqubaisy M, Aljaafari MN, AlAli AO, Baqais L, Molouki A, et al. Nutraceuticals: Transformation of Conventional Foods into Health Promoters/Disease Preventers and Safety Considerations. Molecules. 2021 Apr 27;26(9):2540. doi:10.3390/molecules26092540 PubMed PMID: 33925346; PubMed Central PMCID: PMC8123587.

97. Zhang Z, Li X, Sang S, McClements DJ, Chen L, Long J, et al. Polyphenols as Plant-Based Nutraceuticals: Health Effects, Encapsulation, Nano-Delivery, and Application. Foods. 2022 Jan;11(15):2189. doi:10.3390/foods11152189

98. Purgatorio R, Boccarelli A, Pisani L, de Candia M, Catto M, Altomare CD. A Critical Appraisal of the Protective Activity of Polyphenolic Antioxidants against Iatrogenic Effects of Anticancer Chemotherapeutics. Antioxidants. 2024 Jan;13(1):133. doi:10.3390/antiox13010133

99. Davatgaran-Taghipour Y, Masoomzadeh S, Farzaei MH, Bahramsoltani R, Karimi-Soureh Z, Rahimi R, et al. Polyphenol nanoformulations for cancer therapy: experimental evidence and clinical perspective. Int J Nanomedicine. 2017 Apr 4;12:2689–702. doi:10.2147/IJN.S131973 PubMed PMID: 28435252.

100. Aiello P, Consalvi S, Poce G, Raguzzini A, Toti E, Palmery M, et al. Dietary flavonoids: Nano delivery and nanoparticles for cancer therapy. Semin Cancer Biol. 2021 Feb 1;Cancer Nanotherapeutics: Targeted medicine, therapeutic vaccination and Challenges with cancer nanomedicines69:150–65. doi:10.1016/j.semcancer.2019.08.029

101. Fuloria S, Mehta J, Chandel A, Sekar M, Rani NNIM, Begum MY, et al. A Comprehensive Review on the Therapeutic Potential of Curcuma longa Linn. in Relation to its Major Active Constituent Curcumin. Front Pharmacol. 2022 Mar 25;13:820806. doi:10.3389/fphar.2022.820806 PubMed PMID: 35401176; PubMed Central PMCID: PMC8990857.

102. Abd. Wahab NA, H. Lajis N, Abas F, Othman I, Naidu R. Mechanism of Anti-Cancer Activity of Curcumin on Androgen-Dependent and Androgen-Independent Prostate Cancer. Nutrients. 2020 Mar;12(3):679. doi:10.3390/nu12030679

103. Chen C, Wang Q, Liu J. Curcumin inhibits growth and triggers apoptosis in human castration-resistant prostate cancer cells via IGF-1/PI3K/Akt pathway. J Int Med Res. 2025 Feb 1;53(2):03000605231220807. doi:10.1177/03000605231220807

104. Mazaheri-Tehrani S, Rouzbahani S, Heidari-Beni M. The Association Between Anti-Neoplastic Effects of Curcumin and Urogenital Cancers: A Systematic Review. BioMed Res Int. 2024;2024:9347381. doi:10.1155/2024/9347381 PubMed PMID: 39445208; PubMed Central PMCID: PMC11496585.

105. Esmaeli M, Dehghanpour Dehabadi M. Curcumin in prostate cancer: a systematic review of molecular mechanisms and nanoformulated therapeutic strategies. BMC Cancer. 2025 Oct 18;25(1):1609. doi:10.1186/s12885-025-15152-2

106. Sun X, Huang X, Liu L, Shen W, Zheng F, Liu M, et al. Anti-cancer role of curcumin in prostate cancer cells via regulation of m6A-modified circ0030568-FMR1 signaling pathway. Transl Androl Urol. 2024 Nov 30;13(11):2358–75. doi:10.21037/tau-24-276 PubMed PMID: 39698574; PubMed Central PMCID: PMC11650353.

107. Shahbaz M, Momal U, Mohamed HM, Perween A, Naeem H, Imran M, et al. Elucidating the Anticancer Mechanisms of Tetrahydroxycurcumin: A Comprehensive Review of Preclinical Studies. Food Sci Nutr. 2025;13(11):e71125. doi:10.1002/fsn3.71125

108. Yakubu J, Tagit O, Pandey AV. Clinical hurdles for curcumin and piperine nanoparticles in prostate cancer treatment: a bridge too far or a path to clinical reality? Expert Opin Drug Deliv. 2026 Jan 22;0(0):1–16. doi:10.1080/17425247.2026.2619094 PubMed PMID: 41548083.

109. Schwerdtfeger P. Relativistic effects in properties of gold. Heteroat Chem. 2002;13(6):578–84. doi:10.1002/hc.10093

110. Engel J, Francis S, Roldan A. The influence of support materials on the structural and electronic properties of gold nanoparticles – a DFT study. Phys Chem Chem Phys. 2019 Sep 11;21(35):19011–25. doi:10.1039/C9CP03066B

111. Amendola V, Pilot R, Frasconi M, Maragò OM, Iatì MA. Surface plasmon resonance in gold nanoparticles: a review. J Phys Condens Matter Inst Phys J. 2017 May 24;29(20):203002. doi:10.1088/1361-648X/aa60f3 PubMed PMID: 28426435.

112. Zhou HS, Honma I, Komiyama H, Haus JW. Controlled synthesis and quantum-size effect in gold-coated nanoparticles. Phys Rev B. 1994 Oct 15;50(16):12052–6. doi:10.1103/PhysRevB.50.12052

113. Yeh YC, Creran B, Rotello VM. Gold Nanoparticles: Preparation, Properties, and Applications in Bionanotechnology. Nanoscale. 2012 Mar 21;4(6):1871–80. doi:10.1039/c1nr11188d PubMed PMID: 22076024; PubMed Central PMCID: PMC4101904.

114. Suresh AK. Biocompatibility and Inertness of Gold Nanocrystallites. In: Suresh AK, editor. Metallic Nanocrystallites and their Interaction with Microbial Systems [Internet]. Dordrecht: Springer Netherlands; 2012 [cited 2026 Mar 22]. p. 47–54. Available from: https://doi.org/10.1007/978-94-007-4231-4_4 doi:10.1007/978-94-007-4231-4_4

115. Jia YP, Ma BY, Wei XW, Qian ZY. The *in vitro* and *in vivo* toxicity of gold nanoparticles. Chin Chem Lett. 2017 Apr 1;28(4):691–702. doi:10.1016/j.cclet.2017.01.021

116. Carnovale C, Bryant G, Shukla R, Bansal V. Identifying Trends in Gold Nanoparticle Toxicity and Uptake: Size, Shape, Capping Ligand, and Biological Corona. ACS Omega. 2019 Jan 31;4(1):242–56. doi:10.1021/acsomega.8b03227

117. Vedantam P, Huang G, Tzeng TRJ. Size-dependent cellular toxicity and uptake of commercial colloidal gold nanoparticles in DU-145 cells. Cancer Nanotechnol. 2013;4(1–3):13–20. doi:10.1007/s12645-013-0033-8 PubMed PMID: 26316898; PubMed Central PMCID: PMC4544071.

118. De Jong WH, Hagens WI, Krystek P, Burger MC, Sips AJAM, Geertsma RE. Particle size-dependent organ distribution of gold nanoparticles after intravenous administration. Biomaterials. 2008 Apr;29(12):1912–9. doi:10.1016/j.biomaterials.2007.12.037 PubMed PMID: 18242692.

119. Mesbahi A. A review on gold nanoparticles radiosensitization effect in radiation therapy of cancer. Rep Pract Oncol Radiother J Gt Cancer Cent Poznan Pol Soc Radiat Oncol. 2010 Oct 8;15(6):176–80. doi:10.1016/j.rpor.2010.09.001 PubMed PMID: 24376946; PubMed Central PMCID: PMC3863177.

120. Herizchi R, Abbasi E, Milani M, Akbarzadeh A. Current methods for synthesis of gold nanoparticles. Artif Cells Nanomedicine Biotechnol. 2016;44(2):596–602. doi:10.3109/21691401.2014.971807 PubMed PMID: 25365243.

121. Oliveira AEF, Pereira AC, Resende MAC, Ferreira LF. Gold Nanoparticles: A Didactic Step-by-Step of the Synthesis Using the Turkevich Method, Mechanisms, and Characterizations. Analytica. 2023 Jun;4(2):250–63. doi:10.3390/analytica4020020

122. Kimling J, Maier M, Okenve B, Kotaidis V, Ballot H, Plech A. Turkevich Method for Gold Nanoparticle Synthesis Revisited. J Phys Chem B. 2006 Aug 1;110(32):15700–7. doi:10.1021/jp061667w

123. Benedetto G, Fowler A, Langdon D, Raine M, White ML, Ogle J, et al. Aptamer-Coated PLGA Nanoparticles Selectively Internalize into Epithelial Ovarian Cancer Cells In Vitro and In Vivo. Biomolecules. 2025 Aug 4;15(8):1123. doi:10.3390/biom15081123 PubMed PMID: 40867568; PubMed Central PMCID: PMC12383946.

124. Amina SJ, Guo B. A Review on the Synthesis and Functionalization of Gold Nanoparticles as a Drug Delivery Vehicle. Int J Nanomedicine. 2020 Dec 7;15:9823–57. doi:10.2147/IJN.S279094 PubMed PMID: 33324054; PubMed Central PMCID: PMC7732174.

125. Faraday M. The Bakerian Lecture: Experimental relations of gold and other metals to light. Philos Trans R Soc Lond. 1857;147:145–81. doi:10.1098/rstl.1857.0011.

126. Trzciński JW, Panariello L, Besenhard MO, Yang Y, Gavriilidis A, Guldin S. Synthetic guidelines for the precision engineering of gold nanoparticles. Curr Opin Chem Eng. 2020 Sep;29:59–66.

127. Usman AI, Abdul Aziz A, Abu Noqta O. APPLICATION OF GREEN SYNTHESIS OF GOLD NANOPARTICLES: A REVIEW. J Teknol. 2018 Dec 4;81(1). doi:10.11113/jt.v81.11409

128. Aljabali AAA, Akkam Y, Al Zoubi MS, Al-Batayneh KM, Al-Trad B, Abo Alrob O, et al. Synthesis of Gold Nanoparticles Using Leaf Extract of Ziziphus zizyphus and their Antimicrobial Activity. Nanomaterials. 2018 Mar;8(3):174. doi:10.3390/nano8030174

129. Hammami I, Alabdallah NM, Jomaa AA, Kamoun M. Gold nanoparticles: Synthesis properties and applications. J King Saud Univ – Sci. 2021 Oct 1;33. doi:10.1016/j.jksus.2021.101560

130. Zhao W, Wang L, Chen H, Qi L, Yang R, Ouyang T, et al. Green synthesis, characterization and determination of anti-prostate cancer, cytotoxicity and antioxidant effects of gold nanoparticles synthesized using Alhagi maurorum. Inorg Chem Commun. 2022 Jul;141:109525. doi:10.1016/j.inoche.2022.109525

131. Mohammed MIA, AlGAWHARI F. Gold nanoparticle: Synthesis, functionalization, enhancement, drug delivery and therapy: A review. Int J Drug Deliv Technol [Internet]. 2020 Jul 1 [cited 2026 Mar 23]. Available from: https://repository.uobaghdad.edu.iq/articles/4ReXn5IBVTCNdQwCRrpH?page=1853

132. Kempson I. Mechanisms of nanoparticle radiosensitization. Wiley Interdiscip Rev Nanomed Nanobiotechnol. 2021 Jan;13(1):e1656. doi:10.1002/wnan.1656 PubMed PMID: 32686321.

133. Her S, Jaffray DA, Allen C. Gold nanoparticles for applications in cancer radiotherapy: Mechanisms and recent advancements. Adv Drug Deliv Rev. 2017 Jan 15;109:84–101. doi:10.1016/j.addr.2015.12.012 PubMed PMID: 26712711.

134. Adams S, Thai D, Mascona X, Schwartzberg AM, Zhang JZ. Key Factors Affecting the Reproducibility of Synthesis and Growth Mechanism of Near-Infrared Absorbing Hollow Gold Nanospheres. Chem Mater. 2014 Dec 9;26(23):6805–10. doi:10.1021/cm5033892

135. Adlia A, Tomagola I, Damayanti S, Mulya A, Rachmawati H. Antifibrotic Activity and In Ovo Toxicity Study of Liver-Targeted Curcumin-Gold Nanoparticle. Sci Pharm. 2018 Sep 21;86(4):E41. doi:10.3390/scipharm86040041 PubMed PMID: 30248962.

136. Reiss H, Marvin DC, Heist RH. The use of nucleation and growth as a tool in chemical physics. J Colloid Interface Sci. 1977 Jan 1;International Conference on Colloids and Surfaces58(1):125–41. doi:10.1016/0021-9797(77)90376-9

137. Hainfeld JF, Dilmanian FA, Zhong Z, Slatkin DN, Kalef-Ezra JA, Smilowitz HM. Gold nanoparticles enhance the radiation therapy of a murine squamous cell carcinoma. Phys Med Biol. 2010 Jun 7;55(11):3045–59. doi:10.1088/0031-9155/55/11/004 PubMed PMID: 20463371.

138. Luo D, Wang X, Zeng S, Ramamurthy G, Burda C, Basilion JP. Prostate-specific membrane antigen targeted gold nanoparticles for prostate cancer radiotherapy: does size matter for targeted particles? Chem Sci. 2019 Sep 11;10(35):8119–28. doi:10.1039/C9SC02290B

139. Roa W, Zhang X, Guo L, Shaw A, Hu X, Xiong Y, et al. Gold nanoparticle sensitize radiotherapy of prostate cancer cells by regulation of the cell cycle. Nanotechnology. 2009 Sep 16;20(37):375101. doi:10.1088/0957-4484/20/37/375101 PubMed PMID: 19706948.

140. Soares S, Faria I, Aires F, Monteiro A, Pinto G, Sales MG, et al. Application of Gold Nanoparticles as Radiosensitizer for Metastatic Prostate Cancer Cell Lines. Int J Mol Sci. 2023 Feb 18;24(4):4122. doi:10.3390/ijms24044122 PubMed PMID: 36835538; PubMed Central PMCID: PMC9964626.

141. Wang X, Hu X, Li J, Russe ACM, Kawazoe N, Yang Y, et al. Influence of cell size on cellular uptake of gold nanoparticles. Biomater Sci. 2016 May 24;4(6):970–8. doi:10.1039/C6BM00171H

142. Dreaden EC, Austin LA, Mackey MA, El-Sayed MA. Size matters: gold nanoparticles in targeted cancer drug delivery. Ther Deliv. 2012 Apr;3(4):457–78. doi:10.4155/tde.12.21 PubMed PMID: 22834077; PubMed Central PMCID: PMC3596176.

143. Arnida, Malugin A, Ghandehari H. Cellular uptake and toxicity of gold nanoparticles in prostate cancer cells: a comparative study of rods and spheres. J Appl Toxicol JAT. 2010 Apr;30(3):212–7. doi:10.1002/jat.1486 PubMed PMID: 19902477.

144. Song K, Xu P, Meng Y, Geng F, Li J, Li Z, et al. Smart gold nanoparticles enhance killing effect on cancer cells. Int J Oncol. 2013 Feb 1;42(2):597–608. doi:10.3892/ijo.2012.1721

145. Xia Q, Huang J, Feng Q, Chen X, Liu X, Li X, et al. Size- and cell type-dependent cellular uptake, cytotoxicity and in vivo distribution of gold nanoparticles. Int J Nanomedicine. 2019;14:6957–70. doi:10.2147/IJN.S214008 PubMed PMID: 32021157; PubMed Central PMCID: PMC6717860.

146. Bavelaar BM, Song L, Jackson MR, Able S, Tietz O, Skaripa-Koukelli I, et al. Oligonucleotide-Functionalized Gold Nanoparticles for Synchronous Telomerase Inhibition, Radiosensitization, and Delivery of Theranostic Radionuclides. Mol Pharm. 2021 Oct 4;18(10):3820–31. doi:10.1021/acs.molpharmaceut.1c00442

147. Khoo AM, Cho SH, Reynoso FJ, Aliru M, Aziz K, Bodd M, et al. Radiosensitization of Prostate Cancers In Vitro and In Vivo to Erbium-filtered Orthovoltage X-rays Using Actively Targeted Gold Nanoparticles. Sci Rep. 2017 Dec 22;7(1):18044. doi:10.1038/s41598-017-18304-y

148. Petrovic LZ, Oumano M, Hanlon J, Arnoldussen M, Koruga I, Yasmin-Karim S, et al. Image-Based Quantification of Gold Nanoparticle Uptake and Localization in 3D Tumor Models to Inform Radiosensitization Schedule. Pharmaceutics. 2022 Mar 18;14(3):667. doi:10.3390/pharmaceutics14030667 PubMed PMID: 35336040; PubMed Central PMCID: PMC8953383.

149. Cybulski P, Bravo M, Chen JJK, Zundert IV, Krzyzowska S, Taemaitree F, et al. Nanoparticle Accumulation and Penetration in 3D Tumor Models: the Effect of Size, Shape, and Surface Charge [Internet]. bioRxiv; 2024 [cited 2026 Mar 22]. p. 2024.12.06.626955. Available from: https://www.biorxiv.org/content/10.1101/2024.12.06.626955v1 doi:10.1101/2024.12.06.626955

150. Sokolova V, Ebel JF, Kollenda S, Klein K, Kruse B, Veltkamp C, et al. Uptake of Functional Ultrasmall Gold Nanoparticles in 3D Gut Cell Models. Small. 2022;18(31):2201167. doi:10.1002/smll.202201167

151. Oliveira BB, Fernandes AR, Baptista PV. Assessing the gene silencing potential of AuNP-based approaches on conventional 2D cell culture versus 3D tumor spheroid. Front Bioeng Biotechnol. 2024 Feb 12;12. doi:10.3389/fbioe.2024.1320729

152. Alhussan A, Jackson N, Calisin R, Morgan J, Beckham W, Chithrani DB. Utilizing Gold Nanoparticles as Prospective Radiosensitizers in 3D Radioresistant Pancreatic Co-Culture Model. Int J Mol Sci. 2023 Jan;24(15):12523. doi:10.3390/ijms241512523

153. Khlebtsov NG, Dykman LA. Biodistribution and toxicity of gold nanoparticles. Nanotechnologies Russ. 2011 Feb 1;6(1):17–42. doi:10.1134/S1995078011010101

154. Aborig M, Malik PRV, Nambiar S, Chelle P, Darko J, Mutsaers A, et al. Biodistribution and Physiologically-Based Pharmacokinetic Modeling of Gold Nanoparticles in Mice with Interspecies Extrapolation. Pharmaceutics. 2019 Apr;11(4):179. doi:10.3390/pharmaceutics11040179

155. Hirn S, Semmler-Behnke M, Schleh C, Wenk A, Lipka J, Schäffler M, et al. Particle size-dependent and surface charge-dependent biodistribution of gold nanoparticles after intravenous administration. Eur J Pharm Biopharm Off J Arbeitsgemeinschaft Pharm Verfahrenstechnik EV. 2011 Apr;77(3):407–16. doi:10.1016/j.ejpb.2010.12.029 PubMed PMID: 21195759; PubMed Central PMCID: PMC3051057.

156. Butterworth KT, McMahon SJ, Currell FJ, Prise KM. Physical basis and biological mechanisms of gold nanoparticle radiosensitization. Nanoscale. 2012 Jul 27;4(16):4830–8. doi:10.1039/C2NR31227A

157. Moradi F, Rezaee Ebrahim Saraee K, Abdul Sani SF, Bradley DA. Metallic nanoparticle radiosensitization: The role of Monte Carlo simulations towards progress. Radiat Phys Chem. 2021 Mar 1;180:109294. doi:10.1016/j.radphyschem.2020.109294

158. Howard D, Sebastian S, Le QVC, Thierry B, Kempson I. Chemical Mechanisms of Nanoparticle Radiosensitization and Radioprotection: A Review of Structure-Function Relationships Influencing Reactive Oxygen Species. Int J Mol Sci. 2020 Jan 16;21(2):579. doi:10.3390/ijms21020579 PubMed PMID: 31963205; PubMed Central PMCID: PMC7013516.

159. Mott JHL, Daniel JM. Interactions of Electromagnetic Radiation and Subatomic Particles with Matter - Part 1. Clin Oncol R Coll Radiol G B. 2021 Jul;33(7):451–4. doi:10.1016/j.clon.2021.02.004 PubMed PMID: 33707070.

160. Gerken LRH, Schaller LGS, Nißler R, Habermann S, Beckers C, Dommke M, et al. Chemical vs Physical Radioenhancement from TiO2 and Au Nanoparticles to Overcome Hypoxic Radioresistance in X-ray Therapy. Nano Lett. 2025 Aug 27;25(34):12806–15. doi:10.1021/acs.nanolett.5c02080

161. Lee H, Lee K, Kim IK, Park TG. Fluorescent gold nanoprobe sensitive to intracellular reactive oxygen species. Adv Funct Mater. 2009 Jun 23;19(12):1884–90. doi:10.1002/adfm.200801838

162. Rosa S, Connolly C, Schettino G, Butterworth KT, Prise KM. Biological mechanisms of gold nanoparticle radiosensitization. Cancer Nanotechnol. 2017;8(1):2. doi:10.1186/s12645-017-0026-0 PubMed PMID: 28217176; PubMed Central PMCID: PMC5288470.

163. He M, Zhou W, Li C, Guo M. MicroRNAs, DNA Damage Response, and Cancer Treatment. Int J Mol Sci. 2016 Dec 12;17(12):2087. doi:10.3390/ijms17122087 PubMed PMID: 27973455; PubMed Central PMCID: PMC5187887.

164. Penninckx S, Heuskin AC, Michiels C, Lucas S. Thioredoxin Reductase Activity Predicts Gold Nanoparticle Radiosensitization Effect. Nanomaterials. 2019 Feb;9(2):295. doi:10.3390/nano9020295

165. Chen XY, Yung LYL, Tan PH, Bay BH. Harnessing the Immunogenic Potential of Gold Nanoparticle-Based Platforms as a Therapeutic Strategy in Breast Cancer Immunotherapy: A Mini Review. Front Immunol. 2022 Mar 31;13. doi:10.3389/fimmu.2022.865554

166. Lakshmisha BM, Tra NT, Mai PQ, Fidelix A, Biswal P, Samala SK, et al. 876 Investigating the immune effects of radiation dose enhancement using internalized gold nanoparticles. J Immunother Cancer. 2025 Nov 4;13(Suppl 2). doi:10.1136/jitc-2025-SITC2025.0876 PubMed PMID: 10.1136/jitc-2025-SITC2025.0876.

167. Lawrence TS, Maybaum J. Fluoropyrimidines as radiation sensitizers. Semin Radiat Oncol. 1993 Jan 1;Adjuvant Therapy for Colon and Rectal Cancer3(1):20–8. doi:10.1016/S1053-4296(05)80074-8

168. Schmid S, Omlin A, Higano C, Sweeney C, Martinez Chanza N, Mehra N, et al. Activity of Platinum-Based Chemotherapy in Patients With Advanced Prostate Cancer With and Without DNA Repair Gene Aberrations. JAMA Netw Open. 2020 Oct 1;3(10):e2021692. doi:10.1001/jamanetworkopen.2020.21692 PubMed PMID: 33112397; PubMed Central PMCID: PMC7593810.

169. Le TK, Duong QH, Baylot V, Fargette C, Baboudjian M, Colleaux L, et al. Castration-Resistant Prostate Cancer: From Uncovered Resistance Mechanisms to Current Treatments. Cancers. 2023 Jan;15(20):5047. doi:10.3390/cancers15205047

170. Turco F, Gillessen S, Cathomas R, Buttigliero C, Vogl UM. Treatment Landscape for Patients with Castration-Resistant Prostate Cancer: Patient Selection and Unmet Clinical Needs. Res Rep Urol. 2022;14:339–50. doi:10.2147/RRU.S360444 PubMed PMID: 36199275; PubMed Central PMCID: PMC9529226.

171. Dai Y, Bae K, Siemann DW. Impact of Hypoxia on the Metastatic Potential of Human Prostate Cancer Cells. Int J Radiat Oncol. 2011 Oct;81(2):521–8. doi:10.1016/j.ijrobp.2011.04.027

172. Schwarz K, Dobiasch S, Nguyen L, Schilling D, Combs SE. Modification of radiosensitivity by Curcumin in human pancreatic cancer cell lines. Sci Rep. 2020 Mar 2;10(1):3815. doi:10.1038/s41598-020-60765-1

173. Schmidt RM, Hara D, Vega JD, Abuhaija MB, Tao W, Dogan N, et al. Quantifying Radiosensitization of PSMA-Targeted Gold Nanoparticles on Prostate Cancer Cells at Megavoltage Radiation Energies by Monte Carlo Simulation and Local Effect Model. Pharmaceutics. 2022 Oct 17;14(10):2205. doi:10.3390/pharmaceutics14102205 PubMed PMID: 36297640; PubMed Central PMCID: PMC9611822.

174. Mioc A, Mioc M, Ghiulai R, Voicu M, Racoviceanu R, Trandafirescu C, et al. Gold Nanoparticles as Targeted Delivery Systems and Theranostic Agents in Cancer Therapy. Curr Med Chem. 2019;26(35):6493–513. doi:10.2174/0929867326666190506123721 PubMed PMID: 31057102.

175. Stone KR, Mickey DD, Wunderli H, Mickey GH, Paulson DF. Isolation of a human prostate carcinoma cell line (DU 145). Int J Cancer. 1978;21(3):274–81. doi:10.1002/ijc.2910210305

176. Yu SQ, Lai KP, Xia SJ, Chang HC, Chang C, Yeh S. The diverse and contrasting effects of using human prostate cancer cell lines to study androgen receptor roles in prostate cancer. Asian J Androl. 2009 Jan;11(1):39–48. doi:10.1038/aja.2008.44

177. Rane TD, Armani AM. Two-Photon Microscopy Analysis of Gold Nanoparticle Uptake in 3D Cell Spheroids. PLOS ONE. 2016 Dec 9;11(12):e0167548. doi:10.1371/journal.pone.0167548

178. England CG, Priest T, Zhang G, Sun X, Patel DN, McNally LR, et al. Enhanced penetration into 3D cell culture using two and three layered gold nanoparticles. Int J Nanomedicine. 2013 Oct 1;8(1):3603–17. doi:10.2147/IJN.S51668

179. Huang K, Ma H, Liu J, Huo S, Kumar A, Wei T, et al. Size-Dependent Localization and Penetration of Ultrasmall Gold Nanoparticles in Cancer Cells, Multicellular Spheroids, and Tumors in Vivo. ACS Nano. 2012 May 22;6(5):4483–93. doi:10.1021/nn301282m

180. Rogakou EP, Pilch DR, Orr AH, Ivanova VS, Bonner WM. DNA Double-stranded Breaks Induce Histone H2AX Phosphorylation on Serine 139 *. J Biol Chem. 1998 Mar 6;273(10):5858–68. doi:10.1074/jbc.273.10.5858

181. LeBel CP, Ischiropoulos H, Bondy SC. Evaluation of the probe 2',7'-dichlorofluorescin as an indicator of reactive oxygen species formation and oxidative stress. Chem Res Toxicol. 1992 Mar 1;5(2):227–31. doi:10.1021/tx00026a012

182. Figueroa D, Asaduzzaman M, Young F. Real time monitoring and quantification of reactive oxygen species in breast cancer cell line MCF-7 by 2′,7′–dichlorofluorescin diacetate (DCFDA) assay. J Pharmacol Toxicol Methods. 2018 Nov 1;94:26–33. doi:10.1016/j.vascn.2018.03.007

183. Vermes I, Haanen C, Steffens-Nakken H, Reutellingsperger C. A novel assay for apoptosis Flow cytometric detection of phosphatidylserine expression on early apoptotic cells using fluorescein labelled Annexin V. J Immunol Methods. 1995 Jul 17;184(1):39–51. doi:10.1016/0022-1759(95)00072-I

184. Rieger AM, Nelson KL, Konowalchuk JD, Barreda DR. Modified Annexin V/Propidium Iodide Apoptosis Assay For Accurate Assessment of Cell Death. J Vis Exp JoVE. 2011 Apr 24;(50):e2597. doi:10.3791/2597

185. Chendil D, Ranga RS, Meigooni D, Sathishkumar S, Ahmed MM. Curcumin confers radiosensitizing effect in prostate cancer cell line PC-3. Oncogene. 2004 Feb;23(8):1599–607. doi:10.1038/sj.onc.1207284

186. Chen Y, Yang J, Fu S, Wu J. Gold Nanoparticles as Radiosensitizers in Cancer Radiotherapy. Int J Nanomedicine. 2020 Nov 24;15:9407–30. doi:10.2147/IJN.S272902

187. Zoi V, Galani V, Tsekeris P, Kyritsis AP, Alexiou GA. Radiosensitization and Radioprotection by Curcumin in Glioblastoma and Other Cancers. Biomedicines. 2022 Feb;10(2):312. doi:10.3390/biomedicines10020312

188. Aborig M, Alsefaou M, Osei E, Wettig S. Engineered dual-functional gold nanoparticles enhance radiosensitization in prostate cancer cells: synergistic action of curcumin and gold. Nanoscale Adv. 2025 Sep 24;7(19):5964–77. doi:10.1039/D5NA00376H

189. Wang T, Wu X, Al rudaisat M, Song Y, Cheng H. Curcumin induces G2/M arrest and triggers autophagy, ROS generation and cell senescence in cervical cancer cells. J Cancer. 2020 Sep 25;11(22):6704–15. doi:10.7150/jca.45176 PubMed PMID: 33046993; PubMed Central PMCID: PMC7545669.

190. Darzynkiewicz Z, Huang X, Zhao H. Analysis of Cellular DNA Content by Flow Cytometry. Current Protocols in Immunology. 2017;119(1):5.7.1-5.7.20. doi:10.1002/cpim.36

191. Juan G, Traganos F, Darzynkiewicz Z. Chapter 15 Methods to identify mitotic cells by flow cytometry. In: Cytometry [Internet]. Academic Press; 2001 [cited 2026 Jun 30]. p. 343–54. (Methods in Cell Biology). Available from: https://www.sciencedirect.com/science/article/pii/S0091679X0163019X doi:10.1016/S0091-679X(01)63019-X

192. Pinto B, Henriques AC, Silva PMA, Bousbaa H. Three-Dimensional Spheroids as In Vitro Preclinical Models for Cancer Research. Pharmaceutics. 2020 Dec;12(12):1186. doi:10.3390/pharmaceutics12121186

193. Boulefour W, Rowinski E, Louati S, Sotton S, Wozny AS, Moreno-Acosta P, et al. A Review of the Role of Hypoxia in Radioresistance in Cancer Therapy. Med Sci Monit Int Med J Exp Clin Res. 2021 Nov 3;27:e934116-1-e934116-7. doi:10.12659/MSM.934116 PubMed PMID: 34728593; PubMed Central PMCID: PMC8573967.

194. Riffle S, Hegde RS. Modeling tumor cell adaptations to hypoxia in multicellular tumor spheroids. J Exp Clin Cancer Res. 2017 Aug 3;36(1):102. doi:10.1186/s13046-017-0570-9

195. Supiot S, Rousseau C, Dore M, Cheze-Le-Rest C, Kandel-Aznar C, Potiron V, et al. Evaluation of tumor hypoxia prior to radiotherapy in intermediaterisk prostate cancer using 18Ffluoromisonidazole PET/CT: a pilot study. Oncotarget. 2018 Jan 13;9(11):10005–15. doi:10.18632/oncotarget.24234

196. Riffle S, Pandey RN, Albert M, Hegde RS. Linking hypoxia, DNA damage and proliferation in multicellular tumor spheroids. BMC Cancer. 2017 May 18;17(1):338. doi:10.1186/s12885-017-3319-0

197. Rakotomalala A, Escande A, Furlan A, Meignan S, Lartigau E. Hypoxia in Solid Tumors: How Low Oxygenation Impacts the "Six Rs" of Radiotherapy. Front Endocrinol. 2021 Sep 2;12. doi:10.3389/fendo.2021.742215

198. Beshiri M, Agarwal S, Yin JJ, Kelly K. Prostate organoids: emerging experimental tools for translational research. J Clin Invest. 2023 May 15;133(10):e169616. doi:10.1172/JCI169616 PubMed PMID: 37183816; PubMed Central PMCID: PMC10178834.

199. Puca L, Bareja R, Prandi D, Shaw R, Benelli M, Karthaus WR, et al. Patient derived organoids to model rare prostate cancer phenotypes. Nat Commun. 2018 Jun 19;9(1):2404. doi:10.1038/s41467-018-04495-z

200. Kang S, Park SE, Huh DD. Organ-on-a-chip technology for nanoparticle research. Nano Converg. 2021 Jul 8;8:20. doi:10.1186/s40580-021-00270-x PubMed PMID: 34236537; PubMed Central PMCID: PMC8266951.

201. Nejati B, Shahhosseini R, Hajiabbasi M, Ardabili NS, Baktash KB, Alivirdiloo V, et al. Cancer-on-chip: a breakthrough organ-on-a-chip technology in cancer cell modeling. Med Biol Eng Comput. 2025 Feb 1;63(2):321–37. doi:10.1007/s11517-024-03199-5

202. Nambiar S, Osei E, Fleck A, Darko J, Mutsaers AJ, Wettig S. Synthesis of curcumin-functionalized gold nanoparticles and cytotoxicity studies in human prostate cancer cell line. Appl Nanosci. 2018;8(3):347–57. doi:10.1007/s13204-018-0728-6

203. Turkevich J, Stevenson PC, Hillier J. A study of the nucleation and growth processes in the synthesis of colloidal gold. Discuss Faraday Soc. 1951;11:55–75. doi:10.1039/DF9511100055

204. Dong J, Carpinone PL, Pyrgiotakis G, Demokritou P, Moudgil BM. Synthesis of precision gold nanoparticles using Turkevich method. KONA Powder Part J. 2020;37:224–32. doi:10.14356/kona.2020011

205. Zhao J, Friedrich B. Synthesis of gold nanoparticles via chemical reduction method. 2015 Oct 14. doi:10.13140/RG.2.2.28933.35049

206. Franken NAP, Rodermond HM, Stap J, Haveman J, Van Bree C. Clonogenic assay of cells in vitro. Nat Protoc. 2006 Dec;1(5):2315–9. doi:10.1038/nprot.2006.339

207. Hall EJ, Giaccia AJ. Radiobiology for the radiologist. Eighth edition. Philadelphia: Wolters Kluwer; 2019. 597